Honeywell Report 12018

31 July 1966

FINAL REPORT

Period 1 July 1965 through 30 June 1966

EXPERIMENTAL RESEARCH ON CRITICAL PROBLEMS ASSOCIATED WITH THE LASER INTEGRATING GYRO

NATIONAL AERONAUTICS AND SPACE ADMINISTRATION
ELECTRONIC RESEARCH CENTER

Contract No. NAS-12-27

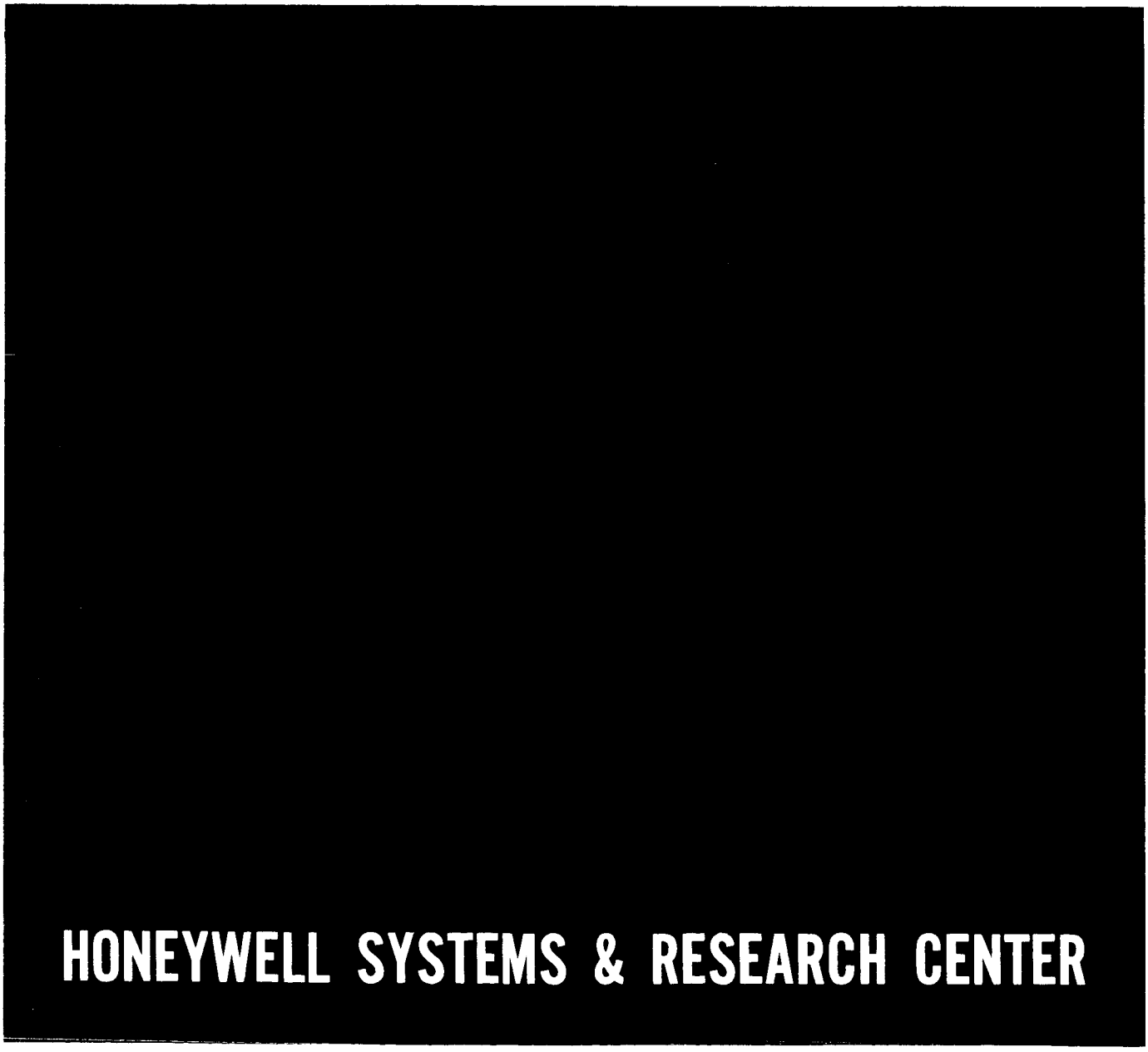

Honeywell Report 12018

31 July 1966

FINAL REPORT

Period 1 July 1965 through 30 June 1966

EXPERIMENTAL RESEARCH ON CRITICAL PROBLEMS ASSOCIATED WITH THE LASER INTEGRATING GYRO

NATIONAL AERONAUTICS AND SPACE ADMINISTRATION
ELECTRONIC RESEARCH CENTER

Contract No. NAS-12-27

Technical Monitor:

Ronald J. Madigan, Jr.

Prepared by:
Frederick Aronowitz
Harry Gustafson

Reviewed by:
Joseph Killpatrick

Approved by:

V. Lewald
Director of Research

Honeywell Inc.
Systems and Research Division
Research Department
2345 Walnut Street
St. Paul, Minnesota

ABSTRACT

The effects of mode coupling due to scattering effects in a traveling-wave He-Ne ring laser are investigated, both theoretically and experimentally.

A Lamb type calculation is made in which the effects of scattering are treated as source terms in Maxwell's Equations. This results in a scattering correction to the self-consistant equations. The scattering correction to the single mode amplitude equations result in mode competition between the oppositely directed beams and possible extinction of one of the beams. The scattering correction to the frequency equations produces frequency synchronization between the oppositely directed beams. Experimental verification of both effects is given.

TABLE OF CONTENTS

ILLUSTRATIONS

I. INTRODUCTION AND SUMMARY

This report relates the results obtained during the one-year contract NAS 12-27, "Experimental Research on Critical Problems Associated with the Laser Integrating Gyro."

The objective of this contract is to establish the ultimate accuracies associated with the use of the ring laser as an inertial component by performing basic research on critical problem areas associated with development of the Laser Gyro.

The particular areas of study and experiment are:

1) To perform a thorough analysis of the fundamental behavior of the Laser.
2) To construct a mathematical model of a laser gyro showing all error sources including non-linearities which may exist.
3) To perform design proof of the math model through testing for the following:
   a) lock-in
   b) anisoptropic scattering as it effects nullshift
   c) mode pulling
   d) g^2 sensitivity
   e) variation of parameters
4) To calculate for the device errors on 1σ, 2σ, and 3σ basis.

A model of a traveling-wave ring laser[1,2] was developed which included mutual coupling between the oppositely directed beams due to scattering effects. The model was a Lamb[3] type calculation where an assumed electromagnetic field in the cavity, polarizes the atoms and acts as a source of scattering. The macroscopic polarization and the scattering are treated as source terms in Maxwell's equations to calculate a reaction field. This reaction field must equal the original assumed field in the cavity for self-consistency. The self-consistency gives a set of equations to determine the amplitudes and frequencies of the modes of oscillation.

For single mode operation there are four coupled self-consistent equations to determine the frequencies and amplitudes of or oppositely

directed traveling waves. For the case of the beams being frequency synchronized, the self-consistent equations reduce to three coupled equations, a pair of amplitude equations and one equation for the phase difference between the oppositely directed beams.

The amplitude equations, under certain conditions, reduce to a pair of coupled cubic equations. From symetry considerations, only four of the nine solutions are independent. The solutions predict that for a single isotope, mode competition occurs at the doppler center. The source of the mode competition is the backscattering of energy from one of the beams into the direction of the other. Depending on the strength of the backscattering, extinction of one of the beams may or may not occur. All four types of modern competition solutions were experimentally observed.

Backscattering was varied by externally retroreflecting one of the beams into the direction of the other. A polarizer was used to control the amount of backscatter. While the beams were frequency locked the phase difference between the oppositely directed beam was measured and correlation with the model was found.

For the case of the beams being unlocked in frequency, the frequency equations predict the lock-in phenomena[4]. The source of lock-in is the mutual coupling by backscattering, of the oppositely directed beams.

Anisotropic forward scattering was shown to produce a differential cavity length for the oppositely directed beams and give rise to a frequency difference in the absence of rotation (null shift). Null shifts were also shown to be produced by velocity flow (Fresnel drag) effecgs.

Lock-in and null shift were experimentally investigated as a function of tuning the frequency of oscillation across the doppler gain profile.

The stability of the laser when operated as an integrating gyro was investigated by rotating the laser in both directions, at a rate much larger than the lock-in threshold. After a period of five hours and after correcting for earths rate, the bias rotation rate was found as 3.6 deg/hr with a 1σ/hour of 0.3 deg/hr.

With the completion of the contract, it is felt that the treatment of a ring laser is on as firm a basis as the treatment of a linear laser. The basic theoretical model has been confirmed experimentally. Due to a limitation in time, however, all the details of the model have not yet been experimentally confirmed.

2. MODIFICATION OF THE LAMB MODEL

In Lamb's model[3] for a SWOM he considered a semiclassical model, in which the electromagnetic field obeyed Maxwell's equations while the gaseous atoms obeyed the laws of quantum mechanics. The treatment was a self-consistent one, in which an assumed electromagnetic field (standing wave) in the cavity polarized (non-linearly) the moving gaseous atoms. The microscopic polarization was then considered as a source term in Maxwell's equations. The derived field was equal to the original assumed field in the cavity. The self-consistency gave conditions on the amplitude of the field and the frequency of oscillation. The latter equations gave conditions on threshold, output power as a function of cavity tuning ("Lamb Dip")[5], frequency pulling and pushing[6], combination tones[7] and the related phenomena of frequency locking.[8]

The nonlinear contribution to the polarization arose from a third order perturbation term in which the atomic system was considered to have interacted three times with the radiation field. Each interaction involved a doppler phase shift such that at the time of observation the net phase shift was zero. The standing wave was considered to have been decomposed into two traveling waves and the atomic system interacted with the traveling waves; twice with the one going in one direction and once with the one going in the other direction. Since the empty cavity normal modes were chosen to be standing waves, a standing wave type radiation field was necessary to obtain the correct contribution to the third order polarization.

In the traveling wave ring optical maser (TWOM) where the waves running in each direction are independent one cannot use Lamb's standing wave formulation.

What will be presented here is a modification of Lamb's formalism to allow treatment of both the traveling and the standing wave optical maser. The results agree with those obtained by Lamb for the SWOM case.

As in the Lamb model, a self-consistent approach is used. An electromagnetic field is assumed to exist in the cavity. The interaction of the radiation with the ensemble of atoms having axial velocity components within an incremental

velocity around velocity $\underline{v}$ is considered. This ensemble sees a Lorentz transformed radiation field in its stationary frame. Thus the interaction between the cavity radiation field and the moving atoms is reduced to an interaction between a doppler shifted radiation field and an ensemble of stationary atoms. In the Lorentz transformation, amplitude transformations are neglected. Only frequency transformations are considered.

In the frame of the moving atoms, the radiation field polarizes the atoms. Applying the inverse Lorentz transformation the polarization is transformed back to the cavity frame. The polarization in the cavity frame is then averaged over all velocity ensembles. The macroscopic polarization is then used as a source term in Maxwell's equations to calculate a reaction field. For self-consistency the calculated reaction field must equal the original assumed radiation field in the cavity. This self-consistency gives a condition on the amplitudes and frequencies of the modes of the radiation field.

A further extension of the Lamb model is made by allowing for the coupling of the oppositely directed travelins waves (ODTW) by the mechanism of scattering. As in the Lamb model, to avoid a complicated boundary value problem, the losses of the cavity are introduced by assuming that a ficticious optical conductivity permeates the entire cavity. The effects of scattering are introduced by assuming a further fictious conductivity caused by scattering. The scattering conductivity term is used as a source term in Maxwell's equations and a scattering correction to the self-consistant amplitude and frequency equations is obtained.

3. ELECTROMAGNETIC FIELD EQUATIONS

In this section the equations to determine the amplitudes and the frequencies of oscillation of the cavity modes, are derived. Starting from Maxwell's Equations in a rotating frame the inhomogeneous wave equation for the electric field is obtained. Since this is a selfconsistent treatment, the source term is the macroscopic polarization which in turn is due to the electric field in the cavity polarizing the gaseous atoms. In addition, the energy which is both forward scattered and back scattered into the cavity, is considered as a source term. This self consistent treatment is represented schematically in Figure (1).

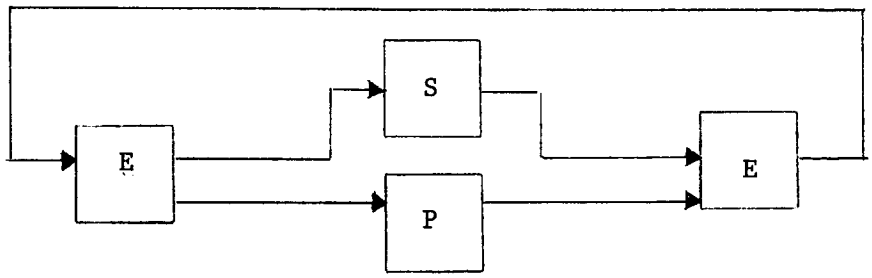

Figure 1. Block Diagram of Self Consistant Treatment

The diagram shows the scattered energy and the macroscopic polarization as source terms for the determination of the electric field intensity. The electric field intensity is the source of the scattered energy and polarizes the atoms. The calculation of the polarization is a quantum mechanical calculation which is done in a later section. In this section the macroscopic polarization is assumed known. It should be noted that the scattered energy does not directly affect the polarization. It indirectly affects the polarization in that the frequencies and amplitudes of the field are affected by the scattered energy and these in turn determine the polarization.

Spontaneous emission is not considered as a source term. Hence for the purposes of the analysis, line width of the oscillating modes is considered much smaller than any other frequency difference.

The calculation to leading to the self consistant equations, which determine

the amplitude, and frequencies of oscillation of the mode of oscillation, will only be outlined here. Details of the calculation can be found in Appendix A.

Maxwell's equations are written for a linearly polarized field and are expressed in a uniformly rotating frame. The equations are separated and the one dimensional inhomogeneous wave equation for the electric field intensity is obtained. The source terms for the wave equation are the microscopic polarization and a term resulting from scattered energy. The wave equation is solved by expanding the solution into the set of the empty cavity normal mode eigenfunctions (ECNME). Substituting back into the wave equation, one then obtains two sets of inhomogeneous equations for the time dependent coefficients of the ECNME. The source terms are now the Fourier components, with respect to the ECNME, of the polarization and the scattering field.

The time dependent coefficients of the ECNME are then written such as to reduce, in an empty cavity, to independent sets of oppositely directed traveling waves. A set of oppositely directed traveling waves, is schematically represented in Fig (2)

Figure 2. Scattering Source Terms

E_1, E_2 and ω_1, ω_2 are the amplitudes and frequencies of the oppositely directed traveling waves. The scattered energy is assumed to be of two types; a forward scattered part and a back scattered part. For forward scattering, it is assumed that a fraction s_1, s_2 , of fields E_1, E_2 is scattered into the original direction, but with an additional phase δ_1, δ_2, respectively. For back scattering, it is assumed that a fraction r_1, r_2 of fields E_1, E_2 is scattered into the opposite direction with an additional phase ϵ_1, ϵ_2 respectively. With this representation of the fields, the self-consistant equations for the determination of the amplitudes and frequencies of oscillation of each mode are

found to be

$$\dot{E}_{1n} + \frac{\omega}{2Q_n} E_{1n} = \frac{\omega}{4\epsilon_o} (\tilde{C}_{1n} - S_{1n}) - \frac{\sigma_s}{2} r_{2n} E_{2n} \cos (\psi_n + \epsilon_{2n}) - \frac{\sigma_s}{2\epsilon_o} s_{1n} E_{1n} \cos \delta_{1n} , \quad (1)$$

$$\dot{E}_{2n} + \frac{\omega}{2Q_n} E_{2n} = \frac{\omega}{4\epsilon_o} \left[(\tilde{S}_{1n} - C_{1n}) \sin \psi_n - (S_{1n} + \tilde{C}_{1n}) \cos \psi_n \right] - \frac{\sigma_s}{2\epsilon_o} r_{1n} E_{1n} \cos (\psi_n - \epsilon_{1n}) - \frac{\sigma_s}{2\epsilon_o} s_2 E_{2n} \cos \delta_{2n} , \quad (2)$$

$$(\Omega_{1n} - \dot{\theta}_{1n}) E_{1n} = \frac{\omega}{4\epsilon_o} (C_{1n} + \tilde{S}_{1n}) + \frac{\sigma_s}{2\epsilon_o} r_{2n} E_{2n} \sin (\psi_n + \epsilon_{2n}) + \frac{\sigma_s}{2\epsilon_o} s_{1n} E_{1n} \sin \delta_{1n} , \quad (3)$$

$$(\Omega_{2n} - \dot{\theta}_{2n}) E_{2n} = \frac{\omega}{4\epsilon_o} \left[(C_{1n} - \tilde{S}_{1n}) \cos \psi_n - (S_{1n} + \tilde{C}_{1n}) \sin \psi_n \right] - \frac{\sigma_s}{2\epsilon_o} r_{1n} E_{1n} \sin (\psi_n - \epsilon_{1n}) + \frac{\sigma_s}{2\epsilon_o} s_{2n} E_{2n} \sin \delta_{2n} , \quad (4)$$

where

$$\psi_n = (\omega_{2n} - \omega_{1n})t + (\varphi_{2n} - \varphi_{1n}) \quad (5)$$

is a slowly varying function of time. The terms in ω/Q represent the losses of the mode. The terms in S and C are the "in phase" and "in quadrature" parts of the Fourier components of the polarization. They can only be determined by a detailed knowledge of the interaction of the atomic system with the electromagnetic field. They will be evaluated in sections 6-9. The terms in Ω_1, Ω_2 represent the empty cavity frequencies for fields E_1, E_2, respectively. In a rotating frame Ω_1 will be different from Ω_2.[8-11]

4. SELF-CONSISTANT EQUATIONS PHYSICAL SIGNIFICANCE

A discussion of the physical significance of the source terms for the inhomogeneous wave equation for the electric field intensity due to scattering effects, is in order at this point. This discussion will be made in conjunction with understanding the signficance of the self-consistent equations.

For simplicity consider the self-constant equations for only a single mode. Rotation removes the directional degeneracy on both frequency and amplitude of the oppositely directed traveling waves and the self-consistent equations can be written as

$$\dot{E}_1 + \frac{\omega}{2Q} E_1 = (\text{Gain})_1 - \frac{\sigma_s}{2\epsilon_o} r_2 E_2 \cos(\psi + \epsilon_2) - \frac{\sigma_s}{2\epsilon_o} s_1 E_1 \cos\delta_1 \qquad (6)$$

$$\dot{E}_2 + \frac{\omega}{2Q} E_2 = (\text{Gain})_2 - \frac{\sigma_s}{2\epsilon_o} r_2 E_1 \cos(\psi - \epsilon_1) - \frac{\sigma_s}{2\epsilon_o} s_2 E_2 \cos\delta_2 \qquad (7)$$

$$(\Omega_1 - \dot{\theta}_1) = \frac{\sigma_s}{2\epsilon_o} r_2 \frac{E_2}{E_1} \sin(\epsilon_2 + \psi) + \frac{\sigma_s}{2\epsilon_o} s_1 \sin\delta_1 \qquad (8)$$

$$(\Omega_2 - \dot{\theta}_1) = \frac{\sigma_s}{2\epsilon_o} r_1 \frac{E_1}{E_2} \sin(\epsilon_1 - \psi) + \frac{\sigma_s}{2\epsilon_o} s_2 \sin\delta_2 \qquad (9)$$

with

$$\psi = \theta_2 - \theta_1 = (\omega_2 - \omega_1)\, t + \varphi_2(t) - \varphi_1(t) \qquad (10)$$

In the self-consistent equations the explicit effects of the polarization of the medium have been suppressed. Only the fact that the medium provides gain has been included in Equations (6, 7). Frequency pulling due to dispersive effects of the medium have also been neglected in Equations (8, 9).

The gain dependence of the active medium and the dispersive effects of the medium can only be discussed in a quantitive fashion after a quantum mechanical treatment of the interaction of the atomic system with the electromagnetic field. Qualitatively, it is seen from Eqs. (8,9) that in the absence of scattering effects, the system will oscillate at the cavity frequency Ω

(modified by a frequency pulling due to the dispersive properties of the active material). For steady state oscillations and in the absence of scattering effects, Eqs. (6,7) give the oscillation condition that "gain equals loss at the frequency of oscillation".

As will be shown in a later section, the gain term in Eqs. (6, 7) is of the form (neglecting mode competition)

$$AE - BE^3 \tag{11}$$

The term in "A" is the linear approximation (polarization proportional to electric field intensity) result. The term in B arises from the saturating effect of the electromagnetic field upon the population inversion of the active medium which produces the gain. The strength of the steady state field can be obtained from Eqs. (6, 11) as

$$BE^2 = A - \omega/2Q \tag{12}$$

Hence the output is proportional to the difference between the unsaturated gain and the loss.

The significance of the scattering term should now be somewhat clearer. In the amplitude equations, the effects of the scattered energy is to increase or decrease the gain, depending on the phase of the scattered energy. In the frequency equations, the effect of the scattered energy is to introduce additional frequency pulling effects. It should be noted that these effects are not necessarily time independent, due to the presence of ψ. It should also be noted, that in addition to coupling effects produced by the induced polarization of the active medium (gain and dispersion) which have not yet been explicitly written, backscattering produces a coupling between the oppositely directed beams, while forward scattering does not.

Consider the special case where the only scattering is forward scattering into beam "one".

Then $r_1 = r_2 = s_2 = 0$, $s_1 \neq 0$, and Eqs. (6-9) become, for steady state

$$\frac{\omega}{2Q} E_1 = (\text{Gain})_1 - \frac{\sigma_s}{2\epsilon_o} s_1 E_1 \cos \delta_1 \tag{13}$$

beam "one" will be shifted in phase, per pass, by the angle α_1. Due to this additional phase shift per pass, the frequancy of the radiation generated by the system will be reduced, such that the net phase shift per pass is still equal to $2m\pi$. The reduction in frequency can be obtained from

$$\alpha_1 = \Delta\Phi/\text{pass} = -\Delta\omega_1 \ (t/\text{pass}) \tag{17}$$

where the time for the radiation to make one pass is (L/C). From Figure 3, for $s_1 << 1$,

$$\alpha_1 = s_1 \sin \delta_1 \tag{18}$$

and Eqs. (17, 18) give

$$\Delta\omega_1 = -\frac{C}{L} s_1 \sin \delta_1 \tag{19}$$

Equation (19) is the physical interpretation of the formally derived self-consistent Equation (15). Comparing the two equations gives

$$\frac{\sigma_s}{2\epsilon_o} = \frac{C}{L} \tag{20}$$

Note that Figure 3 is also consistant with the self-consistent amplitude equation, given by Equation (13). In Equation (13) the "gain" term is of the form

$$AE_1 - BE_1^3, \qquad A, B > 0, \tag{21}$$

as will be shown from the quantum mechanical calculations. This shows that the output intensity in the presence of forward scattering is of the form

$$BE_1^2 = A - \frac{\omega}{2Q} - \frac{C}{L} s_1 \cos \delta_1 \tag{22}$$

Thus when the forward scattered radiation is in phase with the cavity oscillation, the energy generated by the atoms is reduced. This is consistent with Figure 3.

$$\frac{\omega}{2Q} E_2 = (\text{Gain})_2 \tag{14}$$

$$\Omega_1 - \omega_1 = \left(\frac{\sigma_s}{2\epsilon_o}\right) s_1 \sin \delta_1 \tag{15}$$

$$\Omega_2 - \omega_2 = 0 \tag{16}$$

In this special case there is no coupling and Figs (14, 16) give the oscillation conditions for beam "two"; gain-equals loss at frequency of oscillation and in the absence of dispersive effects due to the medium, the frequency of oscillation occurs at the cavity frequency. Eqs. (13, 15) show the effects of scattering on the amplitude and frequency of beam "one".
Refer to Figure 3.

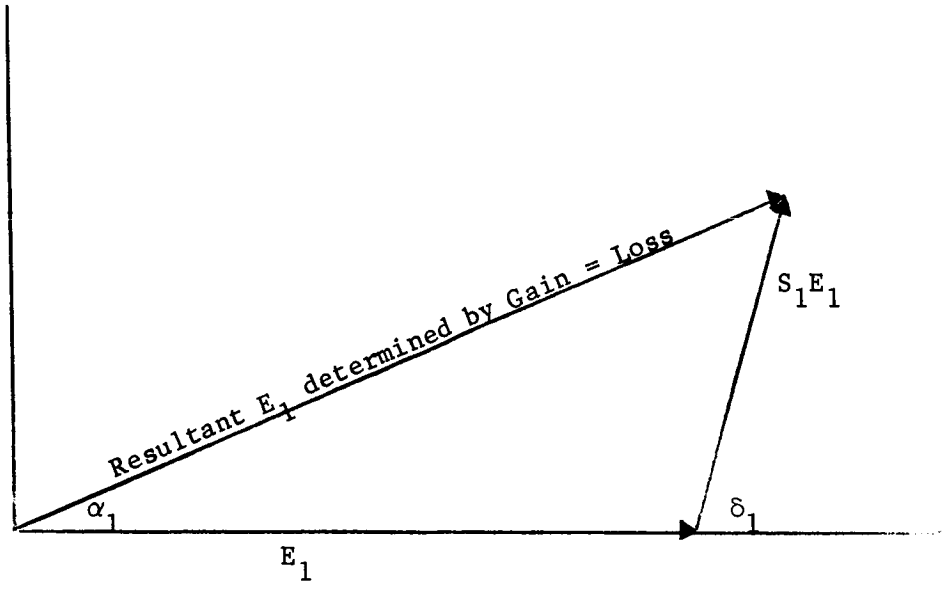

Figure 3. Phase Space Vector Diagram of Oscillation Condition

In the absence of scattering the intensity of beam "one" is represented, on a frame in phase space rotating with the frequency of oscillation of beam "one" equal to the cavity frequency Ω_1, by the factor E_1. The effect of the forward scattering is the addition per pass of a vector of length s_1E_1 with an additional phase angle δ_1. From Figure 3, the resultant radiation of

Fig. 4 shows the phase space vector diagram for the case of pure back scattering. For the case of the frequencies of the oppositely directed waves being different, ψ is a function of time and the vector E_2 rotates about vector E_1 at the beat frequency rate. Likewise the back scattered vector r_2E_2 rotates about the vector E_1 at the beat frequency rate. The net traveling wave field in the cavity at any instant of time is the vector sum of the field produced by stimulated emission and the field arising from back scattering. If forward scattered energy is also present, the resultant field is a simple superposition of all the fields present. For example Eqs. (6, 11) can be written in the form

$$BE_1^2 = AE_1 - \frac{\omega}{2Q}E_1 - \frac{\sigma_s}{2\epsilon_o} s_1E_1 \cos\delta_1 - \frac{\sigma_s}{2\epsilon_o} r_2E_2 \cos(\psi + \epsilon_2) \qquad (23)$$

The first two terms on the right hand side of Eqs (23) represent the difference between the unsaturacted gain and the losses of the system. If the scattered fields are in phase with the stimulated field

$$\delta = \psi + \epsilon_2 = 0,$$

then the amount of energy that must be produced by stimulated emission to made up the losses of the system, is reduced. This is seen in Eq. (23), where BE_1^2 represents the stimulated emission term. Hence scattered radiation in phase with stimulated radiation results in an effective increase in the losses of the system in the sense that increases losses result in decreased stimulated emission.

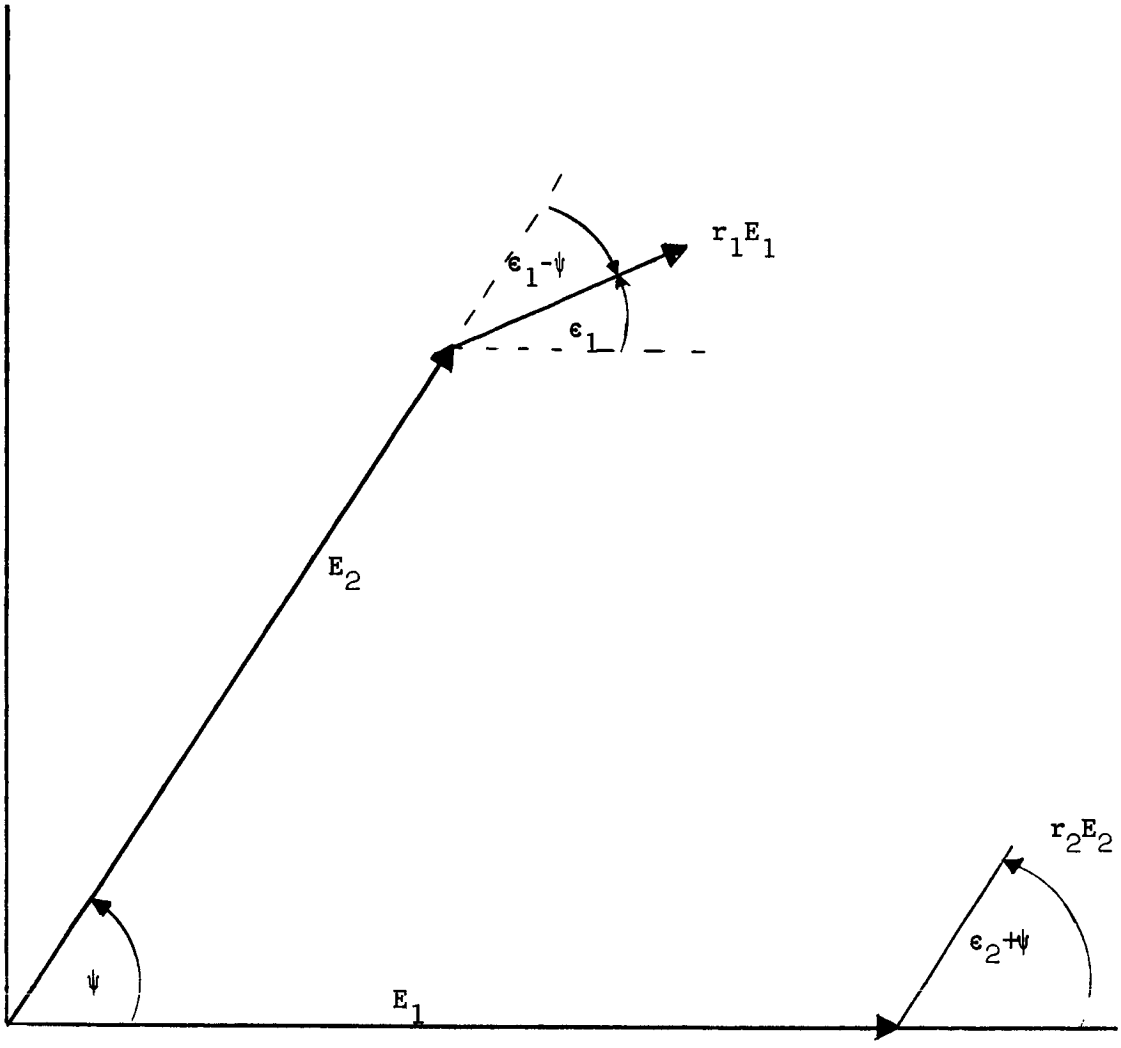

Figure 4. Phase Space Vector Diagram for Mutual Coupling Due to Backscattering

5. FREQUENCY SYNCHRONIZATION (LOCK-IN)

The effect of backscattering has been shown to result in a time dependent pulling of the frequencies of oscillation of the oppositely directe traveling waves. An expression for the frequency difference between the oppositely directed traveling waves can be obtained by subtracting Eqs. (8, 9) and making use of Eq. (10) to write

$$\dot{\psi} = \Omega_2 - \Omega_1 + (c/L)\,[s_1 \sin \delta_1 - s_2 \sin \delta_2] +$$

$$(c/L)\,[\rho_2 \sin (\psi + \epsilon_2) + \rho_1 \sin (\psi - \epsilon_1)], \qquad (24)$$

where

$$\rho_2 = r_2 E_2/E_1 \quad , \quad \rho_1 = r_1 E_1/E_2 \qquad (25)$$

The first term on the right hand side of Eq. (24) is the difference between the cavity frequencies of the oppositely directed traveling waves. This term is proportional to the angular velocity of the rotating frame, upon which the cavity is located, and includes the mode pulling terms arising from the dispersion of the active medium.

The second term is a frequency bias resulting from differential forward scattering. It produces a beat frequency between the oppositely directed traveling waves in the absence of any rotations of the cavity frame, This term arises due to forward scattering producing a change in the optical length of the cavity for both of the traveling waves. If the length change is different for each of the beams, a frequency difference results.

The third term is a time dependent frequency bias resulting from mutual coupling between the traveling waves due to backscattering. Eq. (24) can be put in the form

$$\dot{\psi} = \Delta\Omega + \Delta\Omega_{bias} + \Delta\Omega_{lock} \cos (\psi - B), \qquad (26)$$

$$\Delta\Omega + \Omega_2 - \Omega_1,$$

$$\Delta\Omega\text{bias} = (c/L)\,[s_1 \sin \delta_1 - s_2 \sin \delta_2],$$

$$\Delta\Omega_{\text{lock}} = (c/L)\,[\rho_1^2 + \rho_2^2 + 2\rho_1 \rho_2 \cos(\epsilon_1 + \epsilon_2)]^{1/2} \tag{26}$$

$$\tan\beta = \frac{(r_2 I_2/r_1 I_1)\cos\epsilon_2 + \cos\epsilon_1}{(r_2 I_2/r_1 I_1)\sin\epsilon_2 - \sin\epsilon_1} \quad . \tag{27}$$

In Eq. (27), I_1 and I_2 are the intensities of the traveling waves, as measured in the cavity.

Equation (25) is the lock-in equation and is analyzed in Appendix B. It has the property that for

$$(\Delta\Omega + \Delta\Omega_{\text{bias}}) \geq \Delta\Omega_{\text{lock}},$$

the beat frequency is given by

$$\dot{\psi} = (\Delta\Omega + \Delta\Omega_{\text{bias}})$$

for

$$(\Delta\Omega + \Delta\Omega_{\text{bias}}) < \Delta\Omega_{\text{lock}},$$

the beat frequency becomes a constant, independent of time. For this case the frequencies are said to be locked together. At all points above the lock in region the actual beat frequency is less than the beat frequency in the absence of backscattering and is given by

$$\dot{\psi} = [(\Delta\Omega + \Delta\Omega_{\text{bias}})^2 - \Delta\Omega^2_{\text{lock}}]^{1/2} \tag{28}$$

Figure 5 shows a plot of the beat frequency in the absence of backscatter and the reduced beat frequency due to backscatter and lock in

6. QUANTUM MECHANICAL DERIVATION OF POLARIZATION

The second part of the self-consistant treatment is now carried out. The electric field intensity is now assumed known and from it the polarization of the medium is calculated. Knowledge of the polarization allows the calculation of the lineshape of the atomic maser transition and hence such quantities as intensities of the oppositely directed beams and frequency pulling effects.

The self-consistant method will be carried out in two steps.. As indicated in Fig 1 the effects of scattering indirectly affect the polarization in the sense that the scattering determines the electromagnetic field in the cavity. In the first step only the two oppositely directed traveling waves. as given in Eq(A10) will be used to determine the polarization of the atoms. Then the effects of scattering will be considered to calculate a correction to the polarization.

Consider an ideal two excited level system. Atoms are excited toveither of levels a or b (Energy $\hbar W_a > \hbar W_b$) at some time t_o. The atom can decay spontaneously at rate γ_a, γ_b respectively, or due to the presence of the rediation field, undergo a stimulated transition. For oscillation to occur, it is assumed that a population inversion exists. Expanding the state of the atomic system in terms of the unperturbed set of states of the atom, here taken as only levels a and b, the equation of motion for the expansion coefficients is [3, 12]

$$\dot{\rho} = - i [H, \rho] - \frac{1}{2} (\Gamma \rho + \rho \Gamma) , \tag{29}$$

where

$$\rho = \begin{pmatrix} aa^* & ab^* \\ ba^* & bb^* \end{pmatrix} = \begin{pmatrix} \rho_{aa} & \rho_{ab} \\ \rho_{ba} & \rho_{bb} \end{pmatrix}, \tag{30}$$

$$H = \begin{pmatrix} W_a & V_{ab}(t) \\ V_{ba}(t) & W_b \end{pmatrix} \qquad \Gamma = \begin{pmatrix} \gamma_a & 0 \\ 0 & \gamma_b \end{pmatrix} \tag{31}$$

The matrix element between states a and b of the interaction is given as

$$\hbar V_{ab}(t) = - \mu_{ab} E(z,v,t) \tag{32}$$

where μ_{ab} is the matrix element of the electric dipole moment taken between states a and b and E(z,v,t) is the electric field as seen by the atom. It is this point in which the formalism differs from that as presented by Lamb.[3] Since the atom is described in its own Lorentz frame, the atom always remains at the point where it was excited. Collisions are neglected. Thus ρ is characterized by the following parameters: t_o and z, defined in the moving frame; v, the axial velocity components of the atom with respect to the cavity; α = a, b, the state to which the atom was initially excited at time t_o; t, the time at which we wish to observe the system. Since the atoms are of thermal velocity, simple Galilean transformations are used so that atom time is simultaneous with cavity time and atoms in all frames see the same cavity length. The ρ which described the total ensemble of atoms excited to either state at position a, having velocity component v is written as

$$\rho(a,v,t) = \sum_{\alpha=a,b} \int dz_o \int_{-\infty}^{t} dt_o \, \lambda_\alpha (t_o,z,v) \, \rho(\alpha,t_o,z,v,t) \, \delta(z-z_o) \tag{33}$$

where $\lambda_\alpha(t_o,z,v)$ is the rate per unit volume of exciting atoms having velocity component v, to state α at position z, at time t_o. Equation (33) contains a trivial integration containing a delta function over all the initial excitation points for the velocity ensemble. This occurs because the interaction is treated in the stationary atom frame.

The cavity field as given by Equations (A10-A12 , A21-A23) in Appendix I is seen by an atom at time t and at position z in a moving frame as

$$E(z,v,t) = \Sigma_n \Big[\Big[E_{1n} \cos \big| \omega_{1n}(1 + v/c)t + \varphi_{1n} \big| + E_{2n} \cos \big| \omega_{2n}(1 - v/c)t +$$

$$+ \varphi_{2n}\Big)\Big] U_n(z) + \Big[E_{1n} \sin\Big(\omega_{1n}\,(1 + v/c)t + \varphi_{1n}\Big) \cdots$$

$$- E_{2n} \sin\Big(\omega_{2n}\,(1 - v/c)t + \varphi_{2n}\Big)\Big] V_n(z)\Big] \qquad (34)$$

The coordinate system has been chosen as to arbitrarily cause the velocity ensemble to see the traveling wave E_{1n} and E_{2n} as being doppler shifted up and down, respectively. The K_n in the ECNME are still given by Equation (A13) as $2\pi n/L$.

The contribution to the polarization by the moving atoms at position z is

$$P\,(z,v,t) = \mu_{ba}\rho(z,v,t) + c.c \ldots \qquad (35)$$

The Fourier components of the polarization due to all the atoms in the velocity ensemble located at point z is

$$P_n\,(v,t) = (2/L) \int_o^L P\,(z,v,t)\; U_n(z)\; dz \qquad (36)$$

$$\tilde{P}_n\,(v,t) = (2/L) \int_o^L P\,(z,v,t)\; V_n\,(z)\; dz \qquad (37)$$

The macroscopic Fourier components of the polarization are obtained by transforming $P_n\,(v,t)$ and $\tilde{P}_n\,(v,t)$ back to the cavity frame and averaging over all velocities. In performing the transformation it is first necessary to group $P\,(z,v,t)$ into terms having the form of oppositely directed traveling waves. The terms will be of the form $\exp i\Big[\pm Kz - \omega_{1n}\,(1 \mp v/c)t - \varphi_{1n}\Big]$. Thus to make the inverse Lorentz transformation, it is sufficient to multiply each term by $\exp\Big(\mp i\,\omega_{1n}\,t\,v/c\Big)$ respectively. This will be more clearly shown in what follows.

7. CALCULATION OF POLARIZATION FOR SINGLE MODE

The solution of Equation (29) for $\rho(\alpha,t_o,z,v,t)$ is obtained by treating the interaction between the radiation field and the atomic system as a perturbation and expanding $\rho(\alpha,t_o,z,v,t)$ in orders of the interaction. This has been done by Lamb[3] and will not be repeated here.

For a single mode the interaction is obtained from Equations (32, 34) as

$$V_{ab}(t) = -\frac{\mu_{ab}}{\hbar}\Big[\Big[E_1\cos\left[(\omega_1 + Kv)t + \varphi_1\right] + E_2\cos\Big[(\omega_2 - Kv)t + \varphi_2\Big]\Big] U_n(z) + \Big[E_1\sin\left[\omega_1 + Kv)t + \varphi_1\right] - E_2\sin\left[\omega_2 - Kv)t + \varphi_2\right]\Big] V_n(z)\Big] \tag{38}$$

In Equation (38) the distinction between the ECNME and oscillating wave number has been neglected. The mode subscript on the amplitudes has also been dropped. Calculating the first-order polarization by evaluating the integrals in somewhat the same manner as prescribed by Lamb[3] (details are to be found in Appendix III), the conditions on the amplitudes and frequencies of oscillation of the oppositely directed traveling waves are found as

$$\dot{E}_i + \frac{1}{2}(\omega/Q_i)\,E_i = \frac{1}{2}(\omega/\epsilon_o)\sqrt{\pi}\,A\,E_i \exp -\xi_i^2 \tag{39}$$

$$\omega_i = \Omega_i - (\omega/\epsilon_o)\,A\,F(\xi_i), \quad i = 1,2 \tag{40}$$

where

$$F(\xi_i) = (-\xi_i^2)\int_o^{\xi_i} dx \exp x^2 \tag{41}$$

$$A = |\mu_{ab}|^2\,\bar{N}(t) / (\hbar K u) \tag{42}$$

$$\xi_i = (\omega_i - \omega) / (K u) \tag{43}$$

Scattering effects have not been included here. In writing Equations (39, 40) it has been assumed that the doppler width

$$\Delta\omega = 2(\ln)^{1/2} K u \quad ,$$

is much larger than the natural width. In Equation (42), $\bar{N}(t)$ is the average excitation inversion density.

Equations (39,40) are the standard threshold conditions for independent oscillation. For the case of a SWOM, Equations (39, 40) reduce to those obtained by Lamb[23].

8. POPULATION INVERSION

A second order perturbation expansion gives the average population inversion of a given velocity ensemble as (details are in Appendix IV).

$$\Delta\rho(v,t) = \bar{N}(t)\, W(v) \left[1 - 2I_1 \mathcal{L}(\xi_1 + v/u) - 2I_2 \mathcal{L}(\xi_2 - v/u) \right] \tag{44}$$

where $W(v)$ is the normalized velocity distribution.

The dimensionless intensity of each beam is

$$I_i = \left|\mu_{ab}\right|^2 E_i^2 \,/\, (2\hbar^2 \gamma_a \gamma_b) \tag{45}$$

The Lorentzian function $\mathcal{L}(\xi)$ is defined as

$$\mathcal{L}(\xi) = \left[1 + (\xi/\eta)^2 \right]^{-1} \tag{46}$$

where η is the ratio of the natural to doppler width, or

$$\eta = \gamma_{ab} / Ku = \frac{1}{2} \Delta\omega_n \,/\, (K\, u) \tag{47}$$

Equation (44) shows the saturating effects of the oscillations on the unsaturated population inversion. A plot of average population inversion versus velocity ensemble shows the Gaussian velocity distribution with two Lorentzian holes "burnt" into the curve. This can better be seen by writing Equation (44) in the non-normalized form

$$\Delta\rho(v,t) = \bar{N}(t)\, W(v) \left\{ 1 - 2I_1 \left[1 + \left(\frac{\omega - \omega_1 - Kv}{(1/2)\Delta\omega_n} \right)^2 \right]^{-1} - 2I_2 \left[1 + \left(\frac{\omega - \omega_1 - \Delta\Omega + Kv}{(1/2)\Delta\omega_n} \right)^2 \right]^{-1} \right\} \tag{48}$$

In Equation (48) pulling effects have been neglected and for a first approximation $\Delta\Omega = \omega_2 - \omega_1$. Thus the depth of each hole is determined by the intensity traveling in each direction and the width is equal to the natural width of the atomic transition. For the case when

$$0 < \Delta\Omega << \omega - \omega_1$$

the holes are located on opposite sides of the inversion curve. As the oscillations are tuned through the center of the atomic transition such that $\Delta\Omega = \omega - \omega_1$ one of the holes is found to be symmetrically placed on the inversion curve. As this point is passed it is found that both holes are centered on the same side of the inversion curve. It is in this region that strong mode competition effects are expected, although mode competition effects are present at any point of oscillation. Mode competition is a maximum when the two holes completely overlap, which occurs when $\Delta\Omega = 2(\omega - \omega_1)$. At this point the two oscillation frequencies ω_1 and ω_2 are symmetrically located about the atomic transition frequency ω.

At first sight it is not even obvious that two independent oppositely directed traveling waves can exist at any frequency. This question will be considered after the calculation of the third-order Fourier component of polarization, which will allow calculation of the intensities I_1 and I_2.

It should also be noted that Equation (48) gives the validity condition on the strength of the field such that convergence of the perturbation expansion occurs. Physically it says that the relative depth of the hole burnt into the inversion curve is small, or I_1, $I_2 << 1$.

It should also be noted that Equation (48) is what would be calculated using Lamb's formalism[3] forthe case of a SWOM if $\Delta\Omega = 0$ and

$$(I_1 = I_2)_{TWOM} = \frac{1}{4} I_{SWOM}$$

9. THIRD-ORDER POLARIZATION

The expression for, and the details of the calculation of the third-order Fourier components of the polarization are found in Appendix E. The expression is similar to that as derived by Lamb[3], except for the Lorentzian operator necessary to transform the polarization contribution of a single velocity ensemble from the moving atom frame to the cavity frame.

In the "doppler limit" the self-consistent equations can be approximated as

$$\dot{E}_1 + \frac{1}{2}(\omega/Q_2)\,E_1 = \frac{1}{2}(\omega/\epsilon_o)\,\sqrt{\pi}\,A\,E_1\Big[Z_i(\xi_1)/Z_i(0) - I_1\exp(-\xi_1^2) - I_2\exp(-\xi_2^2)\,\mathcal{L}(\xi)\Big] \tag{49}$$

$$\dot{E}_2 + \frac{1}{2}(\omega/Q_2)\,E_2 = \frac{1}{2}(\omega/\epsilon_o)\,\sqrt{\pi}\,A\,E_2\Big[Z_i(\xi_2)/Z_i(0) - I_2\exp(-\xi_2^2) - I_1\exp(-\xi_1^2)\,\mathcal{L}(\xi)\Big] \tag{50}$$

$$(\omega_1 + \dot{\varphi}_1 - \Omega_1) = \tfrac{1}{2}(\omega/\epsilon_o)\,A\Big[Z_r(\xi_1) + I_2(\xi/\eta)\,\mathcal{L}(\xi)\,Z_i(\xi_2)\Big] \tag{51}$$

$$(\omega_2 + \varphi_2 - \Omega_2) = \tfrac{1}{2}(\omega/\epsilon_o)\,A\Big[Z_r(\xi_2) + I_1(\xi/\eta)\,\mathcal{L}(\xi)\,Z_i(\xi_1)\Big] \tag{52}$$

where Z_r and Z_i are the real and imaginary parts of the "plasma dispersion function"[13], as defined in Appendix C.

For the case of a SWOM, Equations (49-52) reduce to those derived by Lamb, except for the added exponential factor $\exp(-\xi_i^2)$ next to each dimensionless intensity factor I_i. As shown in Appendix E,, the exponential factor arises from the evaluation of the integrals without the delta function approximation. The physical significance in being able to insert or omit the exponential factor arises in the criteria for the validity of the perturbation expansion. The exponential factor becomes significant for large ξ_i, or for operation "away" from the center frequency of the atomic transition. This implies a gain/loss value such that as the oscillation frequency is tuned through the

doppler center, the depth of the hole[14] will be great enough such as to invalidate the perturbation expansion. Hence, the solution is expected to be most valid in the region where the exponential differs little from unity. However, when the effect of multiple isotopes upon the operation of the system is considered it will be essential to keep the exponential factor.

From a study of the form of the interaction which leads to Equation (49-52) it is seen that the dominant contribution to the polarization occurs when the accumulated doppler phase shift cancels. This corresponds to the case of pure inhomogeneous broadening and the third order contribution to Equations (49-52) contain only this dominant part of the interaction. The third order polarization occurs due to the atom undergoing three stimulated interactions with the net radiation field at times $t''' < t'' < t'$. The choice of with which traveling wave the atom interacts, is not arbitrary. From the form of Equations (E6) it is seen that for the dominant contribution to the polarization, the atoms first two interactions are with the same traveling wave, while the third interaction may be with either of the two traveling waves. This order of interaction also applies for the case of SWOM.

For the case of broadening somewhat between pure inhomogeneous and pure homogeneous, contributions to the polarization can occur when the accumulated doppler phase shifts are not zero. Some of these contributions have been evaluated in Appendix E, although they have not been included in the self-consistent Equations (49-52), and have been shown to be of higher order in the parameter (natural width/doppler width).

10. SELF-CONSISTANT EQUATIONS
TWO ISOTOPE CASE

Consider the addition of a second isotope to the system such that the ratio of atoms of each type is f/(1 - f). Let primes signify quantities pertaining to the second isotope. Refer to Figure 6 for a diagramatic definition of the variables. Then the excitation inversion density for each velocity ensemble is

$$N(z,v,t) = f\, N(z,t)\, W(v) + (1 - f)\, N(z,t)\, W'(v) \tag{53}$$

In analogous fashion to the single isotope case, the self-consistency amplitude equations, correct to the third order, are found to be

$$\dot{E}_1 + \tfrac{1}{2}(\omega/Q_1)\, E_1 = \tfrac{1}{2}(\omega/\epsilon_o)\sqrt{\pi}\, A\, E_1 \Big[f \Big[\exp(-\xi_1^2) - I_1 \exp(-\xi_1^2) - I_2 \exp(-\xi_2^2) \mathcal{L}(\xi) \Big] + (m'/m)^{1/2} (1 - f) \Big[\exp(-\xi_1'^2) - I_1 \exp(-\xi_1'^2) - I_2 \exp(\xi_2'^2)\, \mathcal{L}(\xi') \Big] \Big] \tag{54}$$

$$\dot{E}_2 + \tfrac{1}{2}(\omega/Q_2)\, E_2 = \tfrac{1}{2}(\omega/\epsilon_o)\sqrt{\pi}\, A\, E_1 \Big[f \Big[\exp(-\xi_2^2) - I_2 \exp(-\xi_2^2) - I_1 \exp(-\xi_1^2) \mathcal{L}(\xi) \Big] + (m'/m)^{1/2} (1 - f) \Big[\exp(-\xi_2'^2) - I_2 \exp(-\xi_2'^2) - I_1 \exp(-\xi_1'^2) \mathcal{L}(\xi') \Big] \Big] \tag{55}$$

The ratio of the masses of the two isotopes arises from the difference in doppler widths for each isotope. Comparing Equations (54,55) to the amplitude equations for the single isotope, it is seen that the equation could easily be generalized for any number of isotopes. Likewise, the frequency equations can be written by inspection of the equations for the single isotope case as

$$(\omega_1 + \dot{\varphi}_1 - \Omega_1) = \tfrac{1}{2}(\omega/E_o)\, A \Big[f \Big[Z_r(\xi_1) + I_2 (\xi/\eta) \mathcal{L}(\xi)\, Z_i(\xi_2) \Big] + (m'/m)^{1/2} (1 - f) \Big[Z_r(\xi_1') + I_2 (\xi/\eta) \mathcal{L}(\xi')\, Z_i(\xi_2') \Big] \Big] \tag{56}$$

$$(\omega_2 + \dot{\varphi}_2 - \Omega_2) = \frac{1}{2}(\omega/E_o)\, A\Big[f\Big[Z_r(\xi_1) + I_1(\xi/\eta)\mathcal{L}(\xi)\, Z_i(\xi_1)\Big] + (m'/m)^{1/2}(1-f)\Big[Z_r(\xi_2') + I_1(\xi'/\eta)\mathcal{L}(\xi')\, Z_i(\xi_1')\Big]\Big] \tag{57}$$

The average population inversion as a function of velocity ensemble is obtained to second order as

$$\Delta\rho(v,t) = f\,\bar{N}(t)\, W(v)\Big[1 - 2I_1\mathcal{L}(\xi_1 \pm v/u) - 2I_2\mathcal{L}(\xi_2 - v/u)\Big] + (1-f)\,\bar{N}(t)\, W'(v)\Big[1 - 2I_1\mathcal{L}(\xi_1' + v/u) - 2I_2\mathcal{L}(\xi_2' - v/u)\Big] \tag{58}$$

For the single isotope, the population inversion curve versus velocity ensemble and the gain curve versus frequency are quite similar in shape (the hole width in the gain curve is twice, in comparable units, the hole width in the population inversion curve) and it is easy to confuse the meaning of each. For the two isotope case, the curves are radically different. From Equation (58) the population inversion curve is composed of two velocity distribution functions, each located symmetrically about the v = 0 axis. The two holes burnt into each curve are of different depth and are located at different distances from the v = 0 axis. There is no significance to the superposition of the two curves.

The gain curve is obtained from the right-hand sides of Equations (54,55), although strictly speaking the amplitude equations only give the condition that gain equals loss, at the frequency of oscillation. It is the interpretation of the equations that determines gain at a frequency other than the frequency of oscillation. In addition, for a TWOM located on a rotating frame, the gain profile versus frequency in the presence of oscillations at a fixed frequency is different for radiation traveling in different directions. As an illustration, consider the gain profile from the point of view of radiation traveling in the same direction as the radiation oscillating at $\omega_2 < \omega$. See Figure 6a. Then at ω_2 there will be two holes, one in each of the single isotope Gaussian gain profiles. The holes due to the radiation oscillating at ω_1 will burn image holes at $-\xi_1$ and $-\xi_1'$, respectively. From the Lorentzian functions in Equations (54,55), it is seen that the width of the holes burnt into the gain curve is twice the width of the holes burnt into the population inversion curve. In the plot of gain versus frequency of oscillation the superposition of the gain profiles of the individual isotopes gives the resultant gain curve.

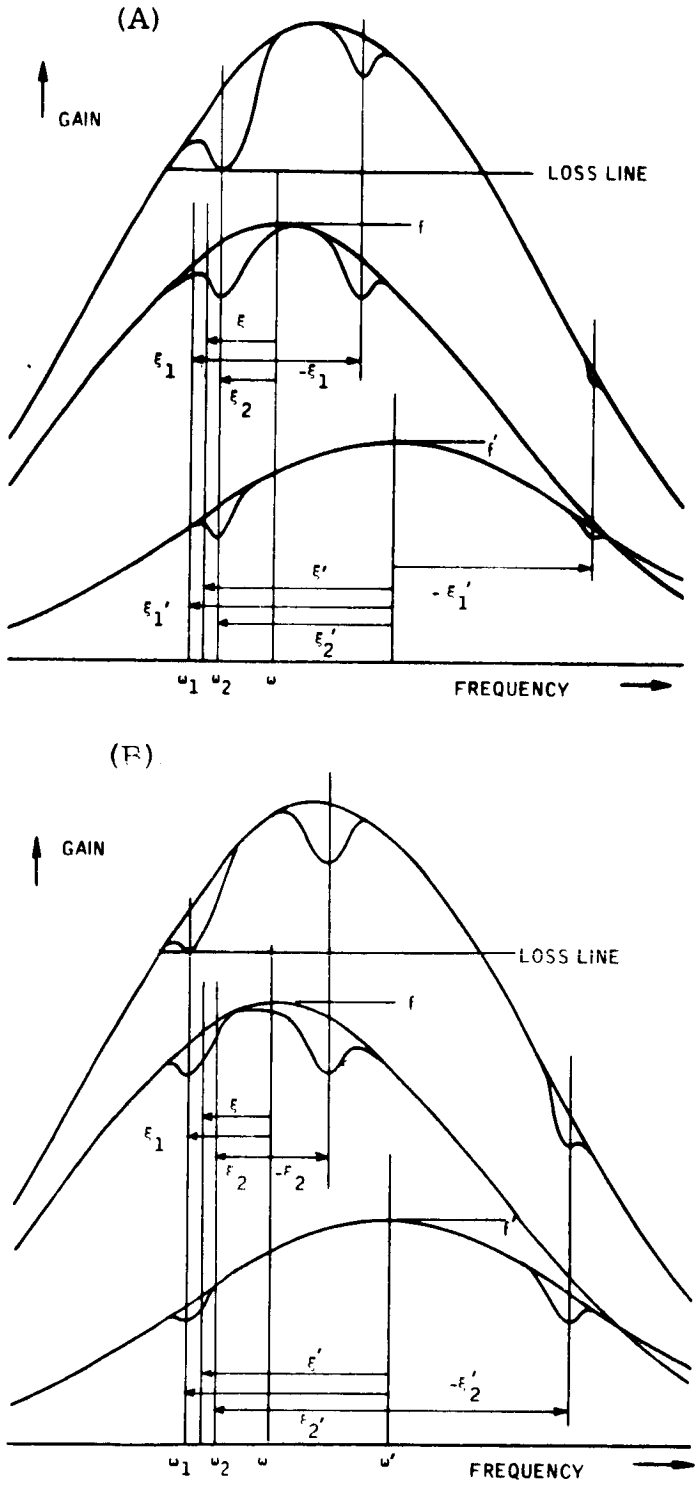

Figure 6 - (A) The gain profile for a test signal traveling in the same direction as the radiation oscillating at ω_2, for two isotopes having relative concentrations of f and f'. The resultant gain curve is a superposition of the single isotope gain curves. (B) The Gain Profile for a test signal traveling in the same direction as the radiation oscillating at ω_1.

Thus in Figure 6a, there will be three holes burnt into the resultant gain curve. At the frequency of oscillation, the gain equals loss condition will be satisfied by the hole being burnt into the resultant gain curve down to the loss line. As the frequency of oscillation is tuned across the atomic transition, the depths of the holes burnt into the single isotope gain profiles will vary as determined by Equations (54,55) such as to always maintain the gain equals loss condition at the frequency of oscillation in the resultant gain profile. If the gain profile is considered from the point of view of radiation traveling in the opposite direction (same direction as radiation oscillating at ω_1) then the hole burnt into the resultant gain curve will satisfy the gain equals loss condition at frequency ω_1. See Figure 6b. The image holes will now correspond to the radiation oscillating at frequency ω_2.

It is interesting to note that the above interpretation of the gain profile as a function of frequency and both the amplitude equations and frequency equations can be obtained using Bennets [14] "hole burning" model. The width of the holes are taken as twice the natural width and the partial depth only due to the radiation which causes the burning of each hole, is given as the dimensionless intensity multiplied by the gain at the point where the hole is burnt. The total hole burnt into each single isotope curve includes the contribution due to the Lorentzian tail of the image hole. It should be noted that, as shown by Appendix E and the discussion in Section 9, Bennets "hole burning" model is valid only in the "doppler limit". When the natural width is comparable with the doppler width, as in the 3.39 micron neon transition, the broadening is neither pure homogeneous nor pure inhomogeneous and to obtain the saturated gain profile it is necessary to carry out the analysis as done in Appendix E.

11. SELF-CONSISTANT EQUATIONS WITH BACKSCATTERING

The self-consistant equations have been found in section 10 to be of the form (taking the single isotope case for the "doppler limit").

$$\dot{E}_1 + \frac{\omega}{2Q_1} E_1 = \frac{\omega}{2\epsilon_o} \sqrt{\pi}\, A\, E_1 \left[\exp(-\xi_1^2) - I_1 \exp(-\xi_1^2) - I_2 \exp(-\xi_2^2)\, \mathcal{L}(\xi) \right] \tag{59}$$

$$\dot{E}_1 + \frac{\omega}{2Q_2} E_2 = \frac{\omega}{2\epsilon_o} \sqrt{\pi}\, A\, E_2 \left[\exp(-\xi_2^2) - I_2 \exp(-\xi_2^2) - I_1 \exp(-\xi_1^2)\, \mathcal{L}(\xi) \right] \tag{60}$$

$$\omega_1 + \dot{\varphi}_1 - \Omega_1 = \frac{\omega}{2\epsilon_o} A \left[Z_r(\xi_1) + \left(\frac{\xi}{\eta}\right) I_2\, Z_i(\xi_2)\, \mathcal{L}(\xi) \right] \tag{61}$$

$$\omega_2 + \dot{\varphi}_2 - \Omega_2 = \frac{\omega}{2\epsilon_o} A \left[Z_r(\xi_2) + \left(\frac{\xi}{\eta}\right) I_1\, Z_i(\xi_1)\, \mathcal{L}(\xi) \right] \tag{62}$$

Referring to Section 4 for the effects of backscatter, it is seen that the effects of forward scattering do not change the form of the above self-consistant equations and need not be written explicitly. The forward scattering amplitude term can be lumped with the loss term while the forward scattering frequency term can be lumped with the passive cavity frequency term.

Before including the backscattering term, it is preferable to express the constants in the self-consistant equations in terms of easily measurable quantities. The Q of the cavity is defined as

$$Q = \frac{2\pi L}{\lambda \gamma}, \tag{63}$$

where λ is the transition wavelength, L the length of the cavity and γ the fractional loss per path. Then

$$\frac{\omega}{2Q} = \frac{c\gamma}{2L} \tag{64}$$

At threshold where the field in the cavity is zero and at line center where $\xi = 0$, Eq. (59) gives ($\dot{E} = 0$ and since A is proportional to population inversion),

$$\frac{\omega}{2Q} = \frac{\omega}{2\epsilon_o}\sqrt{\pi}\, A_t \tag{65}$$

But since A_t is the population inversion where the fraction gain/pass G is equal to the fractional loss/pass γ, then

$$\frac{A}{A_t} = \frac{G}{\gamma} \quad , \tag{66}$$

and

$$\frac{\omega}{2\epsilon_o}\sqrt{\pi}\, A = \frac{\omega}{2\epsilon_o}\sqrt{\pi}\, \frac{A_t G}{\gamma} \tag{67}$$

But from Eqs (64,65), Eq. (67) becomes

$$\frac{\omega}{2\epsilon_o}\sqrt{\pi}\, A = \frac{c}{2L}\, G \tag{68}$$

Now the self-constant equations in the presence of scattering become

$$\frac{2L}{c}\,\frac{\dot{E}_1}{E_1} = \alpha_1 - \beta_1 I_1 - \theta_{12} I_2 - 2\rho_2 \cos(\psi + \epsilon_2) \quad , \tag{69}$$

$$\frac{2L}{c}\,\frac{\dot{E}_2}{E_2} = \alpha_2 - \beta_2 I_2 - \theta_{21} I_1 - 2\rho_1 \cos(\psi - \epsilon_1) \quad , \tag{70}$$

$$\omega_1 + \dot{\varphi}_1 - \Omega_1' = \sigma_1 + \tau_{12} I_2 - \frac{c}{L}\rho_2 \sin(\psi + \epsilon_2) \quad , \tag{71}$$

$$\omega_2 + \dot{\varphi}_2 - \Omega_2' = \sigma_2 + \tau_{21} I_1 - \frac{c}{L}\rho_1 \sin(\epsilon_1 - \psi) \quad , \tag{72}$$

where

$$\alpha_1 = G \exp(-\xi_1^2) - \gamma_1 - 2s_1 \cos\delta_1 \tag{73}$$

$$\beta_1 = G \exp(-\xi_1^2) \tag{74}$$

$$\theta_{12} = \exp(-\xi_2^2)\, \mathcal{L}(\xi) \tag{75}$$

$$\rho_2 = r_2 E_2/E_1 \tag{76}$$

$$\Omega_1' = \Omega_1 - \frac{c}{L} s_1 \sin \delta_1 \tag{77}$$

$$\sigma_1 = \frac{c\ G}{2L} Z_r\ (\xi_1)/\pi^{\frac{1}{2}} \tag{78}$$

$$\tau_{12} = \frac{c\ G}{2L} \left(\frac{\xi}{\eta}\right) Z_i\ (\xi_1)\ \mathcal{L}(\xi)\ /\pi^{\frac{1}{2}} \tag{79}$$

$$\xi_1 = (\omega_1 - \omega)/Ku \tag{80}$$

$$Ku = \Delta\omega_{dop}/2(\ln 2)^{1/2} \tag{81}$$

$$\xi = \frac{1}{2} (\xi_1 + \xi_2) \tag{82}$$

$$\eta = \gamma_{ab}/Ku = \left[\Delta\omega\ (\text{natural}) + \Delta\omega\ (\text{collision}) \right] /2Ku \tag{83}$$

$$Z_i\ (\xi) = \sqrt{\pi}\ \exp\ (-\xi)^2 - 2\eta \left[1 - 2\xi\ F\ (\xi)\right] + O\ (\eta^2) \quad \eta \ll 1 \tag{84}$$

$$Z_r\ (\xi) = -2\ F\ (\xi) + 2\sqrt{\pi}\ \eta\ \exp\ (-\xi^2) + O(\eta^2) \tag{85}$$

$$F\ (\xi) = \exp\ (-\xi^2) \int_0^{\xi} \exp\ (x^2)\ dx \cong \xi \left[1 - \frac{2}{3} \xi^2 + \right.$$

$$\left. + O(\xi^4) \right] \quad \xi < 1 \tag{86}$$

The definitions of α_2, β_2 etc. are analogous.

12. BACKSCATTER CORECTION TO POLARIZATION

Figure (1) shows a block diagram of the self-conistant treatment. There it is seen that an assumed elechromagnetic field in the cavity produces the scattering source terms and polarizes the atoms. The microscopic polarization and the scattering terms are then treated as source terms in Maxwell's equations to calculate an electromagnetic field. This calculated field must equal the original assumed field for self-conisitancy.

In calculating the polarization in section 6 only two oppositely directed traveling waves were taken as the assumed field. Now a correction to the polarization will be calculated by assuming that steady state backscattering fields also exist in the cavity. The form of the backscattered fields are similar to those used for the source terms in Maxwell's equations. They are represented in Fig (2). Using this correction field, a calculation of the first order polarization is carried out in Appendix F.

The results show the first order self-consistant equations (59-62) to be modified to read

$$\dot{E}_1 + \frac{\omega}{2Q_1} E_1 = \frac{\omega A}{2\epsilon_o}\Big[E_1 z_i(\xi_1) + r_2 E_2 \Big[z_i(\xi_2)\cos(\psi+\epsilon_2) - z_r(\xi_2)\sin(\psi+\epsilon_2)\Big]\Big] \tag{87}$$

$$\dot{E}_2 + \frac{\omega}{2Q_2} E_2 = \frac{\omega A}{2\epsilon_o}\Big[E_2 z_i(\xi_2) + r_1 E_1\Big[z_i(\xi_1)\cos(\psi-\epsilon_1) + z_r(\xi_2)\sin(\psi-\epsilon_1)\Big]\Big] \tag{88}$$

$$(\omega_1 + \dot{\varphi}_1 - \Omega_1) E_1 = \frac{\omega A}{2\epsilon_o}\Big[E_1 z_r(\xi_1) + r_2 E_2\Big[z_r(\xi_2)\cos(\psi+\epsilon_2) + z_i(\xi_2)\sin(\psi+\epsilon_2)\Big]\Big] \tag{89}$$

$$(\omega_2 + \dot{\varphi}_2 - \Omega_2) E_2 = \frac{\omega A}{2\epsilon_o}\Big[E_2 z_r(\xi_2) + r_1 E_1\Big[z_r(\xi_1)\cos(\psi-\epsilon_1) - z_i(\xi_1)\sin(\psi-\epsilon_1)\Big]\Big] \tag{90}$$

The modified self-consistant equations (87-90) show additional terms linear in the backscattering coefficients r_1, r_2. These terms are multiplied by factors of cos ψ and sin ψ and are of the form of mode coupling terms in the amplitude equations and frequency pulling terms which lead to lock-in in the frequency equations. When the backscattering effects obtained by considering scattering as a source term in Maxwell's equations are also considered, the self-consistant equations become [combining Eqs. (87-90) with Eqs. (69-72)] equivalent to Eqs. (69-72) with the following changes:

$$\rho_2 \rightarrow \rho_2 \left[1 - \frac{G}{\sqrt{\pi}} \, z_i \, (\xi_2) + \frac{G^2}{4\pi} \left[z_i^{\,2} \, (\xi_2) + z_r^{\,2} \, (\xi_2) \right] \right]^{1/2} \tag{91}$$

$$\epsilon_2 \rightarrow \epsilon_2 - \tan^{-1} \frac{\frac{G}{2} \, z_i(\xi_2)}{\sqrt{\pi} - \frac{G}{2} z_i(\xi_2)} \tag{92}$$

There are analogous equations for the change in ρ_1 and ϵ_1.

For small values of gain ie G $\sim$ .1, Eqs (91,92) can be approximated as

$$\rho_2 \rightarrow \rho_2 \left(1 - \frac{G}{2} e^{-\xi^2}\right), \tag{93}$$

$$\epsilon_2 \rightarrow \epsilon_2 - \frac{G}{2} e^{-\xi^2} \tag{94}$$

13. GAIN DEPENDENCE OF LOCK-IN

From Eq. (26) the expression for the lock-in frequency is given by

$$\Delta\Omega_{lock} = \frac{c}{L}\left[\rho_1^2 + \rho_2^2 + 2\rho_1\rho_2 \cos(\epsilon_1 + \epsilon_2)\right]^{1/2} \tag{26}$$

Making the gain correction, as given by Eqs. (93,94), Eq. 26 becomes

$$\Delta\Omega_{lock} = \frac{c}{L}\left[\rho_1^2 + \rho_2^2 + 2\rho_1\rho_2 \cos(\epsilon_1 + \epsilon_2 - G_e^{-\xi^2})\right]^{1/2}\left(1 - \frac{G}{2}e^{-\xi^2}\right) \tag{95}$$

Thus the gain dependent part of the lock-in threshold should be an even function of tuning the frequency of oscillation across the doppler gain curve, with a minimum at the doppler center.

Equation (95) holds in the limit of small gain.

14. ANALYSIS OF MODE COMPETITION EQUATIONS

The Eqs. (69,70), determining the intensities of the oppostiely directed traveling waves are two simultaneous non-linear coupled first order differential equations in thettwo unknowns I_1, I_2. The intensity I is related to the electric field intensity E by

$$I = (\text{const})\ E^2$$

Defining a normalized electric field intensity so that

$$I = E^2 \tag{96}$$

the mode competition equations for steady state oscillation can be written in the form

$$\alpha_1 E_1 - \beta_1 E_1^3 - \theta_{12}\ E_1 E_1^2 - R_2 E_2 = 0 \quad , \tag{97}$$

$$\alpha_2 E_2 - \beta_2 E_2^3 - \theta_{21}\ E_2 E_1^2 - R_1 E_1 = 0 \quad , \tag{98}$$

where the coefficients are, for a single isotope and no assymetry

$$\alpha_1 = (G/\gamma_1)\ \exp\ (-\xi_1^2) - 1 \tag{99}$$

$$\beta_1 = (G/\gamma_1)\ \exp\ (-\xi_1^2) \tag{100}$$

$$\theta_{12} = (G/\gamma_1)\ \exp\ (-\xi_2^2)\ \mathcal{L}(\xi) \tag{101}$$

$$R_2 = (2r_2/\gamma_1)\ \cos\ (\psi + \epsilon_2) \tag{102}$$

Similar equations exist for the other coefficients.

In analyizing Eqs. (97, 98), R will be assumed to be consistant (independent of θ). The justification for this assumption will be discussed after a discussion of the experimental results. Eq. (97, 98) are a pair of coupled cubic equations. Thus nine sets of solutions for E_1, E_2 exist. One is the null solution and since the equations are odd in E, for each set of solutions (E_1, E_2), $(-E_1, -E_2)$ is also a solution. Thus only four sets of solutions

need be found.

The technique to be used is to write

$$E_1 = x\, E_2 \,, \tag{103}$$

substitute Eqs. (103) into both equations (97,98) and solve each for E_2 to obtain

$$E_2^2 = \frac{\alpha_1 x - R_2}{\beta_1 x^3 + \theta_{12} x} = \frac{\alpha_2 - R_1 x}{\beta_2 + \theta_{21} x^2} \tag{104}$$

Equation (104) gives a quartic equation for the unknown quantity x, which can be written as

$$R_1\beta_1 x^4 + (\theta_{21}\alpha_1 - \alpha_2\beta_1)x^3 + (R_1\theta_{12} - R_2\theta_{21})x^2 + (\beta_2\alpha_1 - \theta_{12}\alpha_2)x - \beta_2 R_2 = 0 \tag{105}$$

As the frequency of oscillation is tuned the parameters will vary, as given by Eqs. (99 - 102). Thus the mode competition equations should be numerically solved by solving the quartic equation (105), for each value of frequency, on a high speed computor. This was done on the Honeywell 1800 and typical results for intensities I_1, I_2 (when $R_1 = 2R_2$), are shown in Figs (7, 8). It should be emphasized that the only collision effect that has been considered here has been a widening of the hole width.[15] Pressure effects in general will be considered after a discussion of the experimental data.

Figs. (7, 8) show the intensities I_1, I_2, respectively. In both figures, curve "a" shows the intensity in the absence of back scattering effects. The power tuning curves show the characteristic Lamb dip around the (doppler) center frequency. Curves b-e correspond to the four possible solutions. It should be noted that the intensities are complementary for the oppositely directed traveling waves. Solution "b" corresponds to the case when I_1 is extinguished over most of the doppler curve. At the center the beam turns on over a range of a few MHz. The complementary solution for I_2 shows a value of I_2 with no competition effects due to the presence of I_1 over most of the

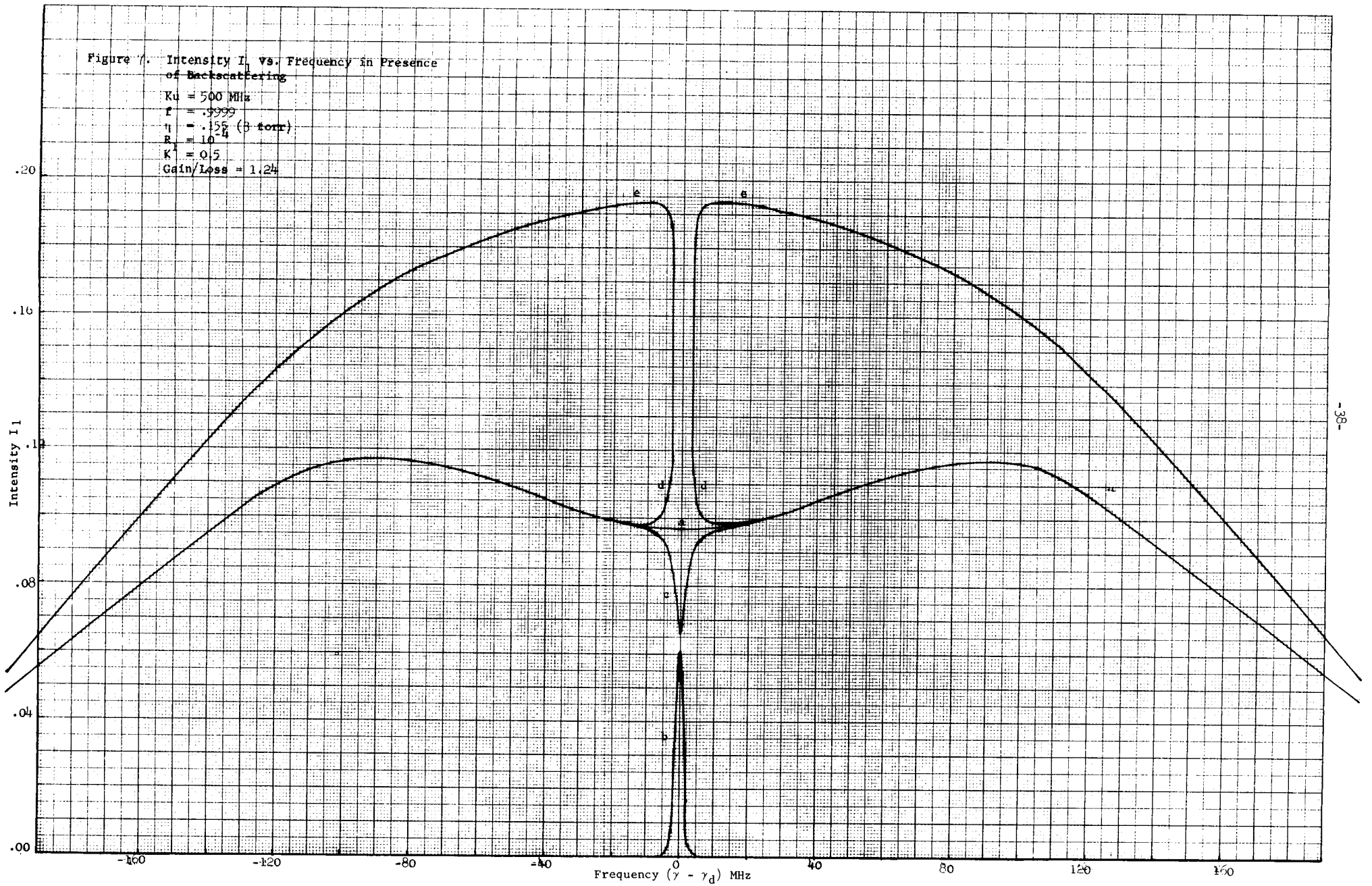
Figure 7. Intensity I_1 vs. Frequency in Presence of Backscattering
Ku = 500 MHz
f = .9999
η = .155 (8 torr)
$R_1 = 10^{-4}$
K = 0.5
Gain/Loss = 1.24
Intensity I_1
.20
.16
.12
.08
.04
.00
-160
-120
-80
-40
0
40
80
120
160
Frequency ($\gamma - \gamma_d$) MHz
a
b
c
d
e
g

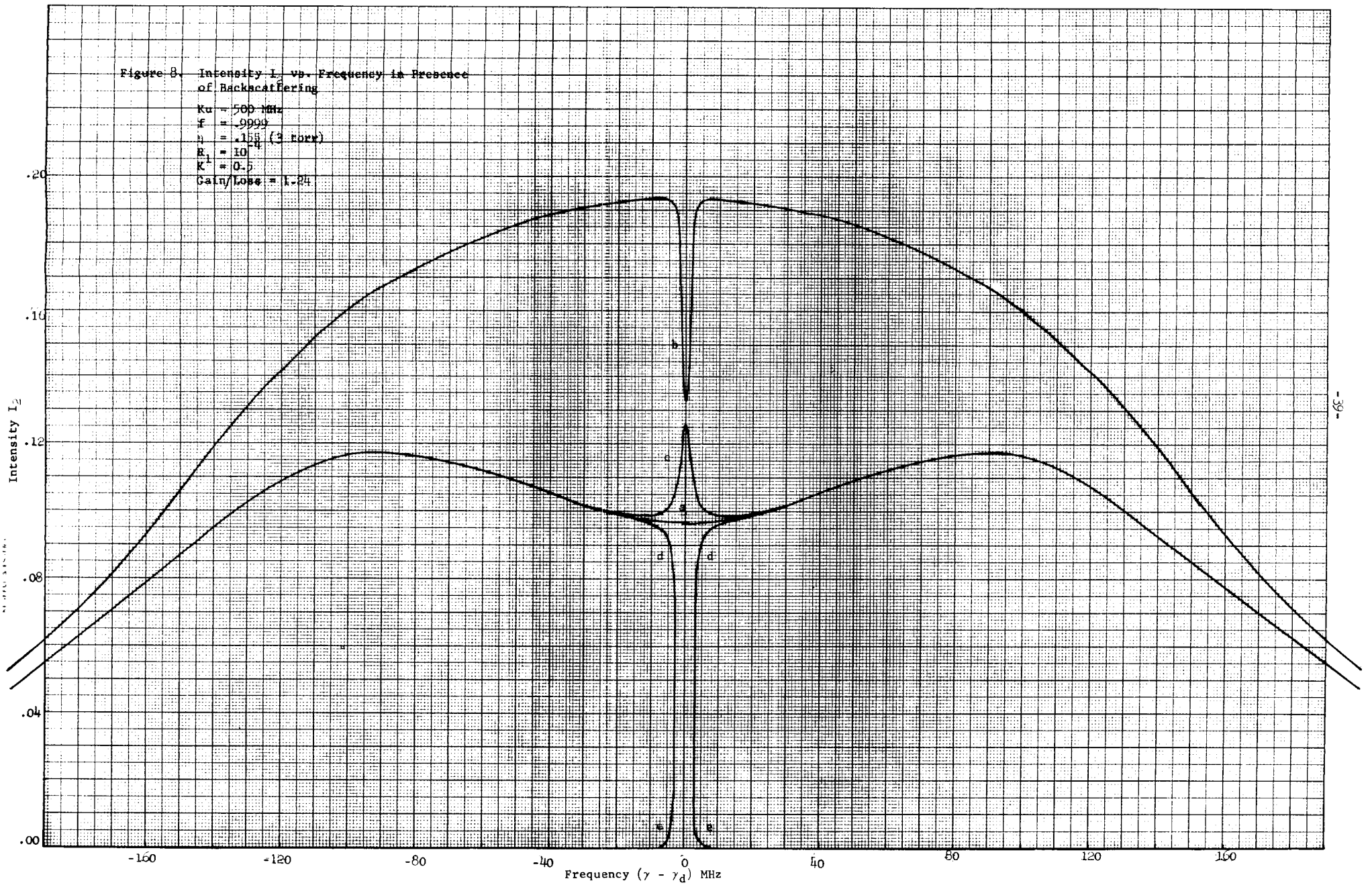
Figure 8. Intensity I_2 vs. Frequency in Presence of Backscattering
Ku = 500 MHz
f = .9999
p = .155 (3 torr)
$R_1 = 10^{-4}$
$K_1 = 0.5$
Gain/Lose = 1.24
Intensity I_2
.20
.10
.12
.08
.04
.00
-160
-120
-80
-40
0
40
80
120
160
Frequency ($\gamma - \gamma_d$) MHz
a
b
c
d
d
e
e

doppler curve. At the center a sharp downward spike occurs, due to the presence of beam I_1.

Curves "c" and "d" show the existance of solutions for I_1 and I_2 which differ only slightly from the non-backscatter solution over most of the doppler curve. At the doppler center, curve "c" shows a competition dip which occurs in the opposite direction to that found in solution "a". At the doppler center no solution exists corresponding to curve "d". The roots of the quartic equation are complex in this region.

Curve "e" corresponds to the solution for which beam I_1 takes over completly and beam I_2 is essentially extinguished. This solution corresponds to the second of the complex roots of the quartic equation. Thus it is possible for either beam to be extinguished.

Whether or not the solutions are all stable is another question that must be answered. A Poincoire analysis was carried out for the case shown in figs (7, 8). The results showed that all the solutions are stable. It should be emphasized at this point that the case being considered is ideal in that collision effects and differential losses have not been considered.

To set a better understanding of the solutions of the mode competition equations, a qualitative description of the quartic equation will be made. For symplicity, equal losses for both directions will be assumed and the beams will be assumed to be frequency locked. Then Eq. (105) reduces to

$$R_1 x^4 - \alpha(1 - \mathcal{L})\, x^3 + \mathcal{L}(R_1 - R_2)\, x^2 + \alpha(1 - \mathcal{L})\, x - R_2 = 0 \qquad (106)$$

For the non-backscattering case, $R_1 = R_2 = 0$ and Eq. (106) gives $x = 0, \pm 1$.

From Eq. (104), the solution corresponding to $x = 0$ is

$$I_1 = 0,\ I_2 = \frac{\alpha}{\beta} = 1 - \frac{\gamma}{G} \exp \xi^2 \qquad (107)$$

This corresponds to solution "b" without the backscatter spike in figs (7,8)

The solution corresponding to $X = \pm 1$ is

$$I_1 = I_2 = [1 - (\frac{\chi}{G}) \exp \xi^2] [1 + \mathcal{L}(\xi)]^{-1} \qquad (108)$$

This corresponds to solution "a" in figs (7, 8). A value of $G/\gamma = 1.24$, $\frac{Ku}{2\pi} = 500$ MHz, $\eta = .155$ was chosen, where

$$\xi = \frac{2\pi (\nu - \nu_d)}{Ku} , \qquad (109)$$

$$\mathcal{L}(\xi) = [1 + \xi^2/\eta^2]^{-1} . \qquad (110)$$

To consider the effects of backscatter, let

$$R_2 = K R_1 , \quad K < 1 \qquad (111)$$

Note that the results for the case of $R_2 > R_1$ can be obtained from the $R_2 < R_1$ case by interchanging the subscripts "one" and "two" and letting $K \rightarrow 1/K$. In Figs (7, 8), $K = 0.5$.

Using Eq. (111), Eq. (106) becomes with $R_1 \rightarrow R$

$$x^4 - \frac{\alpha}{R} (1 - \mathcal{L}) x^3 + \mathcal{L}(1 - K)x^2 + \frac{\alpha}{R} (1 - \mathcal{L})x - K = 0 \qquad (112)$$

Consider the solution of Eq (112) at the doppler center. From Eqs (109, 110), the doppler center corresponds to $\xi = 0$ and $\mathcal{L} = 1$. Eq (111) becomes

$$x^4 + (1 - K) x^2 - K = 0$$

or (113)

$$X = \pm\sqrt{K}, \pm i$$

Thus at the doppler center two of the solutions are complex. This corresponds to solutions "d" and "e". Solutions "b" and "c" are equal and the intensities are related, as seen from Eq. (103), by

$$I_1 = K I_2 \qquad (114)$$

Note that Eq. (114) is only approximately satifified in figs (7, 8) since the curves were not calculated for a single isotope. The isotopic impurity was taken to be 10^{-4}, but this impurity is sufficient to restore the odd terms in x in Eq (112).

Using DeMoivre's theorem to determine the sign of the roots of Eq. (112), it is found that there are, at most, three positive roots and at most one negative root. Euqation (114) shows that there exists a negative root and that the root corresponds to either curve "b" or "c". Equation (114) also shows that as the scattering becomes highly assymetric (K→0) the spike amplitude in solution "b" drops to zero and the dip amplitude in solution "c" increases. In both cases intensity I_1 drops to zero. The solutions for I_2 are again complementary. Thus the relative strengths of the competition spikes are independent of the absolute scattering into each direction. Again it should be emphasized that this relation holds only in the limit of a single isotope.

Again consider the case of assymetric scattering, or K = 0. Equation (112) then becomes

$$x\left[x^3 - \frac{\alpha}{R}(1-\mathcal{L})x^2 + \mathcal{L}x + \frac{\alpha}{R}(1-\mathcal{L})\right] = 0 \qquad (115)$$

The x = 0 root corresponds to

$$I_1 = 0$$

and from Eq (107)

$$I_2 = 1 - \frac{\gamma}{G}\exp \xi^2.$$

At the doppler center, the cubic equation (115) has two complex roots and another root of x=0. This x=0 root corresponds to the minimum intensity I_1 of curve "c" being zero. For frequencies slightly off the doppler center, $x \sim 0$ and $1 - \mathcal{L} + \frac{\xi^2}{\eta^2} \sim 0$. Thus an approximate root of Eq (115) corresponding to this case is obtained as

$$x = -\frac{\alpha}{R}\,\frac{(1-\mathcal{L})}{\mathcal{L}}$$

or

$$x = -\frac{(G-\alpha)\,\xi^2}{\gamma R \eta^2} \qquad (116)$$

Thus curve "c" corresponds to the negative root.

15. COMPUTOR SOLUTIONS OF MODE COMPETITION EQUATIONS

Figures (7,8) show the four possible solutions for the intensities I_1, I_2, respectively. The parameters used were those for the neon-20 transition (99.99 percent isotopic purity). The doppler width was taken as 800MHz (Ku = 500 MHz corresponding to a temperature of 413°K. The gain/loss ratio was taken to be 1.24 for both beams. The pressure used was 3 torr giving a value of $\eta = 0.158$. The backscattering parameters were chosen as $R_1 = 10^{-4}$, $K = 0.5$.

In Figs (7,8) and in those that follow, the only effect of collisions that is considered is the broadening[15] of the hole. Assymetry due to phase shift effects and the reduction in the hole depth due to velocity shift effects[15] have not been considered. These effects will be considered in a later section.

Figure (10) shows the effect of varying the pressure and hence the hole width. Only intensity I_1 is shown and only (half) the center region is shown. The intensity curves are even functions about the doppler center and the curves for I_2 are complementary to those shown for I_1. It is seen that as the pressure increases from 1-7 torr, the half range over which two of the solutions are imaginary increases from approximately 1-5.5 MHz. In addition it is seen that both the width of the dip and the center spike increases. However the depth of both the spike and the dip remains constant. These results have been summarized in Fig (11) which shows the values of the various widths as a function of pressure with the equivalent value of η. It is seen that the widths are approximately a linear function of pressure.

Figs (12, 13) show the values of the intensity I_1 at the doppler center for values of $R_1 = 10^{-5}$, 10^{-6} respectively. Pressure is included as a parameter. The results show that for decreasing values of scattering, the competition widths decrease, roughly as the square root of the scattering.

Figures (14, 15) show the intensity I_1 for varying values of K (the ratio of the backscattering coefficients) for values of $R = 10^{-4}$, 10^{-3}, respectively.

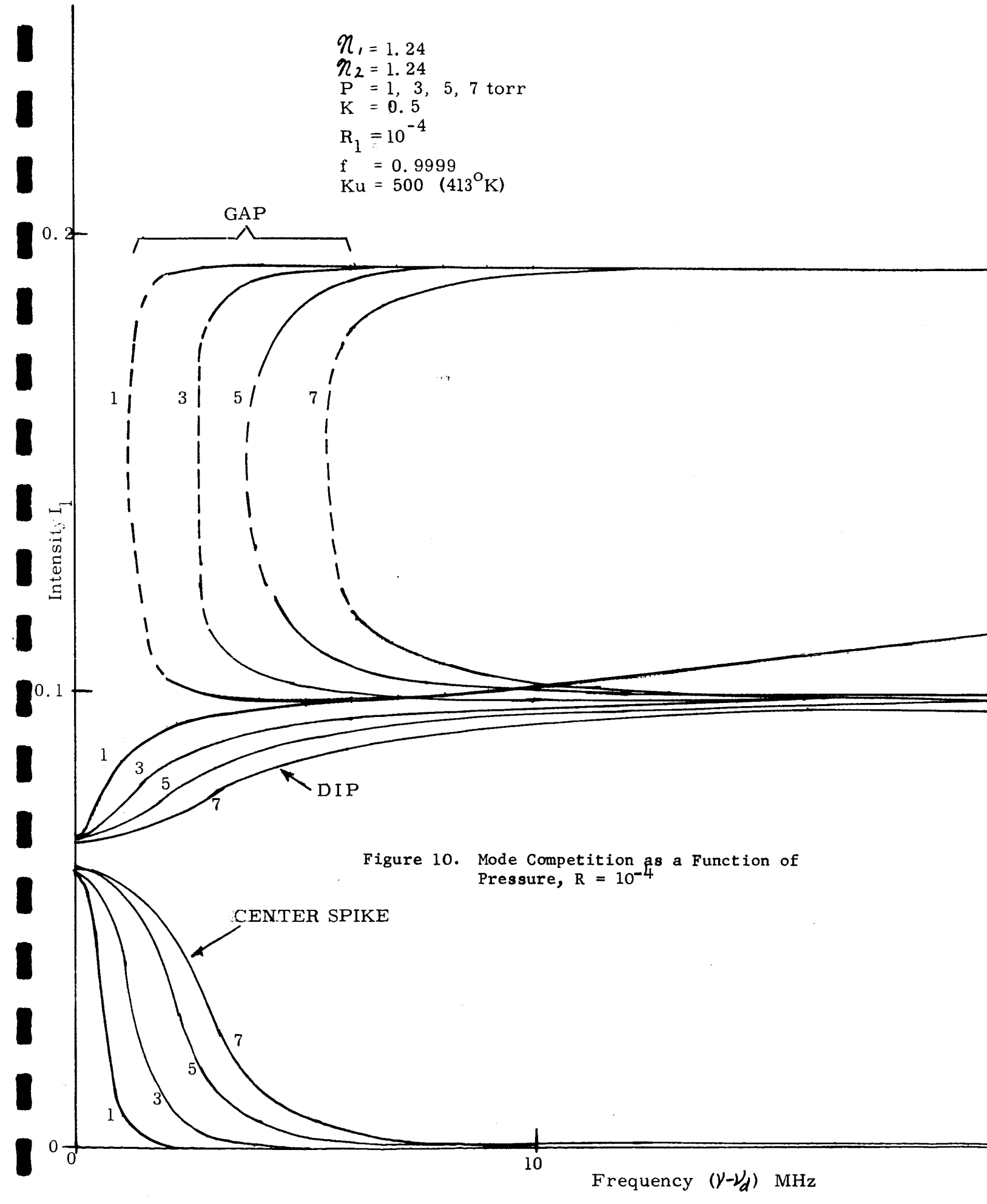

Figure 10. Mode Competition as a Function of Pressure, R = 10^{-4}

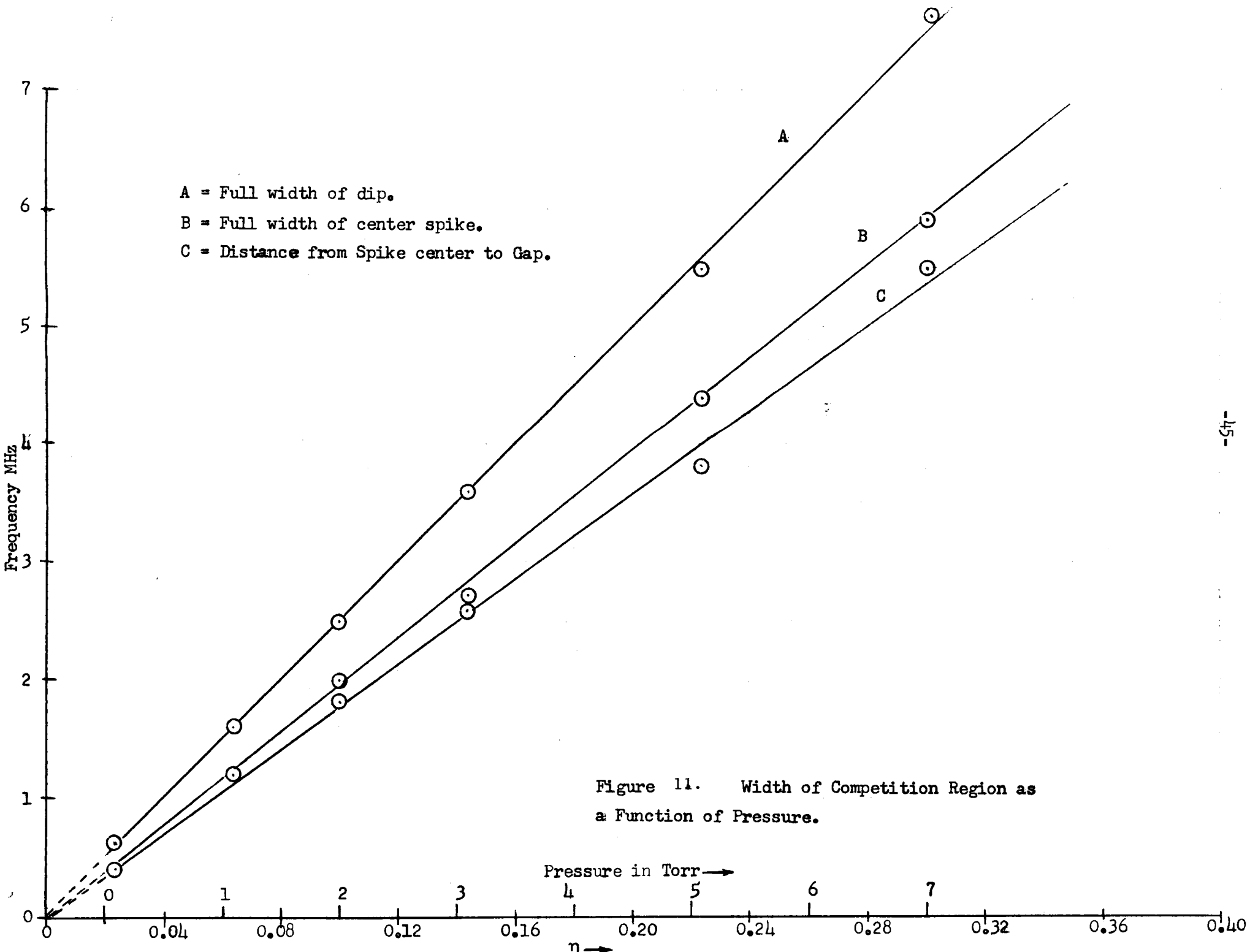

Figure 11. Width of Competition Region as a Function of Pressure.

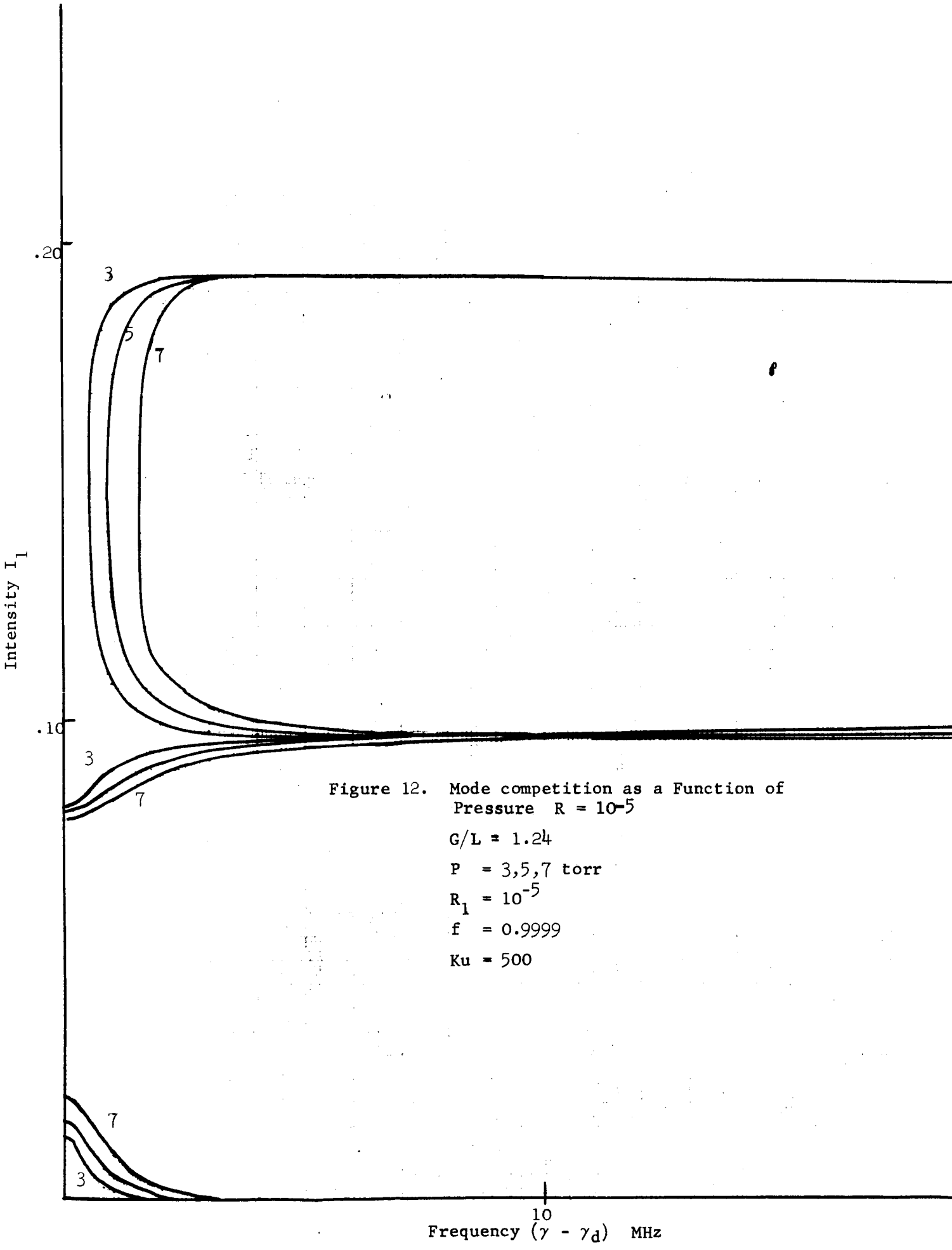

Figure 12. Mode competition as a Function of Pressure R = 10^{-5}

G/L = 1.24

P = 3,5,7 torr

R_1 = 10^{-5}

f = 0.9999

Ku = 500

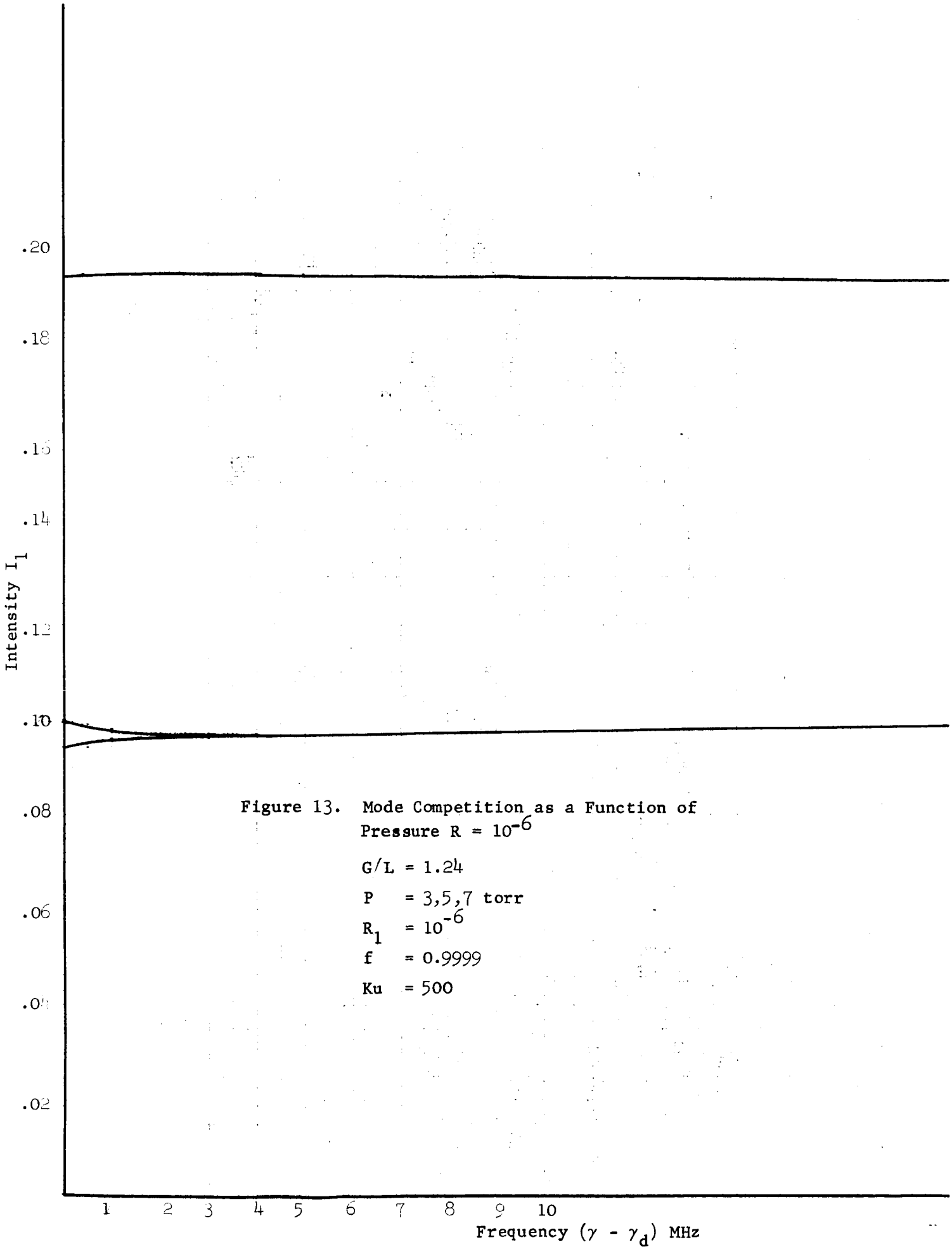

Figure 13. Mode Competition as a Function of Pressure R = 10^{-6}

G/L = 1.24

P = 3,5,7 torr

R_1 = 10^{-6}

f = 0.9999

Ku = 500

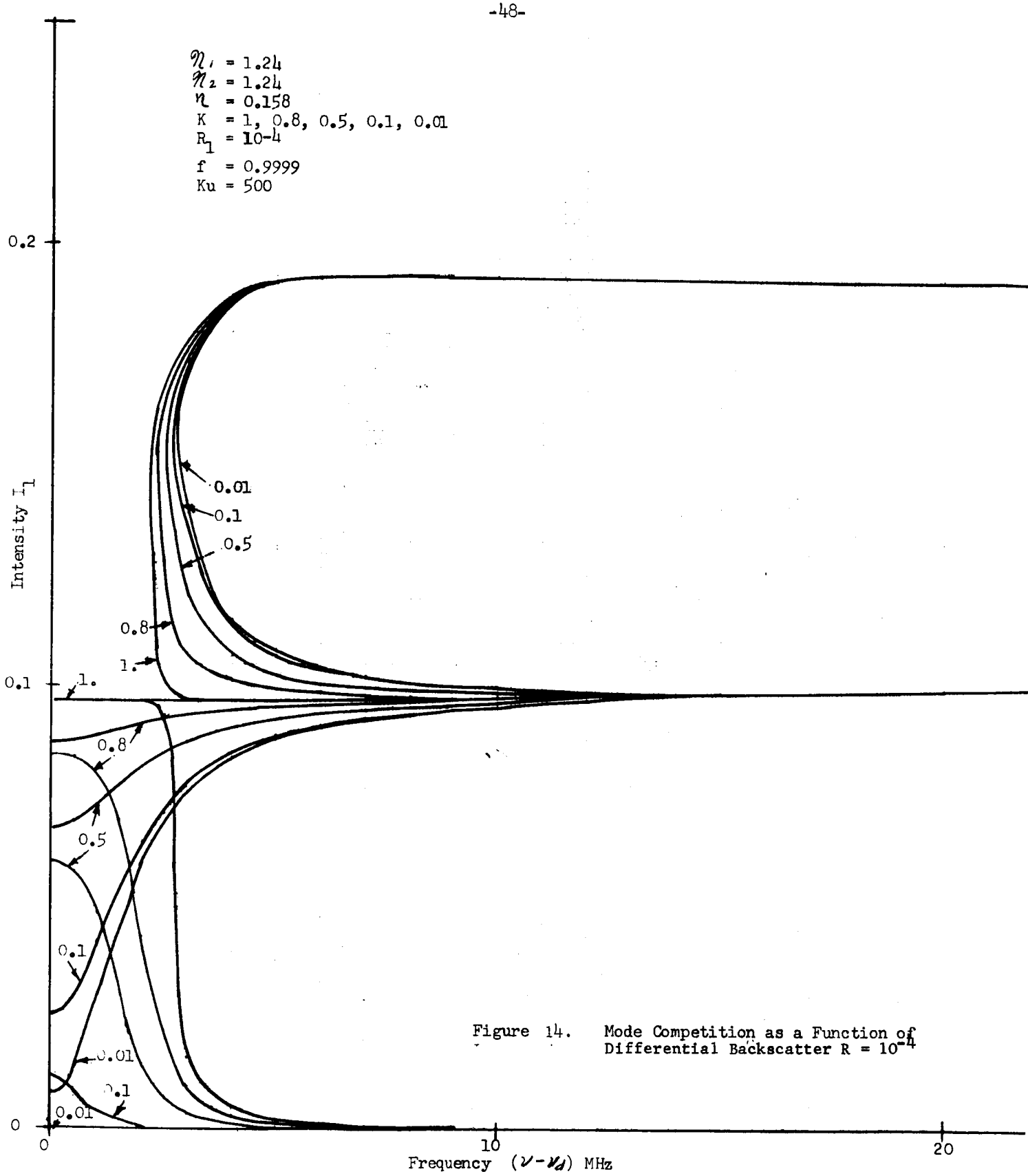

Figure 14. Mode Competition as a Function of Differential Backscatter R = 10^{-4}

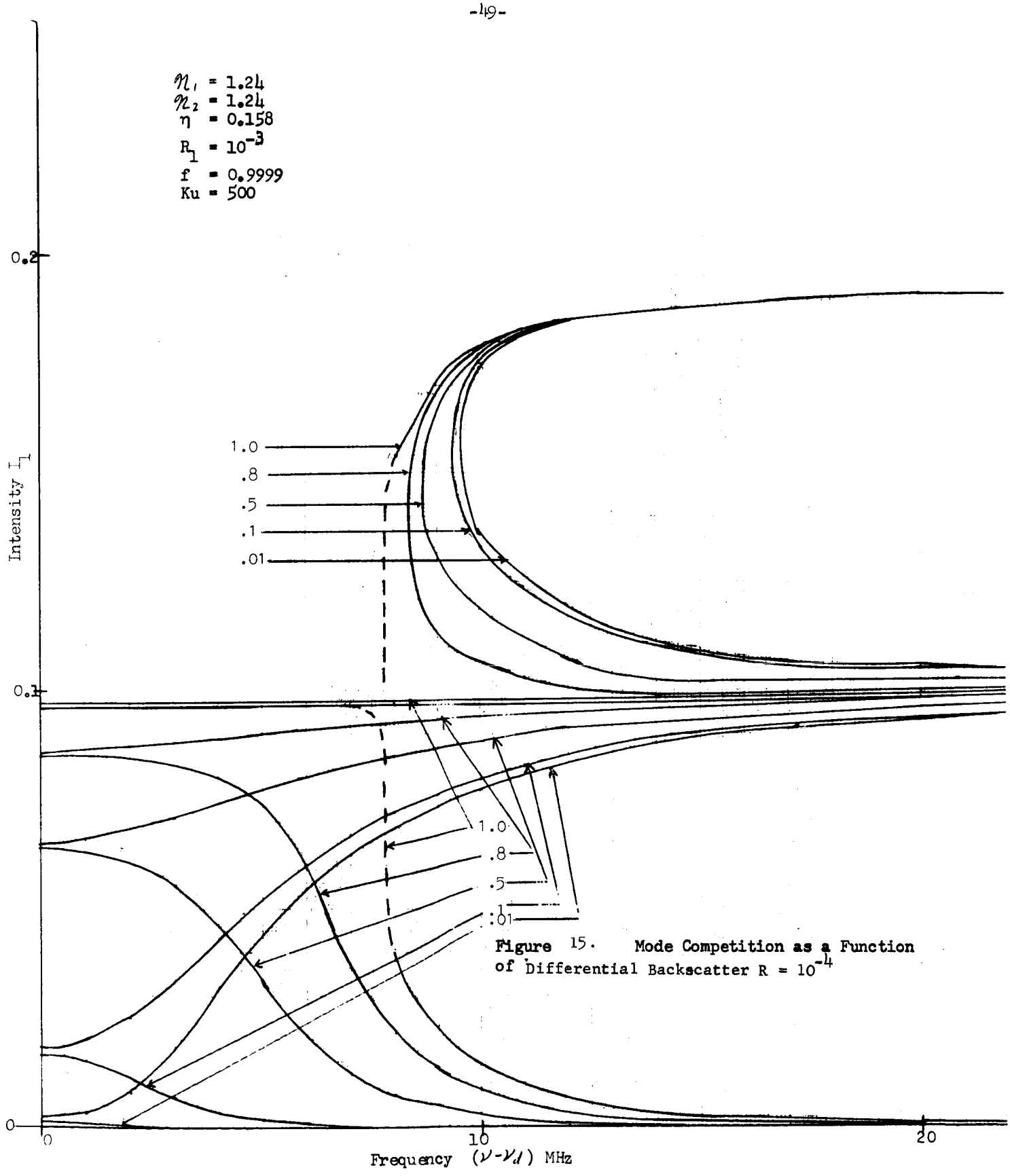

Figure 15. Mode Competition as a Function of Differential Backscatter R = 10^{-4}

The hole width chosen corresponds to a pressure of 3 torr. The results show agreement with $R^{1/2}$ width dependence rule, and show that the rule $I_1 = KI_2$, $K < 1$, at the doppler center is more nearly satisfied for larger values of R.

In all the curves shown, the gain/loss ratio has been made equal for both beams. Figures (16, 17) show the zero backscatter solutions for the intensities I_1, I_2, respectively, for zero pressure and a differential gain/loss ratio. It is seen that for increasing values of the differential gain/loss, the frequency range over which mode competition occurs, increases. For large values of differential gain/loss ($\sim 10^{-4}$), the beam discriminated against (I_1) is shown to be extinguished.[17] Figures (18-21) show intensity I_1 for both backscatter ($R_1 = 10^{-4}$) and differential gain/loss ($\pm 10^{-4}$, $\pm 10^{-5}$). The pressure is 3 torr and the scattering ratio K is a parameter. It is seen that for the value of the backscattering chosen the backscattering competition dominates. Also the dip acts in the same manner as the zero-backscatter solution in the sense that as the losses favor beam I_2, the intensity I_1 dips towards zero. However, the spike acts in the opposite sense in that it increases. The effect is more pronounced for greater differential gain/loss.

$\eta_1 = 1.24$
$\eta_2 = 1.24 + 10^{-n}$, n = 3, 4, 5, 6, ∞
P = 0
f = 0.9999

Figure 16. Intensity I_1 vs Frequency With Differential Gain/Loss as a Parameter. (Pressure = 0)

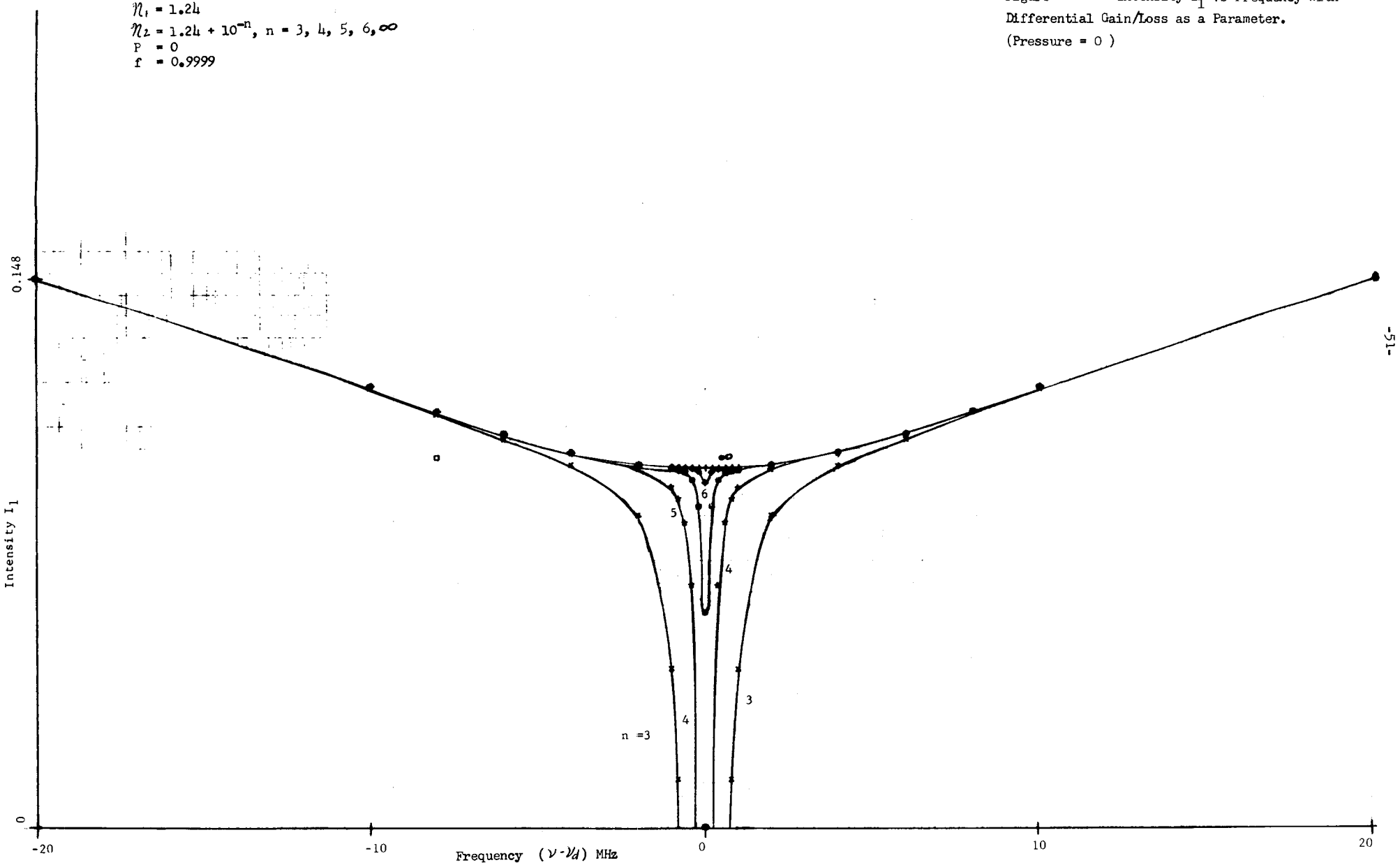

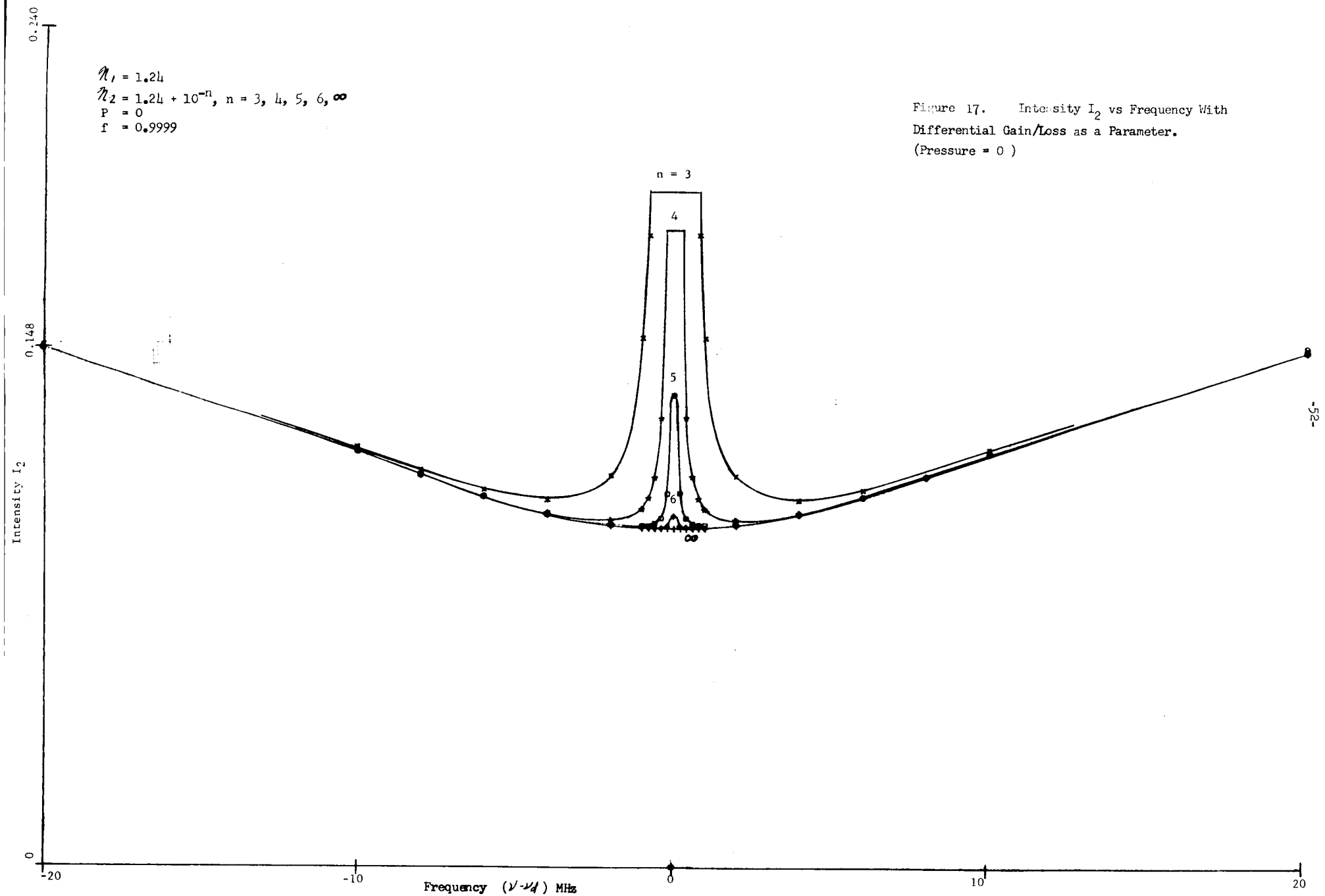

Figure 17. Intensity I_2 vs Frequency With Differential Gain/Loss as a Parameter. (Pressure = 0)

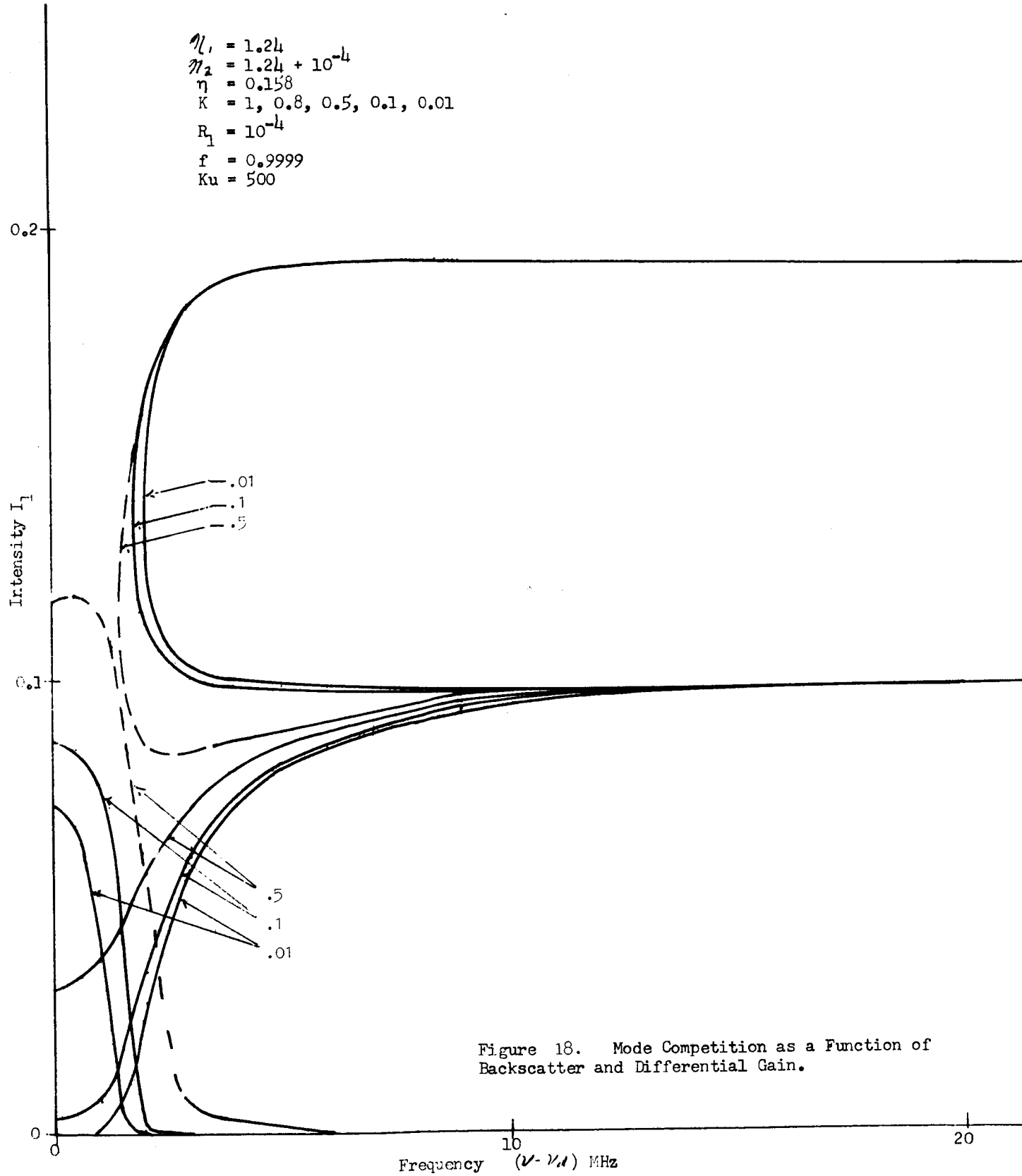

Figure 18. Mode Competition as a Function of Backscatter and Differential Gain.

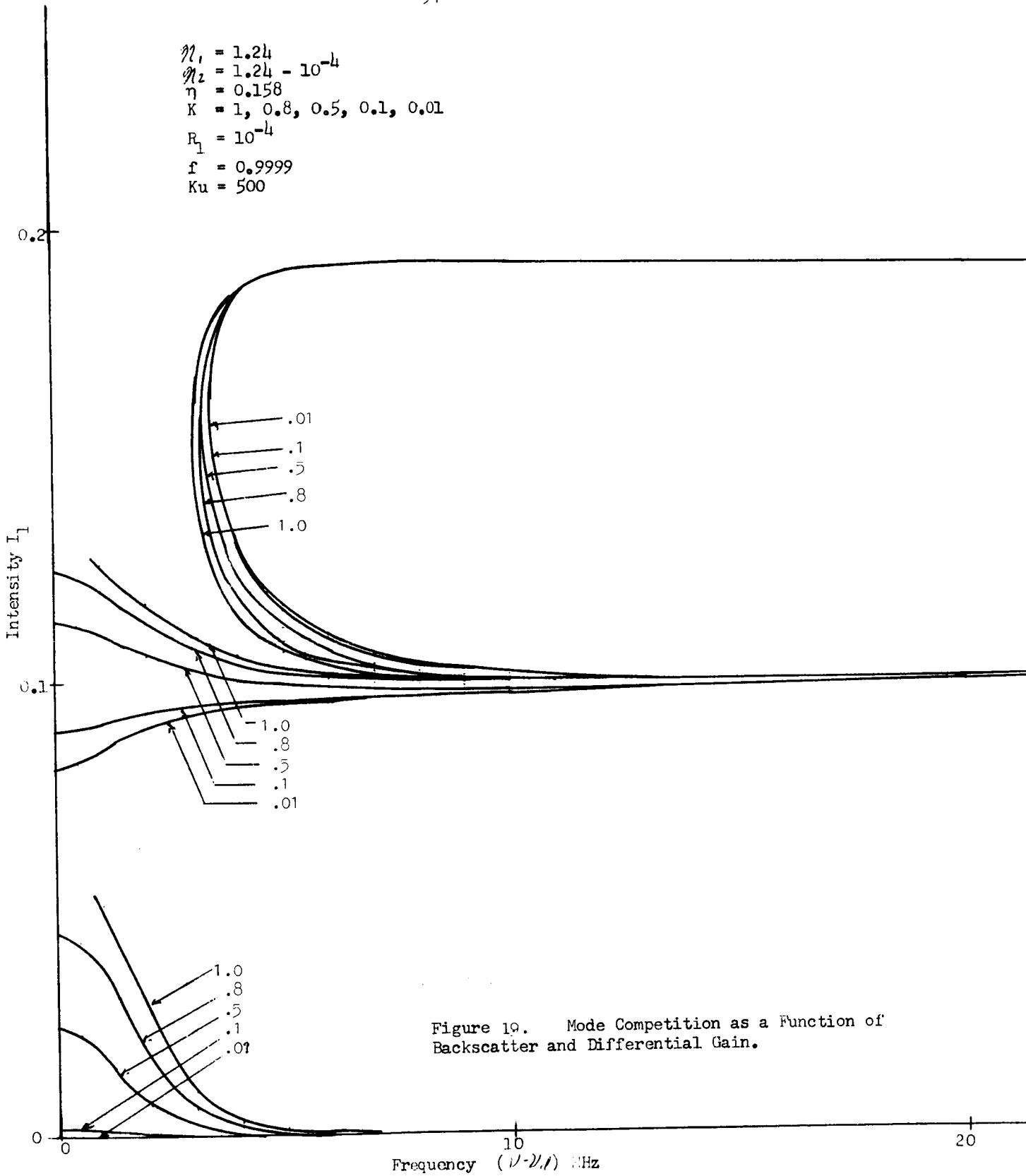

Figure 19. Mode Competition as a Function of Backscatter and Differential Gain.

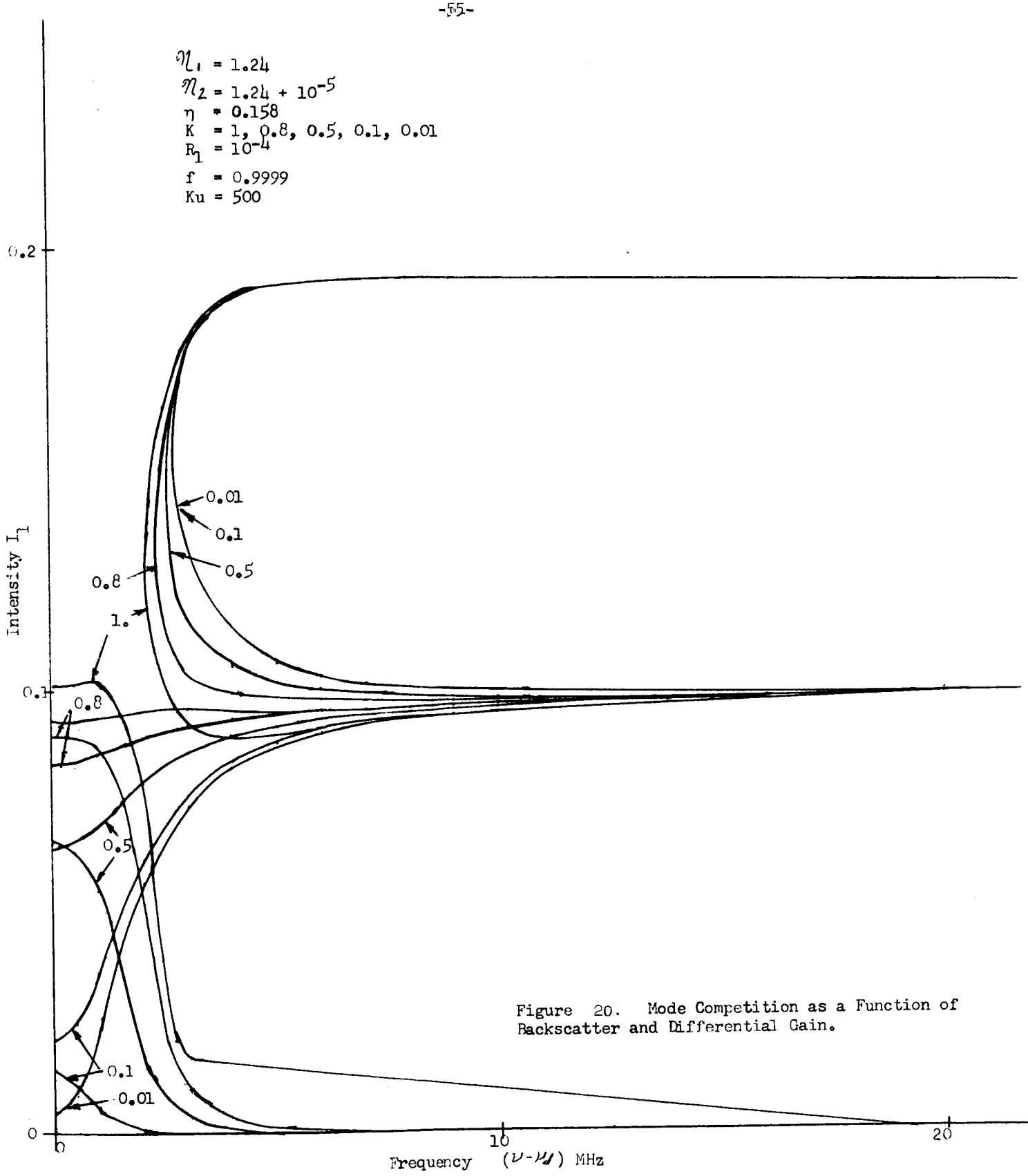

Figure 20. Mode Competition as a Function of Backscatter and Differential Gain.

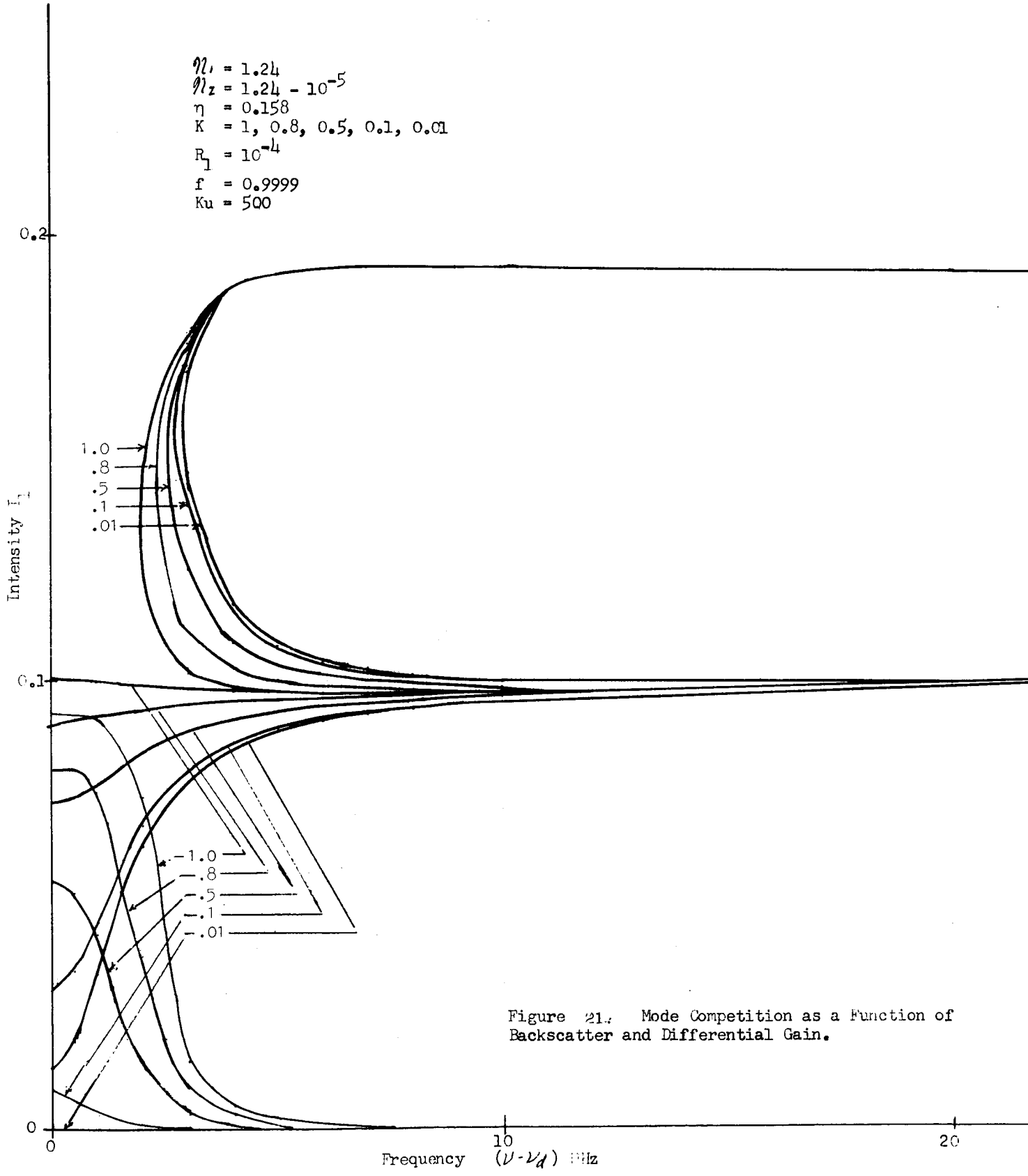

Figure 21. Mode Competition as a Function of Backscatter and Differential Gain.

16. COLLISION EFFECTS IN THE MODE COMPETITION EQUATIONS

From the work of Szoke, Javan,[15] Fork, Pollack[16] and others, it is known that the effects of collisions cannot always be neglected in the analysis of the He-Ne laser. In Fork and Pollacks[16] work mode competition between successive longitudinal modes in a linear laser was observed as the two modes were symetrically spaced about the doppler center. Their experimental results were explained by making two modifications in Lamb's theory.[3] The hole width was taken to be a linear function of the total pressure of the helium and neon. The gain curve (imaginary part of the "plasma dispersion function") was considered to be a linear combination of the gain curve plus the dispersion curve (real part of the plasma dispersion function). The coupling constant was a linear function of pressure. The mixing of the gain and dispersion curves produces an assymetric line shape.

Assymetry was taken into account in the mode competition equations (97, 98) by writing, for the doppler limit and for "low" pressures, ($c \ll 1$),

$$\exp(-\xi^2) \rightarrow \exp(-\xi^2) + cF(\xi) \ , \tag{117}$$

$$F(\xi) \rightarrow F(\xi) - \frac{\pi}{4} c \exp(-\xi^2) \tag{118}$$

From Eq (117), the maximum of the gain curve is shifted to

$$\xi_{max} = \frac{c}{2} \tag{119}$$

In frequency units,

$$\Delta\nu_{shift} = 250\ c\ (\text{MHz}) \tag{120}$$

The pressure shift has been measured as 4.2 MHz/torr[18] which give a value of c to be

$$c = 0.02\ p \qquad \left(p \text{ in torr}\right) \tag{121}$$

Using the form of assymetry given by Eqs (117, 118), the mode competition equations (97, 98) were solved for the intensities I_1, I_2. The results for I_1 are shown in Fig (22). Equation (121) was not used and value of c was

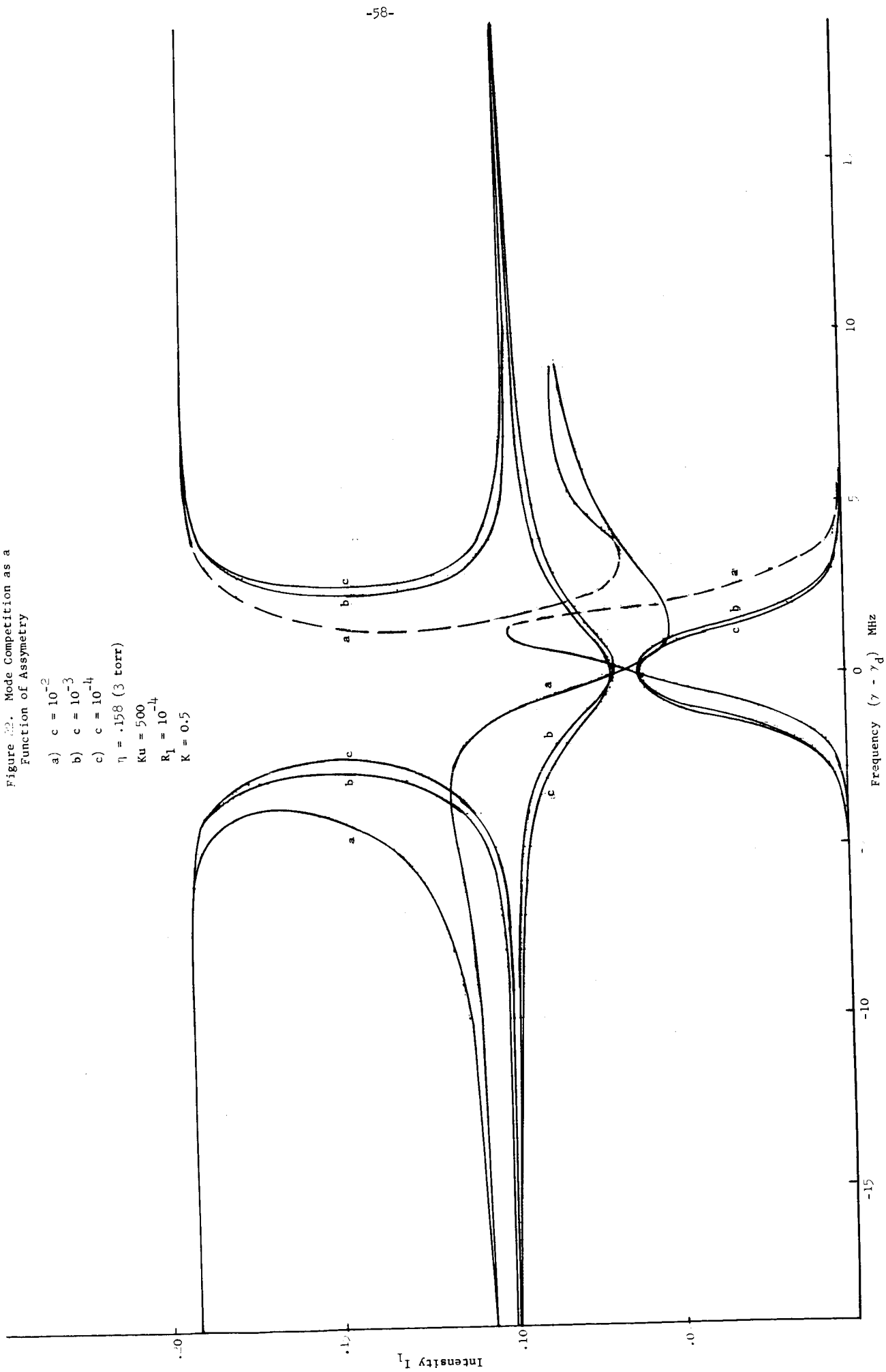

Figure 22. Mode Competition as a Function of Assymetry

a) $c = 10^{-2}$
b) $c = 10^{-3}$
c) $c = 10^{-4}$
$\eta = .158$ (3 torr)
Ku = 500
$R_1 = 10^{-4}$
K = 0.5

taken as 10^{-2}, 10^{-3}, 10^{-4}. The pressure (to determine hole width) was 3 torr, $R_1 = 10^{-4}$, $K = 0.5$. The results show the competition spike and dip to be shifted towards ξ_{max}, but the shift is much smaller than the shift of the maximum of the gain curve.

When Szoke and Javan[15] investigated velocity shift effects in a linear laser, they found that mode competition between the waves traveling in opposite directions was reduced. The reduction in competition could be expressed by replacing the Lorentzian factor in Eqs (97, 98) (in the standing wave case) by

$$\mathcal{L}(\xi) \rightarrow \frac{\eta}{\eta'} \mathcal{L}(\xi) \tag{122}$$

Both η and η' are linear functions of pressure and $\eta \leq \eta'$. The equality holds for zero pressure.

The mode competition equations were solved on the computor using the velocity shift effect given by Eq (122). The results showed no mode competition at the doppler center. The solution showed only complete extinction possible for either beam and complete co-existance. An investigation of the equations showed that whenever the maximum value of the Lorentzian factor was appreciably different from unity. The competition at the doppler center disappeared.

A mixture of isotopes will effectively reduce the maximum value of the Lorentzian function from unity and hence should eliminate the backscattering mode competition. The equations were run for the case of natural neon and this was found to be so.

17. EXPERIMENT - GENERAL DESCRIPTION

The first part of this report presents a theoretical description of a traveling wave ring laser in the presence of scattering effects. This part will present the experimental work performed with the aim of showing correlation with the theoretical model.

To this end the following experimental program was carried out. A ring laser was built and operated on the neon 1.15 micron transition. Mode competition between the oppositely directed traveling waves of a single longitudinal mode was investigated by tuning the frequency of oscillation across the doppler gain profile and measuring the intensities of the beams. The total pressure of the gas was treated as a parameter. In addition mode competition was investigated as a function of reflecting a portion of one of the transmitted beams back into the direction of the other.

While the beams were frequency locked changes in the phase difference between the oppositely directed beams were investigated as a function of tuning the frequency of oscillation across the doppler gain profile. The phase difference was also measured as a function of varying the phase of the back scattered energy from one of the beams, which was scattered into the direction of the other beam.

A block diagram of the experimental system is shown in Fig. (23).

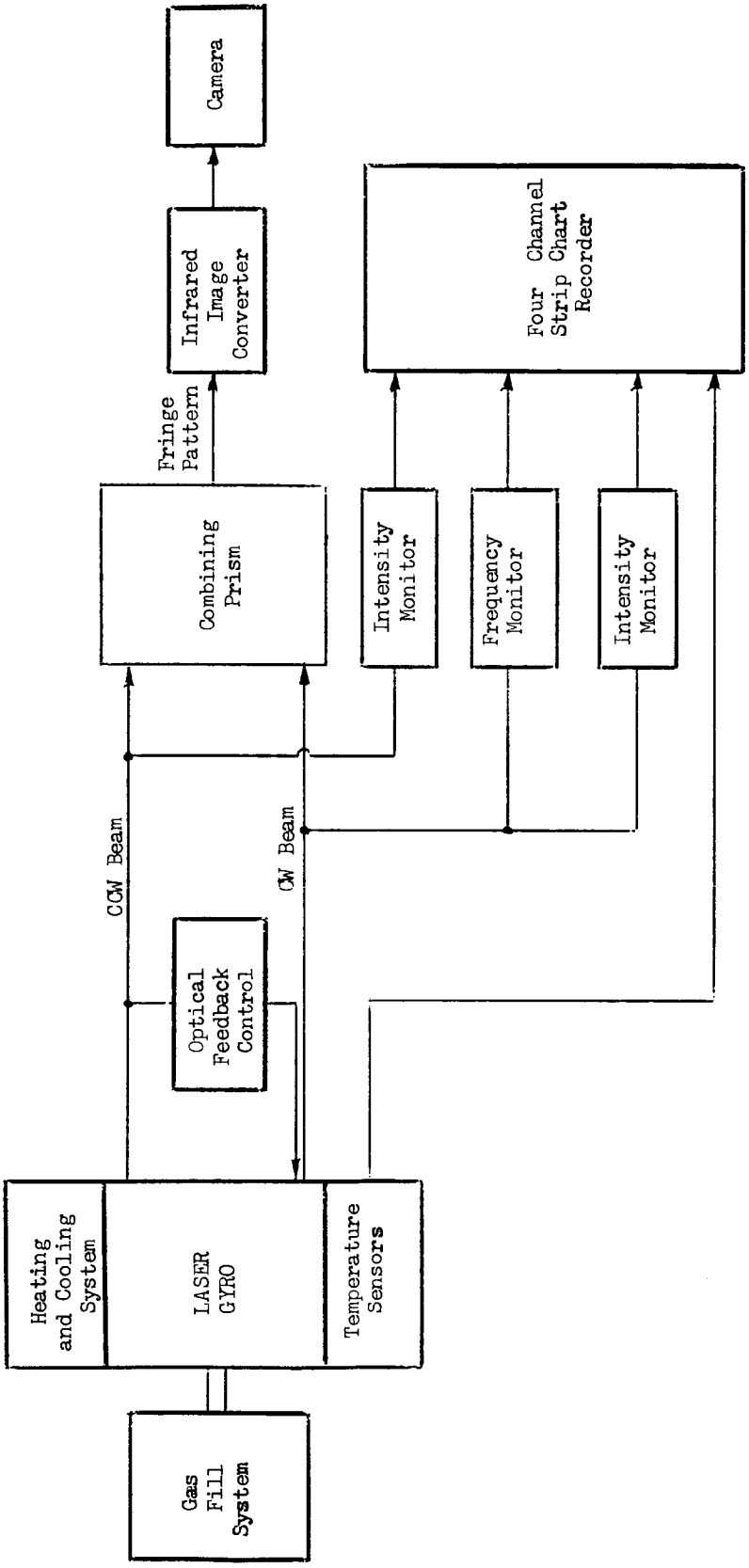

Figure 23 Block Diagram of Experimental System.

18. QUARTZ BLOCK RING LASER

The ring laser used in the experiments has been constructed from a single piece of fused quartz. The holes (4.5 mm diameter) defining the laser paths were made in the form of an equilateral triangle. The total path length is 58.9 cm giving a longitudinal mode spacing of 509 MHz. Excitation is d.c. with provision of exciting, by halves, a maximum of two legs. Two of the mirrors are flat ($\lambda/10$) and one is curved with a radius of curviture of 3 meters.

The mirrors are coated for operation on the neon 1.15 micron transition. One of the mirrors has a transmission of 0.62 percent, while the other two have a transmission of 0.28 percent. All three have a scattering loss of 0.2 - 0.3 percent. The diffraction loss is 0.1 - 0.2 percent giving a total loss of 2 percent. A design analysis is given in Appendix F. Operation is restricted to a single transverse mode by means of a 2.2 mm aperature placed symetrically with respect to the curved mirror. Visual confirmation was made of single transverse mode operation by means of an infra-red image converter. Both beams were observed to be linearly polarized in the low reflection loss plane. Typical current excitation (8 mm) allowed operation with either one or two longitudinal modes, depending on the position of the cavity modes with respect to the doppler gain profile.

The laser was always operated while attached to a vacuum fill station, allowing the total pressure of a 10:1 mixture of He^3 - Ne^{20} (99.99 percent) to be varied. Frequency tuning was accomplished by thermally heating the quartz block structure as a whole. Tuning could thus be varied in both directions. For a temperature change of ΔT, the cavity length changes by

$$\Delta L = L \alpha \Delta T \tag{123}$$

where $\alpha = 5.5 \times 10^{-7}/^{o}C$ (Linear expansion of quartz)

The frequency change due to a change in cavity length ΔL is

$$\Delta\nu = -\nu\Delta L/L \tag{124}$$

The negative sign implies that increasing the length causes the frequency to decrease. For a cavity length increase of 1 wavelength,

$$\Delta\nu_L = -\varepsilon/L \tag{125}$$

and the temperature change, ΔT for a mode spacing of 509MHz, is

$$\Delta T = \frac{\lambda \Delta\nu_L}{\alpha c} = 3.6^{\circ}C \tag{126}$$

Tuning has been accomplished over five modes with no difficulty.

The thermal time constant of the quartz block has been measured by heating one surface and measuring the time intervals over which successive cavity modes are tuned across the doppler gain profile. Meausrements indicate a time constant of 22 - 25 minutes. A rough theoretical estimate of the time constant of a homogeneous rectangular parallelopiped where one dimension is much smaller than the others, is

$$\tau = \frac{4\rho C A^2}{\pi^2 K} = 16 \text{ min} \tag{127}$$

where

ρ - density (2.2 gm/cm^3)
K - thermal conductivity (3.2×10^{-3} cal/sec. cm$^{\circ}$C)
C- specific heat (0.17 cal/gm$^{\circ}$C)
A- thickness of quartz (4.44 cm)

19. ZEEMAN CELL FREQUENCY MONITOR

In operating the laser it appeared desirable to have an instrument which could directly measure the frequency of oscillation, rather than rely on something indirect, such as power measurements. The measurement of the temperature of the quartz block would not be conclusive, since a question could arise as to the actual response of the cavity length to the temperature at a given point. In addition, for tuning over a small frequency range, there would be a question as to what point under the doppler curve the frequency is oscillating.

To avoid uncertainties of this kind, it was decided to design and build a device to directly measure the frequency of oscillation. Resolution should be as good as possible with a minimum resolution of a few MHz. To this end the Zeeman cell frequency monitor was designed.

Frequency Monitor

The frequency monitor operates on the output of one laser gyro beam to determine the laser operating frequency as defined by the cavity dimensions. Operation of the frequency monitor is explained with reference to Figure 24. (Further circuit details are found in Figure 26 and are subsequently explained.) The linearly polarized light from one laser gyro beam passes through a quarter wave plate to become circularly polarized. The light then passes through the absorption (or gain) tube containing a helium-neon mixture operated with a d.c. discharge. An alternating axial magnetic field is generated by an a.c. current in the coil surrounding the discharge tube. The laser light passing through the gain tube is modulated by the axial magnetic field at a modulation depth which depends on the laser operating frequency relative to the center of the doppler curve as shown in Figure 25a. Operation at frequencies higher or lower than the center of the doppler curve is identified by the relative phase of the modulated light referred to the modulating current. The modulated light signal is sensed by a lead sulphide detector, preamplified, and then demodulated in a phase sensitive demodulator. The output of the phase sensitive demodulator is then a typical "discriminator" curve as shown in Figure 25b. From the phase sensitive demodulator the signal goes to a current amplifier which superposes a d.c. current in the coil generating the magnetic field. In operation as a closed loop system the d.c. current takes on a value such that the d.c. magnetic

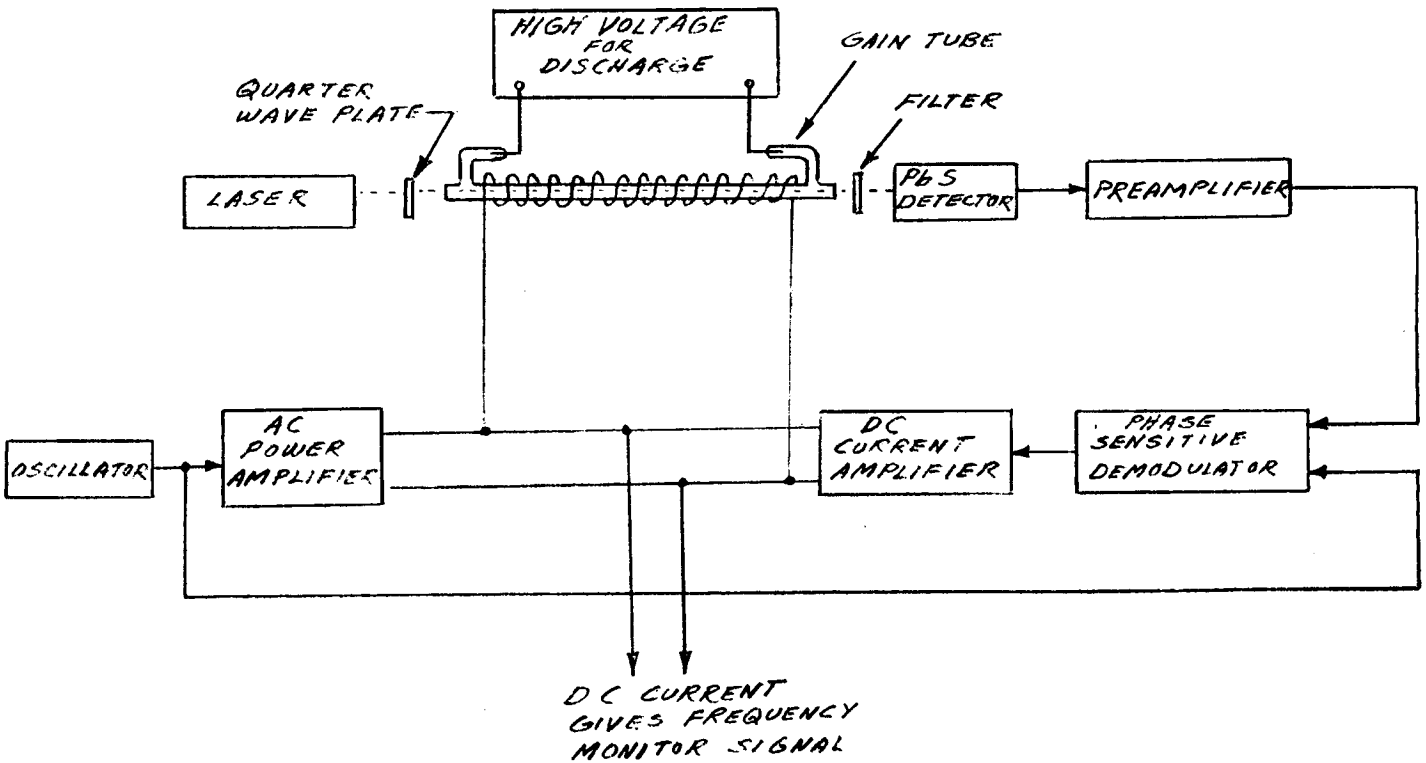

Figure 24 Frequency Monitor Block Digram

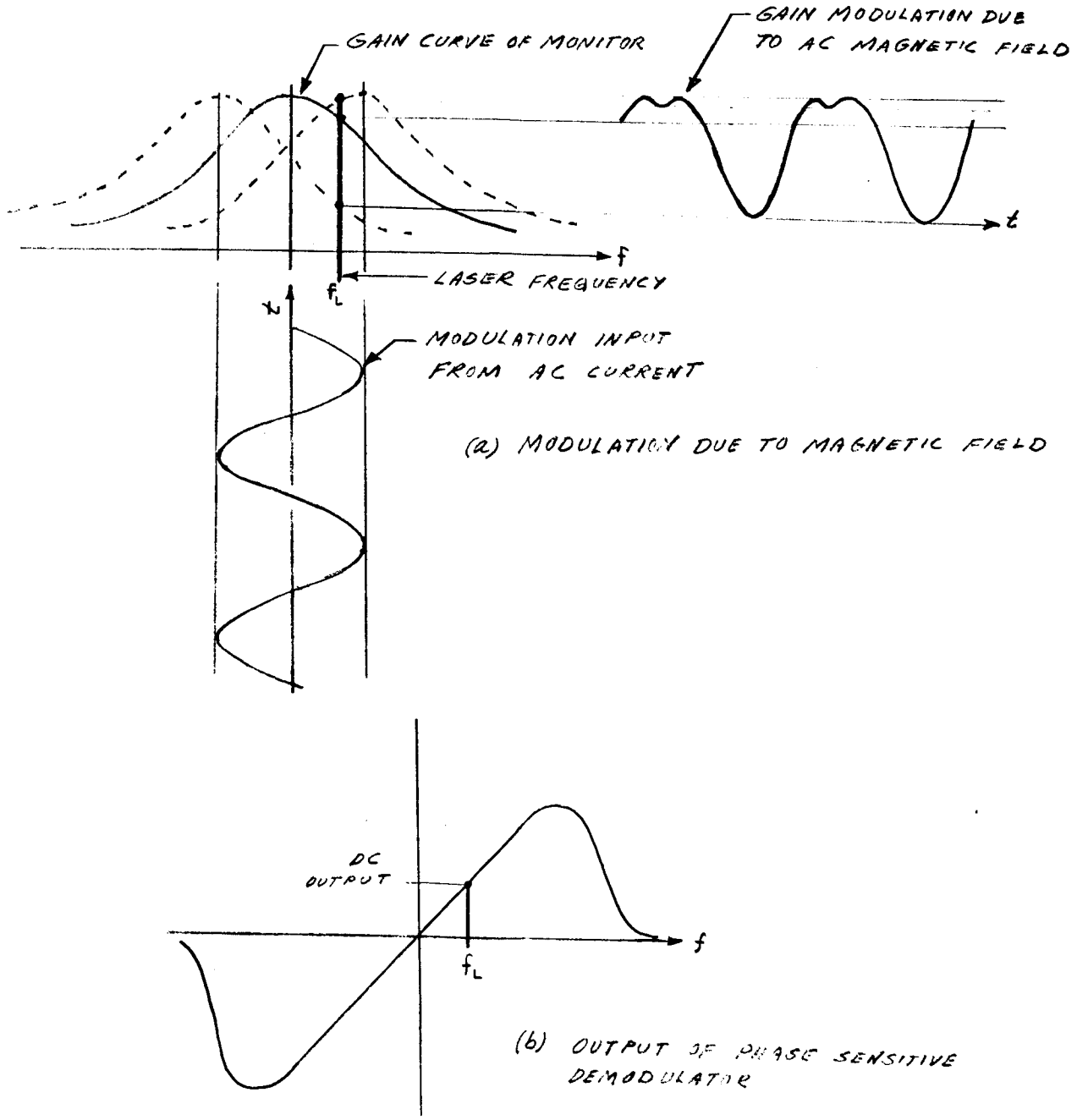

Figure 25 Modulation In Frequency Monitor and Resulting DC Output

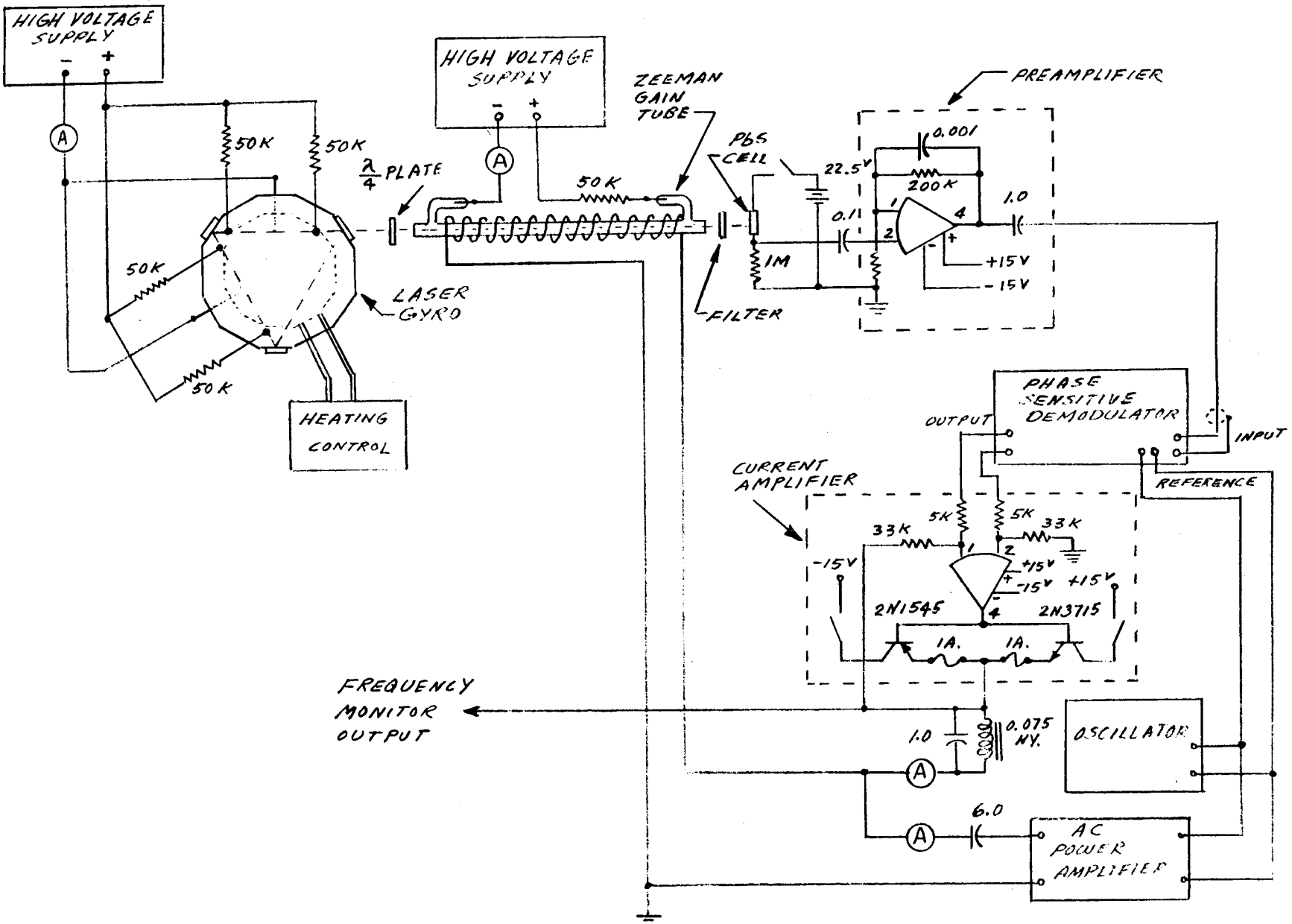

Figure 26 Circuit Details of Frequency Monitor

field bias nulls the a.c. signal at the fundamental of the reference (or modulation) frequency. When the system is operating closed loop in a nulled condition the magnitude of the d.c. current is a measure of the laser oscillating frequency. By using closed loop operation, the frequency measurement is largely independent of fluctuations in laser intensity, peak values of the a.c. magnetic field, and absorption or gain of the discharge tube.

Further details of the frequency monitor are described with reference to Figure 26. The discharge tube is 7mm internal diameter and 16.5 inches long. The active discharge length is 15.5 inches. The coil surrounding the tube is wound with 12 layers No. 20 copper wire, giving a total of 4450 turns or 318 turns per inch. The d.c. resistance of the coil is 13 ohms, and the inductance at 400 cycles is 32 millihenries.

The discharge tube is filled to a pressure of 6.4 torr with a 10:1 mixture of He^3 and Ne^{20}. The discharge is operated from a high voltage power supply at a current of 10 ma. A 50K ohm resistor in series with the discharge tube stabilizes the discharge with a 1400 volt drop across the tube.

To isolate the effects of the magnetic field from the laser, the coil is enclosed in a mu-metal shield.

An infrared-pass filter is located ahead of the detector and serves to reject the visible light generated by the discharge and the laser. The lead sulphide cell is operated with a 2215 volt bias and a 1 megohm load resistor. The a.c. signal developed across the load resistor is coupled by an 0.1 mfd capacitor to the preamplifier.

The preamplifier consists of a Burr-Brown model 1506 solid state operational amplifier having an open loop gain of 106 db. The amplifier is connected to give a gain of 1000 in a non-inverting configuration which provides high impedance input to the lead sulphide cell. A 0.001 mfd capacitor in parallel with the feedback resistor produces a roll-off of the frequency response above the 400 modulation frequency for the purpose of noise rejection. Low frequencies are rejected by the 1.0 mfd output coupling capacitor.

The phase sensitive demodulator is a Princeton Applied Research Corporation model JB-4 having a gain of 10,000, and selectable filtering time constants from 0.001 to 10 seconds. The input a.c. amplifier in the phase sensitive demodulation is highly frequency selective with respect to the reference frequency (400 cps). The second harmonic is rejected by a factor of 1000. Second harmonic rejection is highly desirable because a relatively large second harmonci component (compared to the signal) is produced when the system is operating in a closed loop condition near null. (Second harmonic signal content is shown in Figure 25a.).

The d.c. output of the phase sensitive demodulator is of push-pull form, offset 6 volts below ground. This output is conveniently coupled into the current amplifier using the Burr Brown model1506 solid state amplifier as a differential operational amplifier because a common mode voltage up to 10 volts can be tolerated. The current amplifier is designed to operate the output power transistors in class B operation for maximum efficiency. The power transistors are selected to operate as a complimentary symmetry, NPN-PNP pair. Operating the high gain amplifier into the output power transistors effectively reduces the "turn-on" effect (or dead zone) near zero to a negligible value. The feedback around the high gain operational amplifier is closed from the power transistor output point. This places the feedback from the load (current coil) to the amplifier input. The feedback arrangements produces good linearity in the current amplifier and results in low quiescent current in the power transistors at null.

Isolation between the a.c. and d.c. current circuits driving the coil is provided by the 0.075 henry choke and 1.0 mfd capacitor operated in parallel. The two elements present a high impedance at 400 cps, but present a resistance of only 0.075 ohms to the flow of d.c. current.

The amplifier which drives the a.c. current in the coil is a Bogen model MU130 power amplifier capable of a 30 va output. Its output transformer is operated with the secondary floating to allow a ground reference to be established only by the d.c. current amplifier. The common and 16 ohm impedance taps on the output transformer are used for connection to the current coil. In operation

the power amplifier delivers 1 ampere peak current at 400 cps into the current coil. The a.c. power amplifier is connected to the coil in series with a 6 mfd capacitor. This capacitor series resonates with the coil to match into the power amplifier impedance. The capacitor also serves to block any d.c. current into the power amplifier output transformer secondary. The a.c. and d.c. currents are metered at the respective amplifier outputs.

The oscillator is a Hewlett-Packard model 200 CD. The oscillator output provides the reference voltage for the phase sensitive demodulator and also the input signal for the a.c. power amplifier. An oscillator output setting of 0.3 volts is adequate to drive the power amplifier through its auxiliary input. The same oscillator output level is adequate as the reference signal in the phase sensitive demodulator since adjustment of the reference level can be made internal to the demodulator.

The frequency monitor output point shown in Figure 26 goes to the data recording system. This point appears across the current coil (with a negligible d.c. drop in the choke) and registers the d.c. voltage across the coil. This output voltage is proportional to the d.c. current in the coil, and is therefore a measure of the laser gyro operating frequency.

20. FREQUENCY MONITOR AND MODE COMPETITION

The amplitudes of both oppositely directed traveling waves were monitored while the laser was operated with a d.c. discharge currentoof 8-9 m.a. The detectors were Hoffman EA7 photovoltaic silicon cells with an infrared-pass optical filter. The outputs were fed to two microvoltmeters, a Kintel model 207B and a Keithley Instruments model 610A electronmeter operating as a microvoltmeter. The microvoltmeters also served as a high gain d.c. amplifier which allowed the meter output to be recorded directly on a strip chart recorder.

The frequency of the laser output was tuned by thermally heating the quartz block structure as a whole. A 3/16 inch thick copper heat transfer plate in contact with the bottom surface of the quartz block was warmed or cooled by circulating water in copper coils soldered to the bottom surface of the plate. Heating and cooling rate was controlled by selecting the water temperature and flow rate.

Figure (27) shows a typical amplitude vs frequency scan as monitored on a four channel strip recorder. The third and fourth channels are recordings of the counterclockwise and clockwise laser beam intensities. The Kintel meter monitored the counterclockwise beam intensity. The time consistant of this meter, as measured from the laser output, was 0.25 sec. The time constant of the Keithley meter was at least an order of magnitude faster and thetime response for the clockwise beam was determined by the recorder itself.

It was possible to monitor the output from each beam from all three mirrors.

One of the output signals from the clockwise beam was fed into the frequency monitor gain tube. The d.c. closed loop output current from the frequency monitor is shown recorded in the second channel. The first recorder channel shows the temperature difference between the bottom and top surfaces of the quartz block. Increasing temperature difference is down. The strip chart recorder was run at a speed of 0.25 mm/sec. Each mark at the top of the strip chart corresponds to 75 mm.

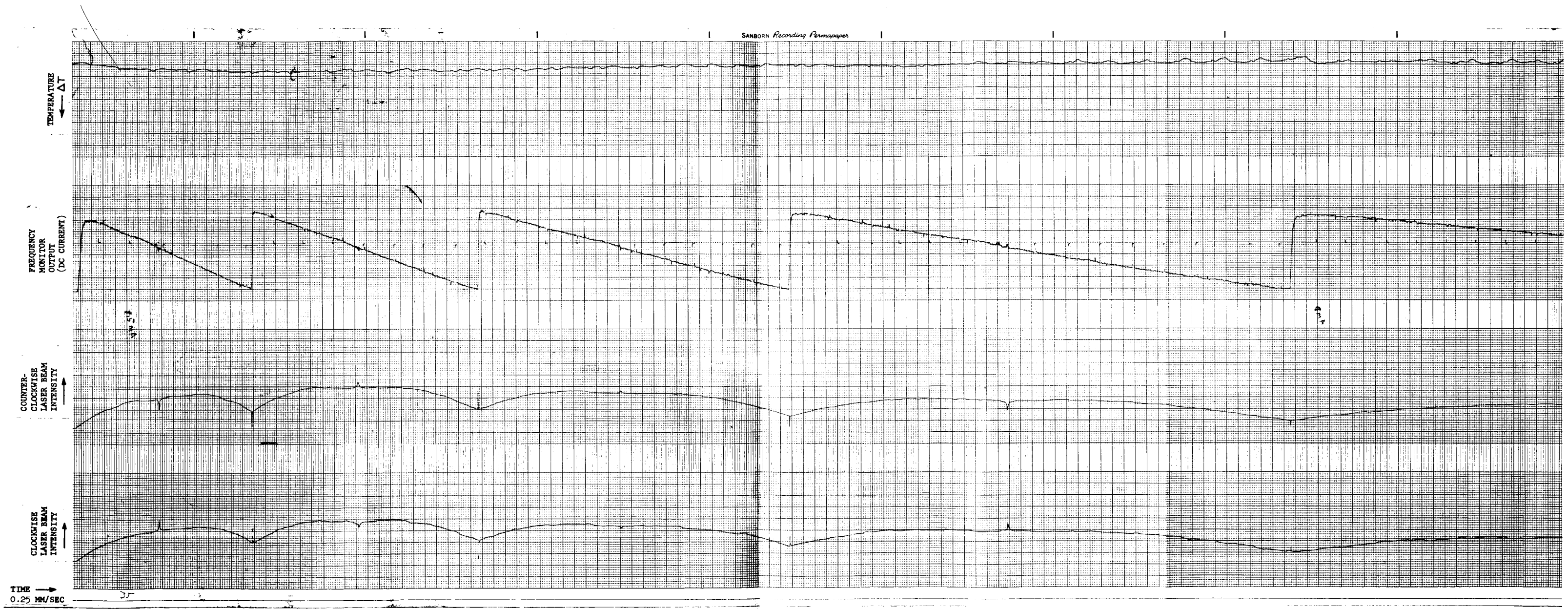

Figure 27 | Mode Competition at 3.2 Torr Pressure, With Zeeman Frequency Monitor.

As discussed in section 19, the d.c. current output from the frequency monitor is a linear function of the difference between the frequency of oscillation of the laser and the frequency at which the gain in the Zeeman cell is a maximum. The operation of the frequency monitor requires single mode operation. As a cavity mode is tuned across the doppler gain profile, the output is a ramp type function as shown in Fig 27. The sharp jump in the ramp occurs as one mode on the low frequency side (tuning is accomplished by heating which increases the cavity length and decreases the oscillation frequency) drops below threshold and another on the high frequency side comes above threshold. As shown in Fig 27, the gain/loss ratio is high enough such that when two adjacent cavity modes are symetrically spaced about the doppler center, both are above threshold.

Figure 27 shows five cavity modes being tuned across the doppler gain profile. The intensity date shown the characteristic linear laser tuning peak around the doppler center. In addition, sharp competition regions are found when one mode is oscillating near the doppler center and when two modes are symetrically spaced about the doppler center.

The cavity mode spacing is 509 MHz. The off center competition spike are rather sharp (0.3-0.6 MHz) and provide a frequency marker to calibrate the frequency scale. The competition spikes near the doppler center are 2-3 MHz wide.

As a means of checking the operation of the frequency monitor, the position of the peak of the center competition spike was measured by two methods. In both cases it was assumed that the thermal heating of the quartz block can be described by one thermal time constant. Three known frequencies can determine the time constant. In the first case the three frequencies used were three adjacent off center competition spikes.. Fig. (27) shows that there are four off center competition frequencies, as three complete modes are scanned across the doppler gain profile. Thus two time constants were calculated using two groups of adjacent competition points. The first time constant is used for calculations involving the first two complete cavity modes while the second is used for the

Table I - Measurement of Position of Center Competition Spike

	Time Const. (min)***	Position of Center Spike (MHz)					Mode Spacing		
		Zeroth	First	Second	Third	Fourth	First	Second	Third
Intensity Data I	24.7	257	257	256			509*	509*	
Intensity Data II	24.2			256	259			509*	509*
Freq. Monitor I	24.9		257	255			509**	510**	
Freq. Monitor II	25.1		256	255	262		507**	509**	517**
Freq. Monitor III	24.9			255	261	254		508**	515**

* Mode Spacing set equal to 509 MHz

** Mode Spacing calculated from time constant.

*** To determine time constant write $\nu = \nu_{oo} [1 - e^{-t/\tau}]$:
Use this equation to obtain ν_1, ν_2, ν_3 at known times t_1, t_2, t_3.
Since $\nu_3 - \nu_2 = \nu_2 - \nu_1 = 509$ MHz. Two equations are obtained from which one can determine τ and ν_{oo}.

second and third modes. The position of the center spike (measured with respect to the previous off center competition spike) was calculated. The results are shown in Table I. The spacing between off center spike was chosen as 509 MHz. In all cases the center spike was on the low frequency side of one half the mode seperation.

The second method made use of the frequency monitor data. Again three points were used to determine the time constant. This time the points chosen were those where the d.c. feedback current was the same over three successive modes. The currents were chosen at 5 mm intervals. Six time constants were chosen in each group and averaged. Three groups were used. The incomplete modes at both ends were able to be used for this type analysis. Using the averaged time constant in each group, the position of the center competition spike was again calculated. They are summarized in Table I. In addition, using the frequency monitor data, the spacing between successive off center competition spikes was calculated and included in Table I.

From Table I, it is seen that there is good correspondence between the results obtained with the power data and those obtained with the frequency monitor data. Only in the third complete mode is there a discrepancy from the expected results. This might be due to the fact that the tuning time for the third mode was 15 minutes and the single time constant assumption may not be valid over this range of the exponential.

An error analysis was made of the expected accuracy in calculating frequency intervals. It was assumed that the dominent error arises from an inability to exactly read the times at which mode competition occurs. It was assumed that this error was $\pm$ 0.1 mm and is random for each time interval. This gave an accuracy for each frequency interval of $\pm$ 2 MHz. The results in Table I show correlation to within this error. But with this error, the displacement of the center competition spike from the midpoint of the two off center competition spikes, becomes questionable.

21. DETERMINATION OF GAIN/LOSS FROM INTENSITY DATA

As seen from Figs (7,8), the effects of small values of backscattering are seen only at the doppler center. At frequencies away from the center, the intensities of the oppositely directed beams are essentially equal. The self consistant amplitude equations can be used to fit the data in Fig (27) under this condition. The center competition spike will be neglected here and the intensity curve will be considered to vary smoothly through the center.

For this case of equal intensities and neglecting backscattering and for the beams being frequency locked, Eq. (97) can be solved for the intensity (of either beam) and is written as

$$I = \frac{\alpha}{\beta+\theta} \tag{128}$$

Using the expressions for the coefficients as given by Eqs. (99-101), Eq. (128) becomes

$$I = \frac{1 - \eta^{-1} \exp \xi^2}{1 + \mathcal{L}(\xi)} \tag{129}$$

where η is the ratio of gain/loss.

From the date in Fig (27), it is seen that η is large enough such that there is at least one longitudinal mode above threshold at all frequencies. Since the mode spacing is 509 MHz, a lower bound can be placed on η. Taking the doppler width as Ku = 500 MHz, Eq. (129) gives, for I = 0,

$$\eta_{min} = \exp [(509/2) /500]^2 = 1.3 \tag{130}$$

The hole width to be used in the Lorentzian function is, for a pressure of 3.2 torr[15]

$$\eta' = 22.1p + 11.4 = 82.1 \text{ MHz} \tag{131}$$

Using this hole width and η_{min}, Eq. (129) predicts intensity tuning data with a much larger Lamb dip than is seen in Fig (27). To get correlation with the theory, the collision correction to the Lorentzian function, as given by Eq. (122) must be used. Thus Eq. (129) must be modified to read[15]

$$I = \frac{1 - \eta^{-1} \exp \xi^2}{1 + \frac{\eta}{\eta'} \zeta(\xi)} \tag{132}$$

The ratio η/η' is pressure dependent and is given by[15]

$$\frac{\eta}{\eta'} = \frac{1.5p + 11.4}{22.1p + 11.4} \tag{133}$$

Using the collision corrected expression for the intensity given by Eq. (132) the value of η will be determined from the data given in Fig (7). First it should be noticed that the magnitude of the intensity follows the differential temperature curve. This has been attributed to a misalignment of the aperature. As the block is heated from the bottom, the block bends and brings the aperature into better alignment. As heating continues, the thermal gradient in the block decreases and the alignment problem gets worse. Thus the valve of η will be a function of mode position.

To calculate η, two valves of intensity must be known, since the data is in arbitrary units of intensity. One point is the doppler center ($\xi=0$). Thus

$$I_o = K \frac{1 - \eta^{-1}}{1 + \eta/\eta'} \tag{134}$$

For the second point, the value of the intensity used is when the two modes are symetrically placed about the doppler center. To eliminate problems of mode competition, the values of the intensity at the tips of the off center mode competition spokes (always assumed up) were used and the value was divided in half. Note that when these spikes are down, they determine the point of zero laser intensity. This is quite important because this allows the subtraction of backgroup light from the laser discharge.

Writing Eq (132) at $\xi = \xi_\ell$

$$I_\ell = K \frac{1 - \eta^{-1} \exp \xi_\ell^2}{1 + \frac{\eta}{\eta'} \zeta(\xi_\ell)} \tag{135}$$

Eliminating the arbitrary constant in Eqs. (134, 135) and solving for η, one finds

$$\eta = \frac{\left[\frac{I_o}{I_\ell}\,\frac{1+(\eta/\eta')}{\left[1+(\eta/\eta')\right]\mathcal{L}(\xi_\ell)}\right]\exp\left(\xi_\ell^{\,2}\right) - 1}{\left[\frac{I_o}{I_\ell}\,\frac{1+(\eta/\eta')}{\left[1+(\eta/\eta')\right]\mathcal{L}(\xi_\ell)}\right] - 1} \qquad (136)$$

However the data from Fig (27) cannot be directly substituted in Eq. (136) since the valuse of I_o and I_ℓ are obtained at different times and hence at different values of η. It is necessary to plot I_o and I_ℓ as a function of tuning frequency and use pairs of instaneous values. The results are shown in Fig (28). The abscissa is units of tuning across doppler centers for successive modes. At each doppler center andat each frequency midway between centers a value of I_o and I_ℓ was used inEq (136) to calculate a value of η. The way in which η varies as a function of frequency tuning is shown on the same figure. A smooth curve has been sketched through all the points. It is seen that η ranges from about 1.3-1.5. A plot of differential temperature is also shown on the same axis (obtained from the first channel in Fig (27)). The differential temperature is seen to have the same shape as η, although it leads η by $\frac{\lambda}{2}$.

Using Eq. (132), a set of curves of intensity vs frequency were plotted for various values of η and pressure and are shown in Figs (29-32) . It is seen that the data in Fig (27)agrees with the calculated curves (ie) (p=3 torr, η= 1.3-1.5). Figures (33-37) show intensity tuning data at various gas pressures. Figure (33) is at a pressure of 2.9 torr. The Lamb dip is more pronounced and is due to an increased η. Figure (34) is for a pressure of 3.2 torr. The center competition spikes are more pronounced here and it is seen that at the end of the third mode, the loss has increased such that the mode has dropped below threshold. Figure (35,36,37) are for a pressure of 4.4, 5.0 and 6.4 torr. In Fig (37), the intensity jumps are gain adjustments.

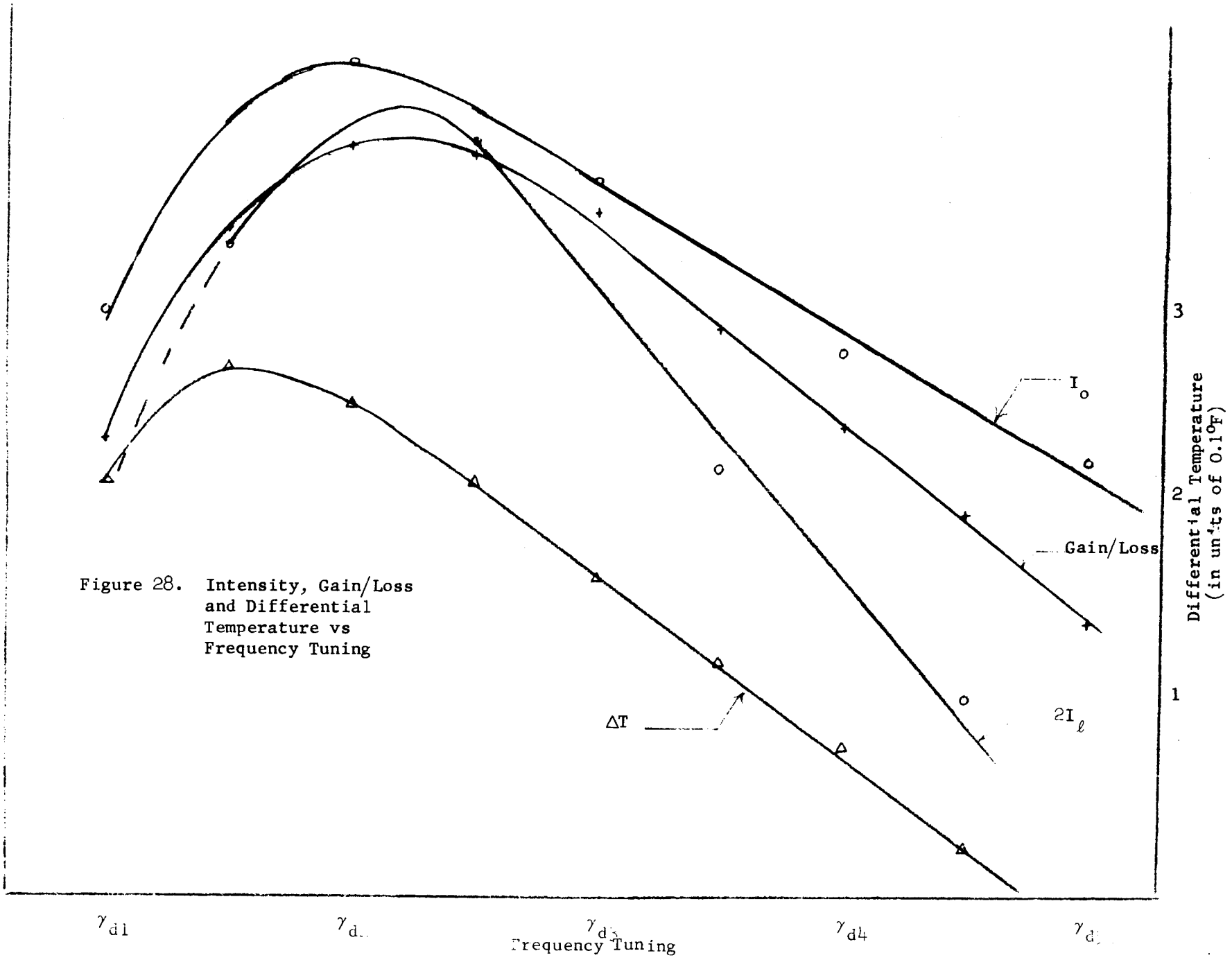

Figure 28. Intensity, Gain/Loss and Differential Temperature vs Frequency Tuning

Figure 29. Intensity vs Frequency for case of Reduced Saturation Effect Pressure = 1 torr

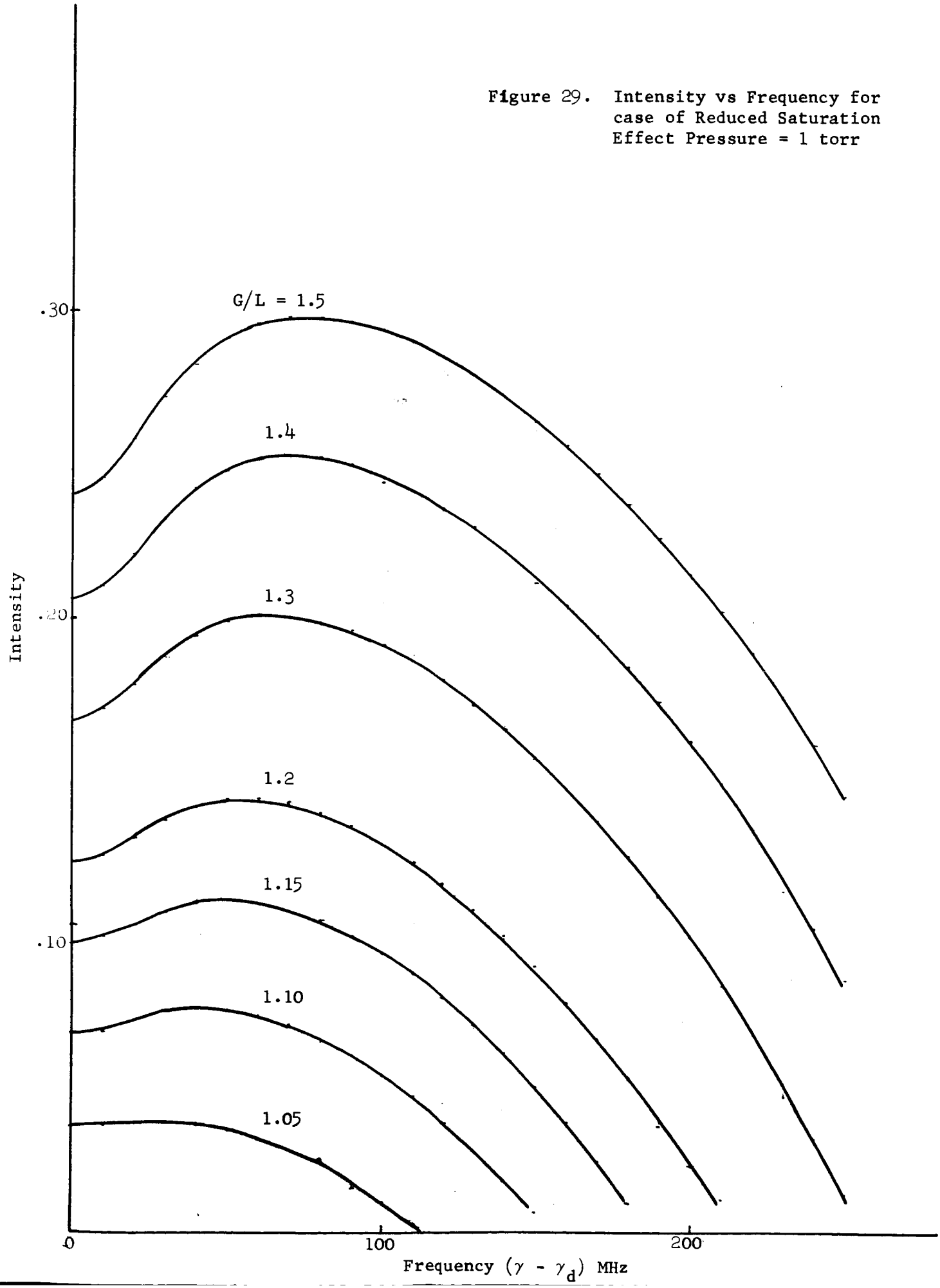

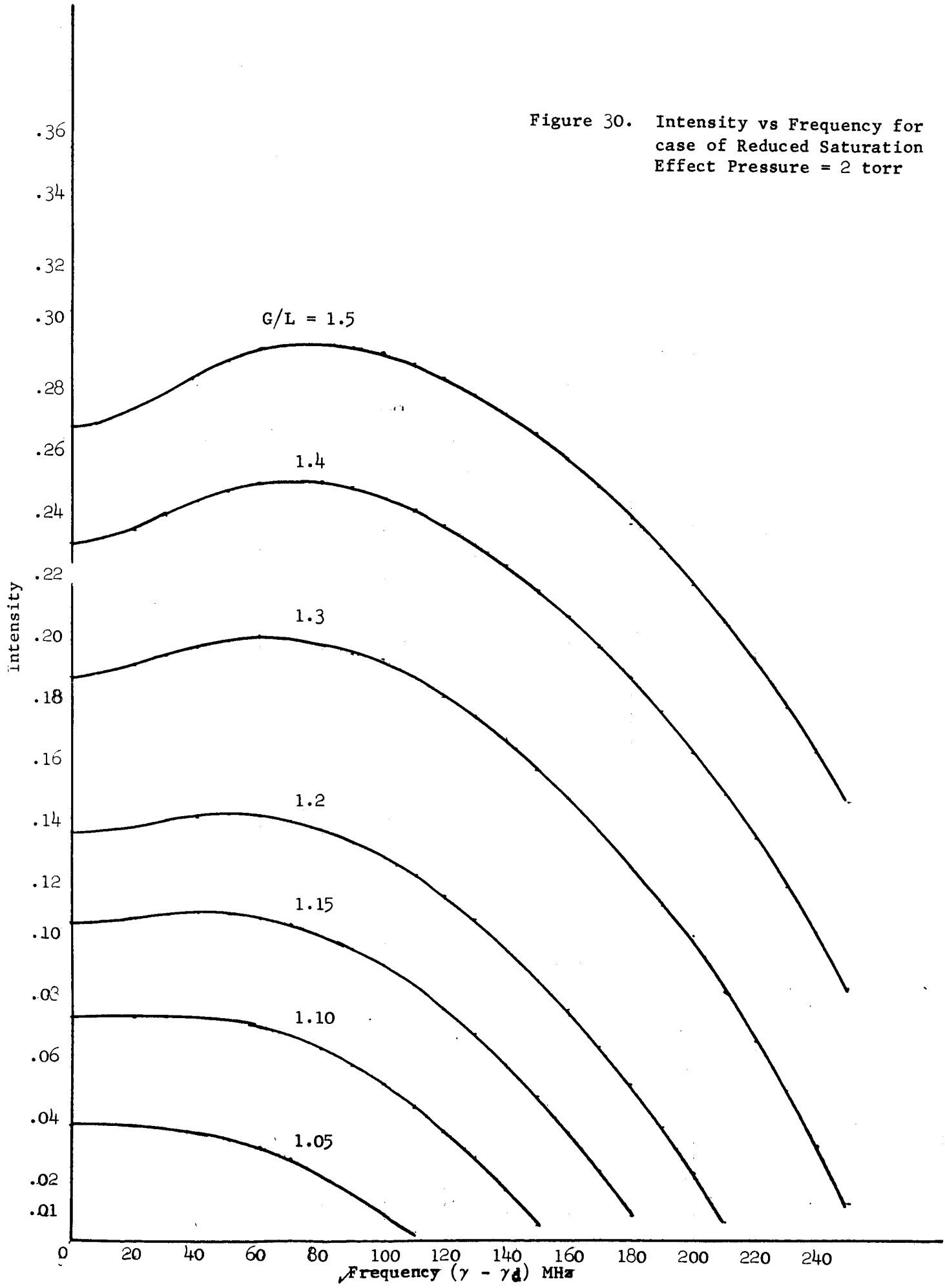

Figure 30. Intensity vs Frequency for case of Reduced Saturation Effect Pressure = 2 torr

Figure 31. Intensity vs Frequency for case of Reduced Saturation Effect Pressure = 3 torr

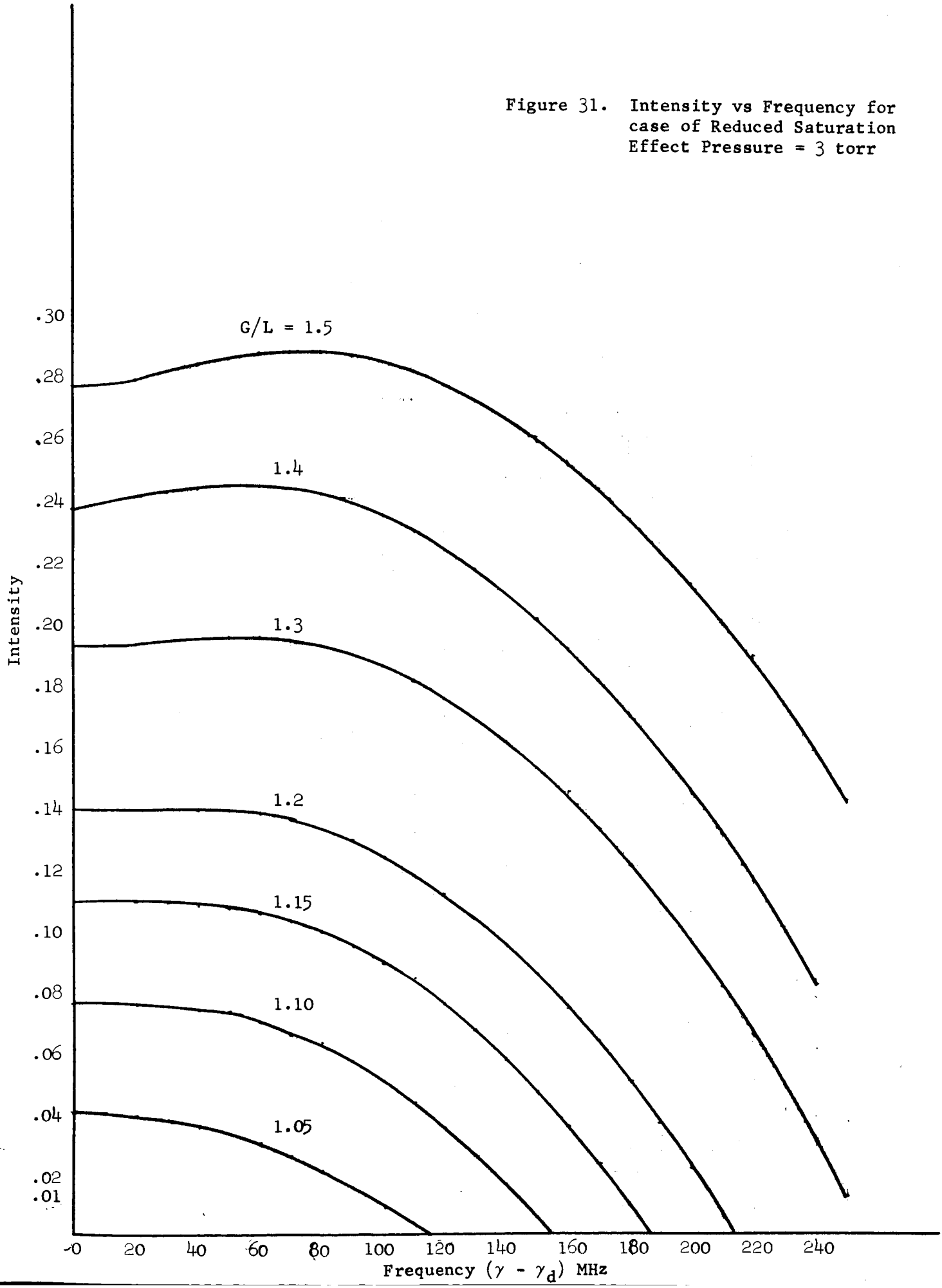

Figure 32. Intensity vs Frequency for case of Reduced Saturation Effect Pressure = 5 torr

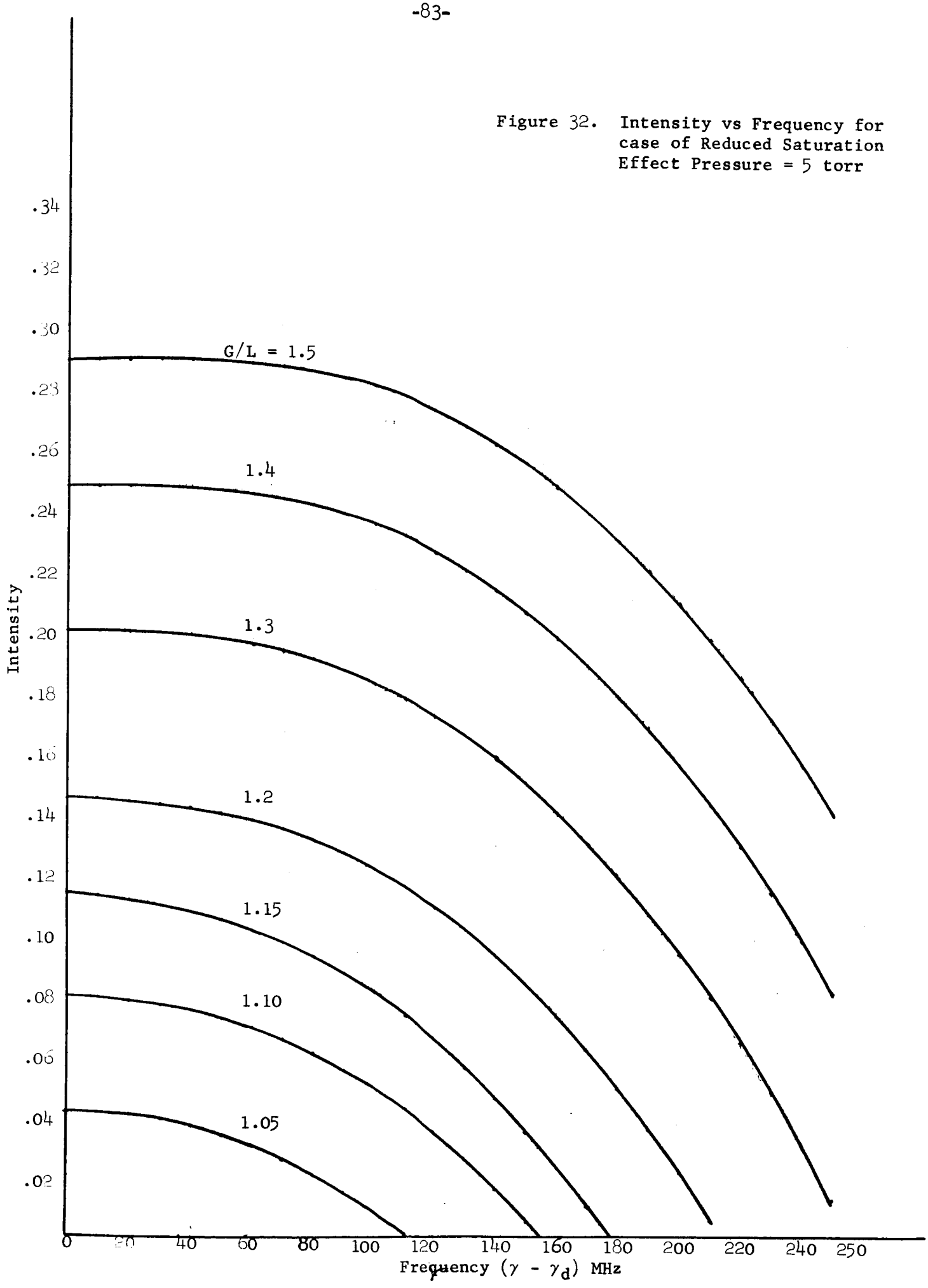

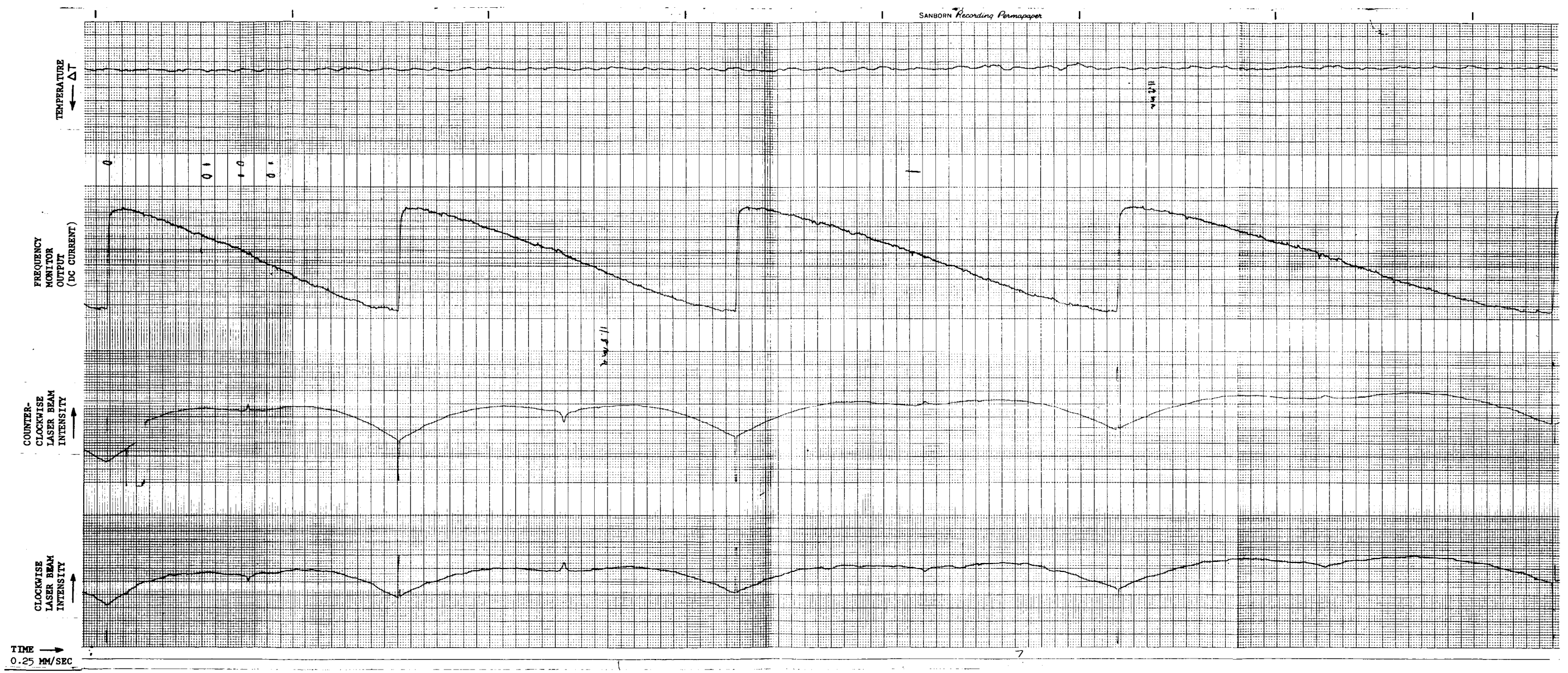

Figure 33 Mode Competition at 2.6 Torr Pressure, With Zeeman Frequency Monitor.

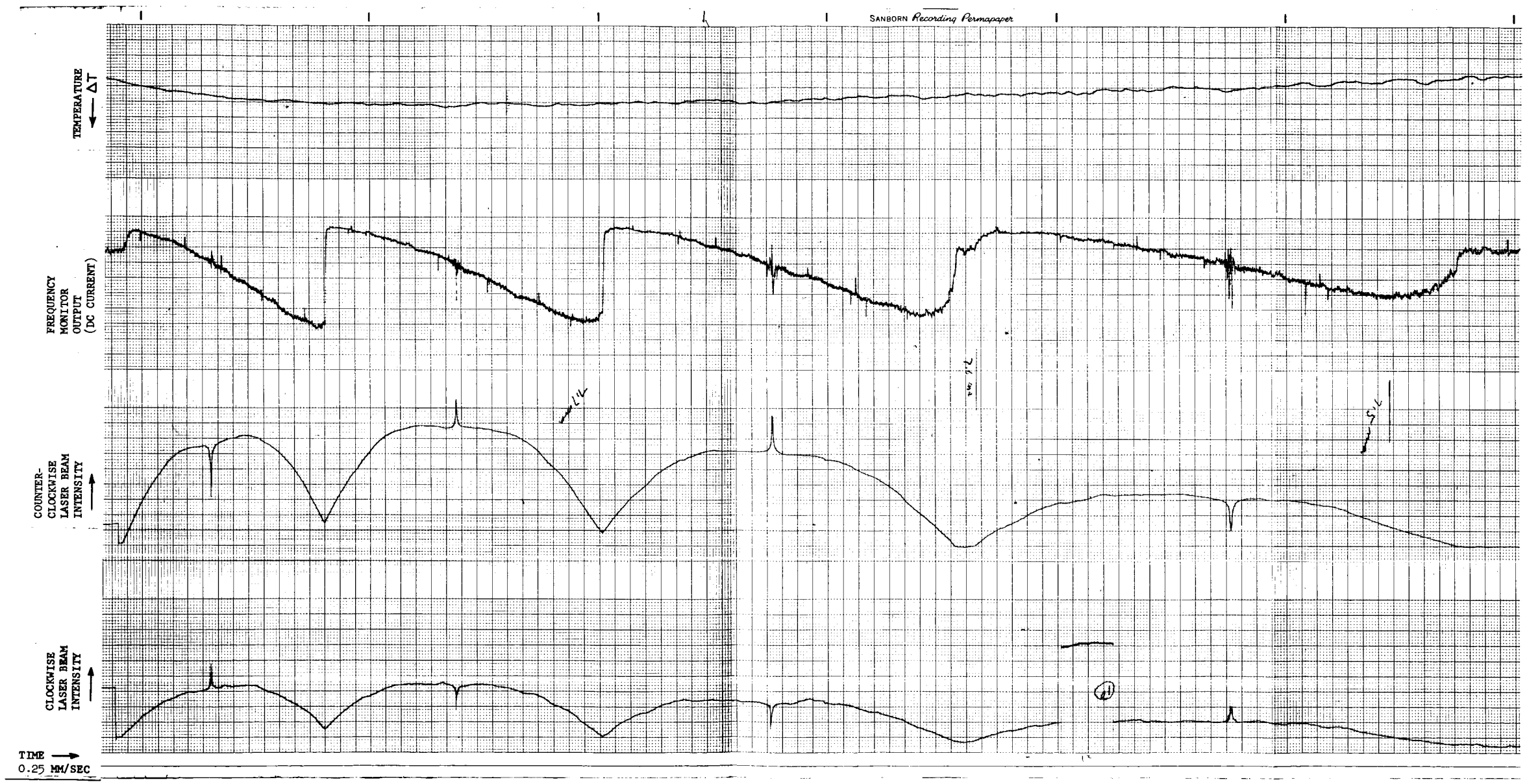

Figure 34 Mode Competition at 3.2 Torr Pressure, With Zeeman Frequency Monitor.

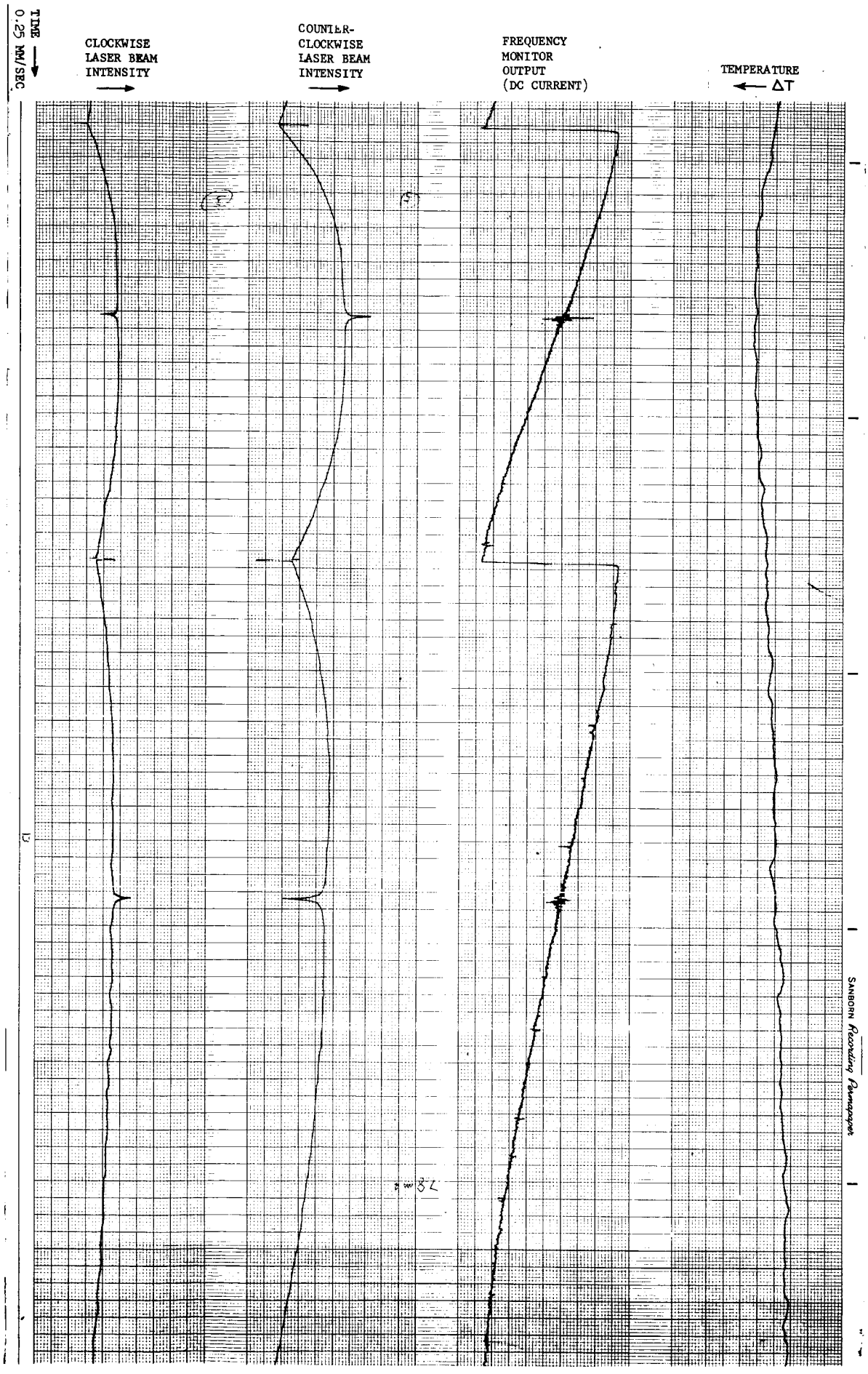

Figure 35 Mode Competition at 4.4 Torr Pressure, With Zeeman Frequency Monitor.

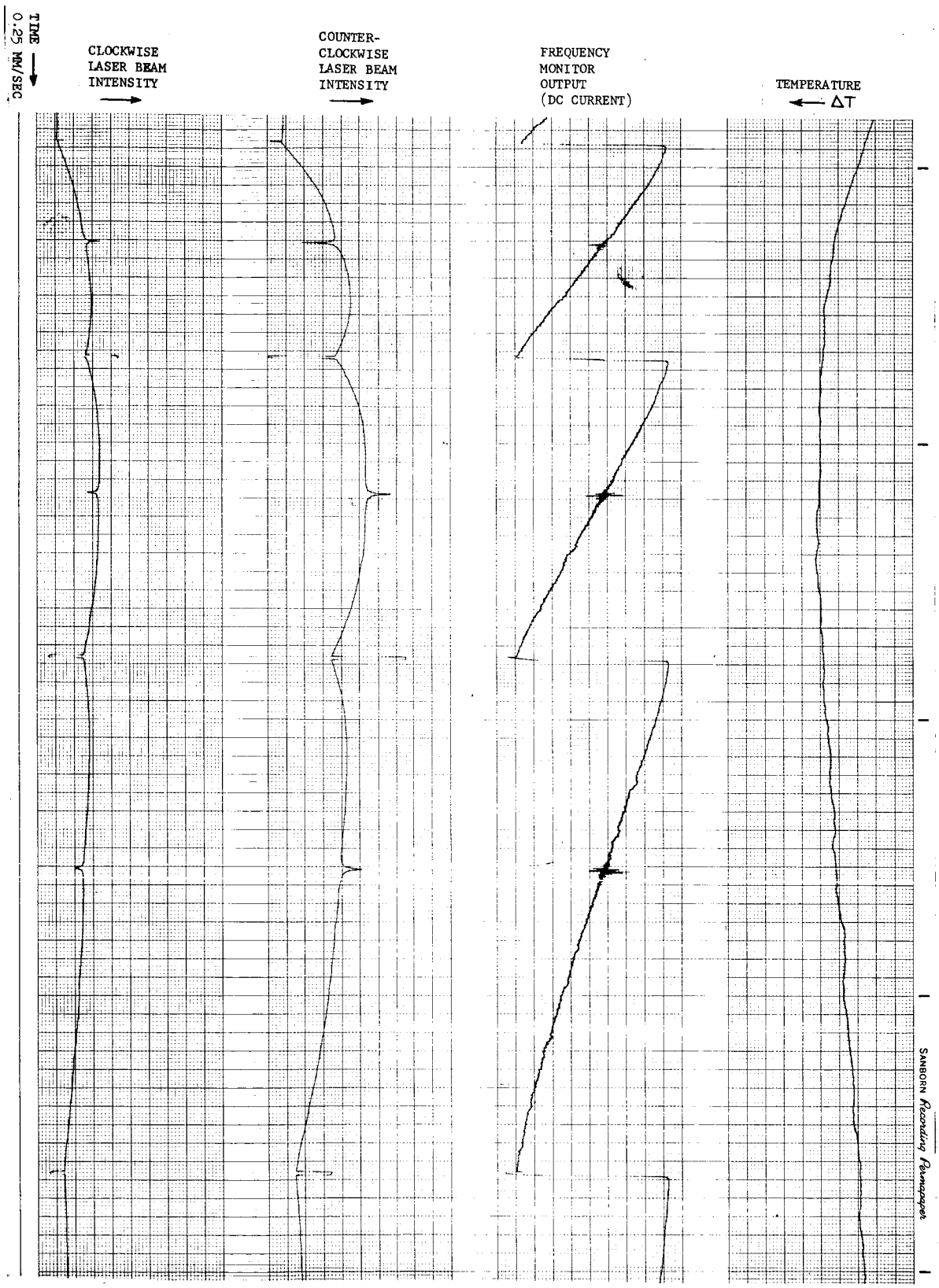

Figure 36 Mode Competition at 5.0 Torr Pressure, With Zeeman Frequency Moni

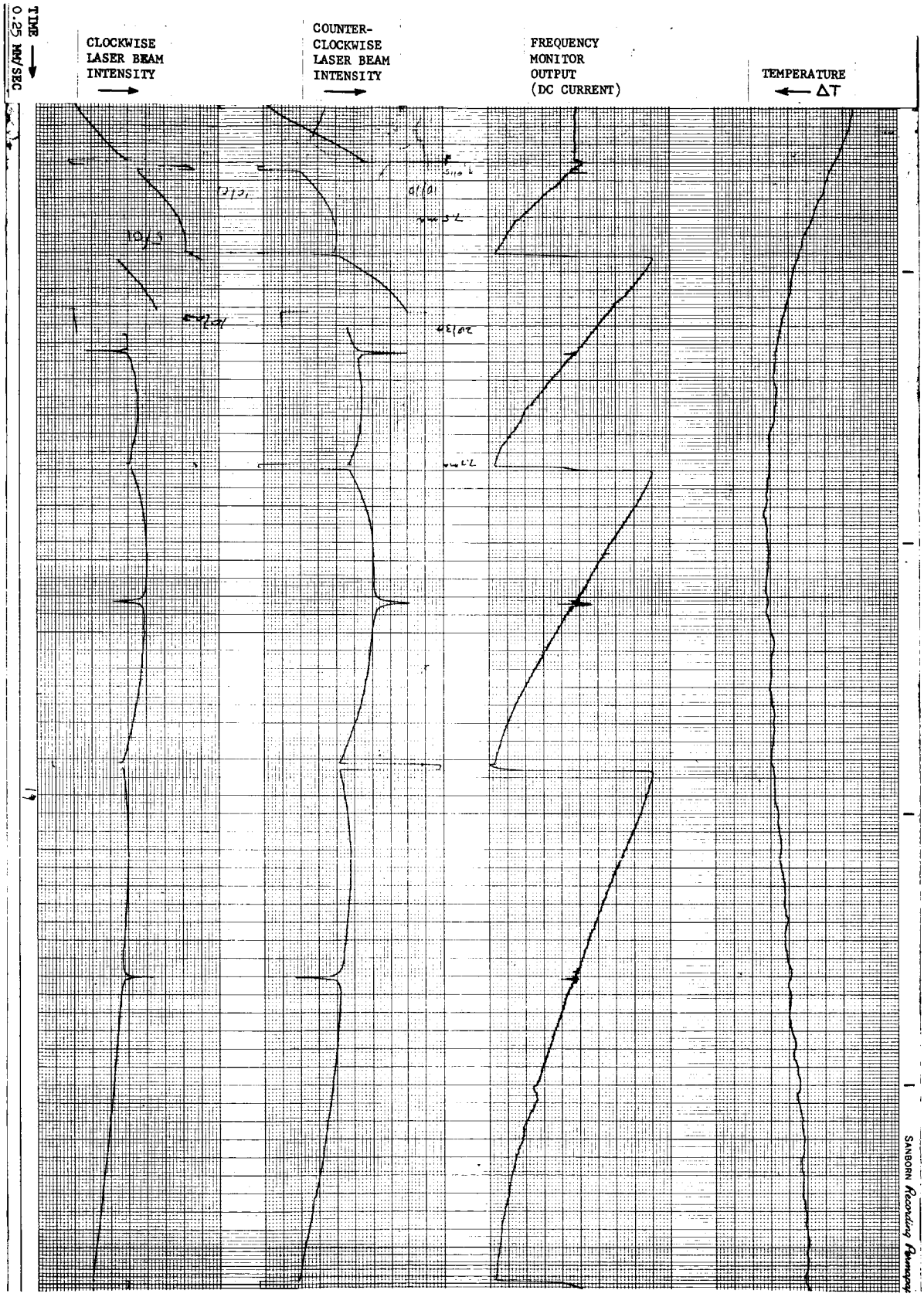

Figure 37 Mode Competition at 6.4 Torr Pressure, With Zeeman Frequency Monit

22. MODE COMPETITION - EXTINCTION

The computor solution of the mode compettiion equations for I_1 and I_2, as shown in Figs (7,8) predict four possible solutions. The mode competition discussed in the previous section has been of type "c", as labeled in Figs, (7,8). Figure (38) shows a more complicated type of mode competition at a pressure of 6.4 torr. It shows one cavity mode being tuned back and forth about the doppler center by heating and cooling the quartz block. I_1 is the lower trace. Comparing Figs (7,8,38), it is seen that I_1 and I_2 both leave solution "c"(or possibly "d") and jump to solution "b". After passing through the center spike, the intensities jump back to solution "c" or "d". Upon cooling, the intensities jump to solution "e" but solution "e" becomes complex right at the center and the intensities quickly jump to solution "b", pass through the center spike and jump back to solution "d" or "c".

Figures (39-41) show a traversal of the center region with the chartspeed increased by a factor of 200 (50mm/sec). I_1 is again the lower trace. Fig. (39) shows a jump to solution "e". At this chart speed the time constant of 0.25 sec in the meter monitoring I_2 becomes apparent. Figure (40) shows a jump to solution "b". After passing through the center spike, Fig (41) shows a return to solution "d" or "c". Notice an oscillation between solutions "c" and "d" in Fig (41).

Figs (42,43) show mode competition at 6.9 torr for one cavity mode being tuned back and forth (many times) around the doppler center. From the slope of the frequency monitor, it is seen that each pair is a cooling-heating (increasing-decreasing frequency)cycle. I_1 is the lower (clockwise) beam. The frequency monitor tracks I_1. Hence if beam I_1 is extinguished, there is no beam to track and the output drifts. It is of interest to note that when I_1 is extinguished and I_2 doubles, the frequency monitor output remains constant. However, the frequency monitor output does reflect intensity surges.

Due to the slower response time of the detector of I_2, it is preferable to look at this beam for a description of the mode competition. Consider the second cycle. The sequence of solutions are (c,d)-b-(c,d)-e-b-(c,d). The sequence for the third cycle is (c,d)-b-e-(c,d)---b-e-(c,d). The sequence for the fourth cycle is (c,d)-e-b-e-(c,d)---b-e-(c,d). Note that the center spike is always downwards for every cycle indicating that the backscattering into beam I_2 is always greater than

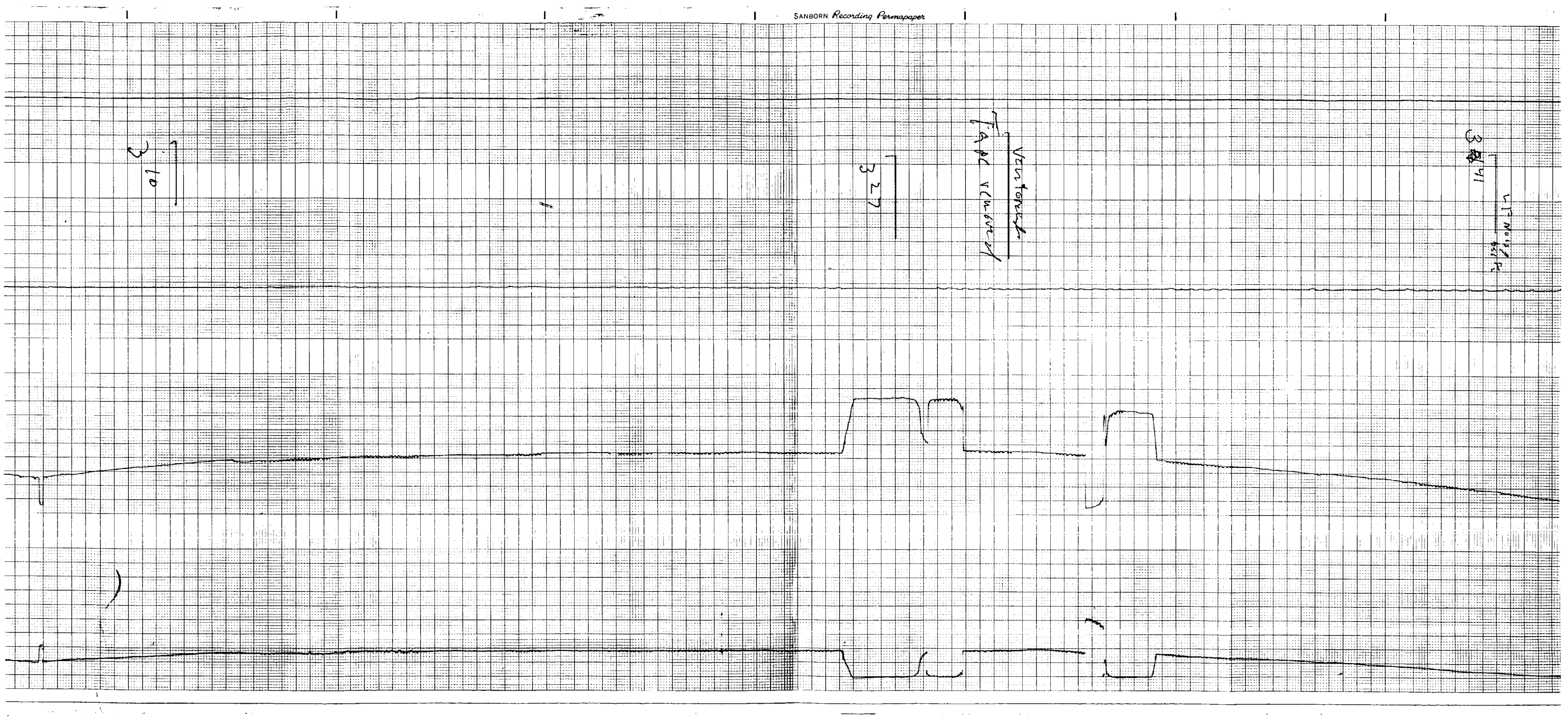

Figure 38 , Intensity VS Frequency-Heating and Cooling (One Cycle)

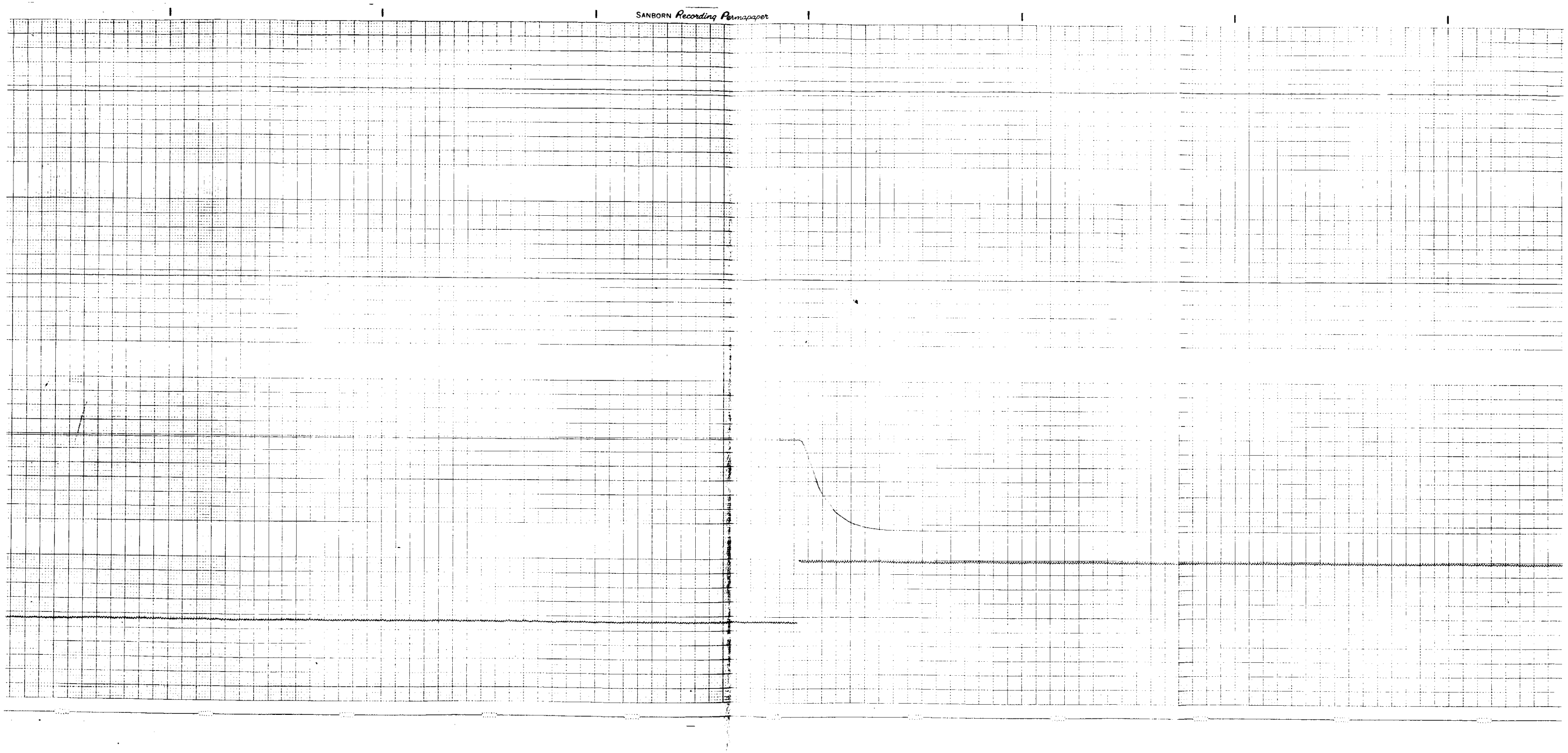

Figure 39 Intensity VS Frequency-High Chart Speed (Competition Region Entered)

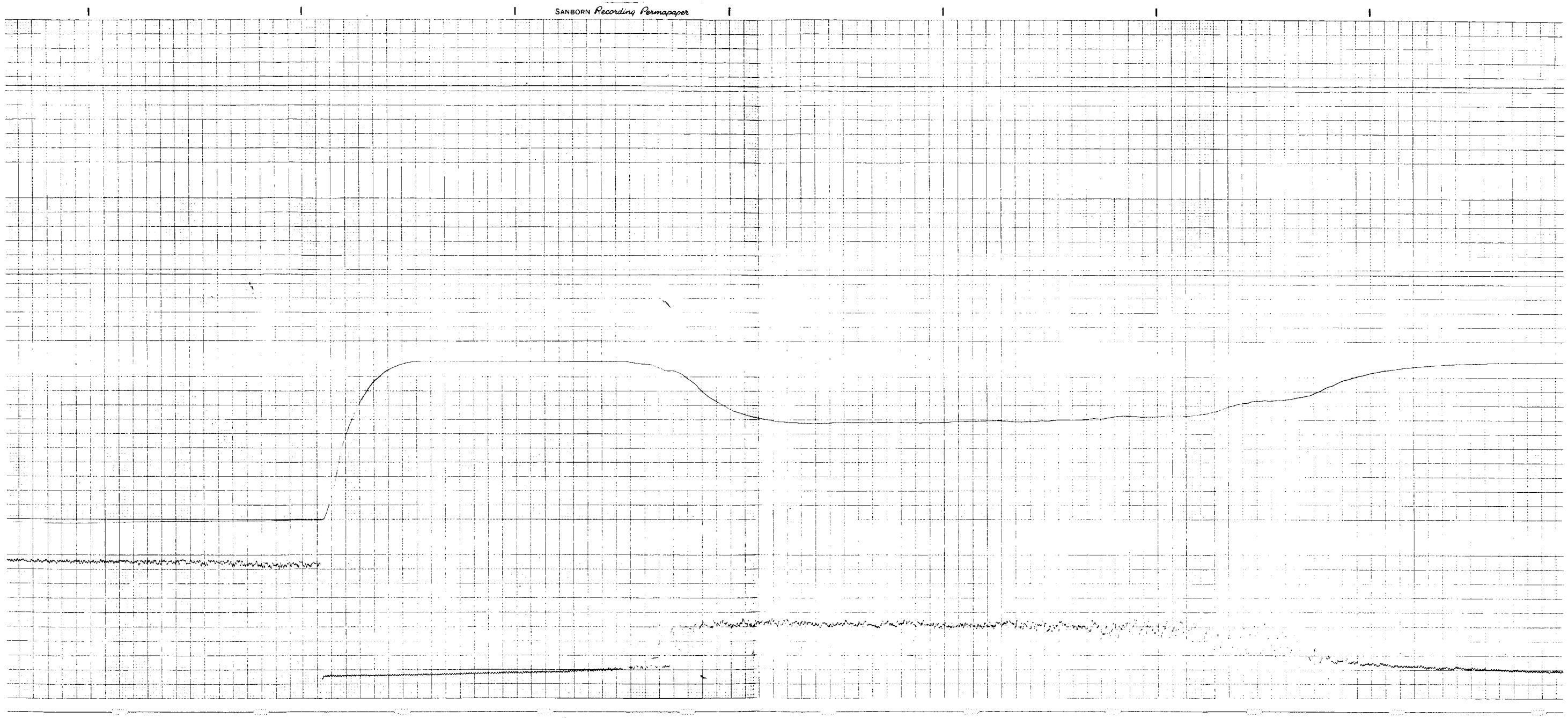

Figure 40 Intensity Vs Frequency-High Chart Speed (Center Spike)

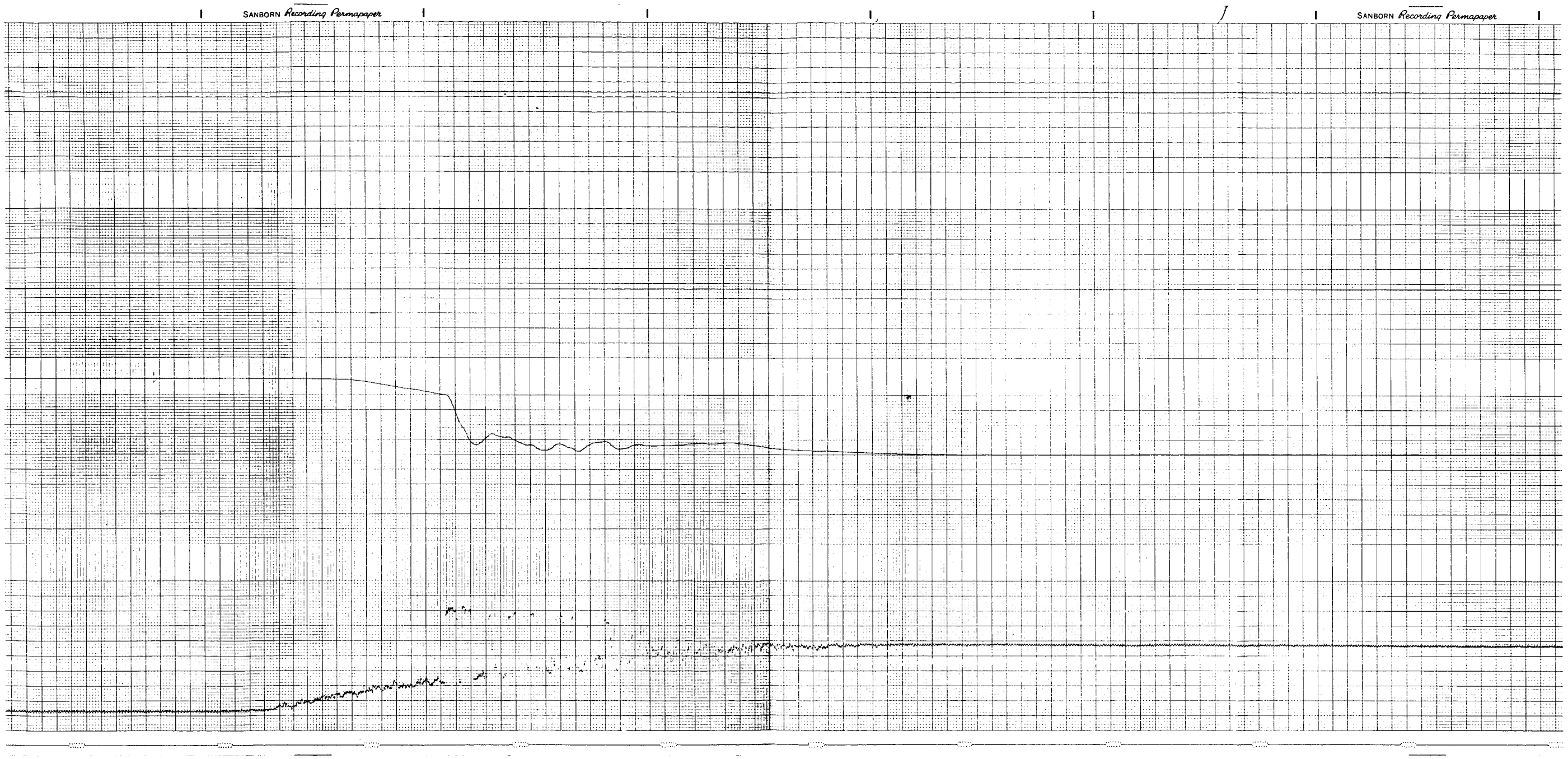

Figure 41 Intensity VS Frequency-High Chart Speed (Comptition Region Left)

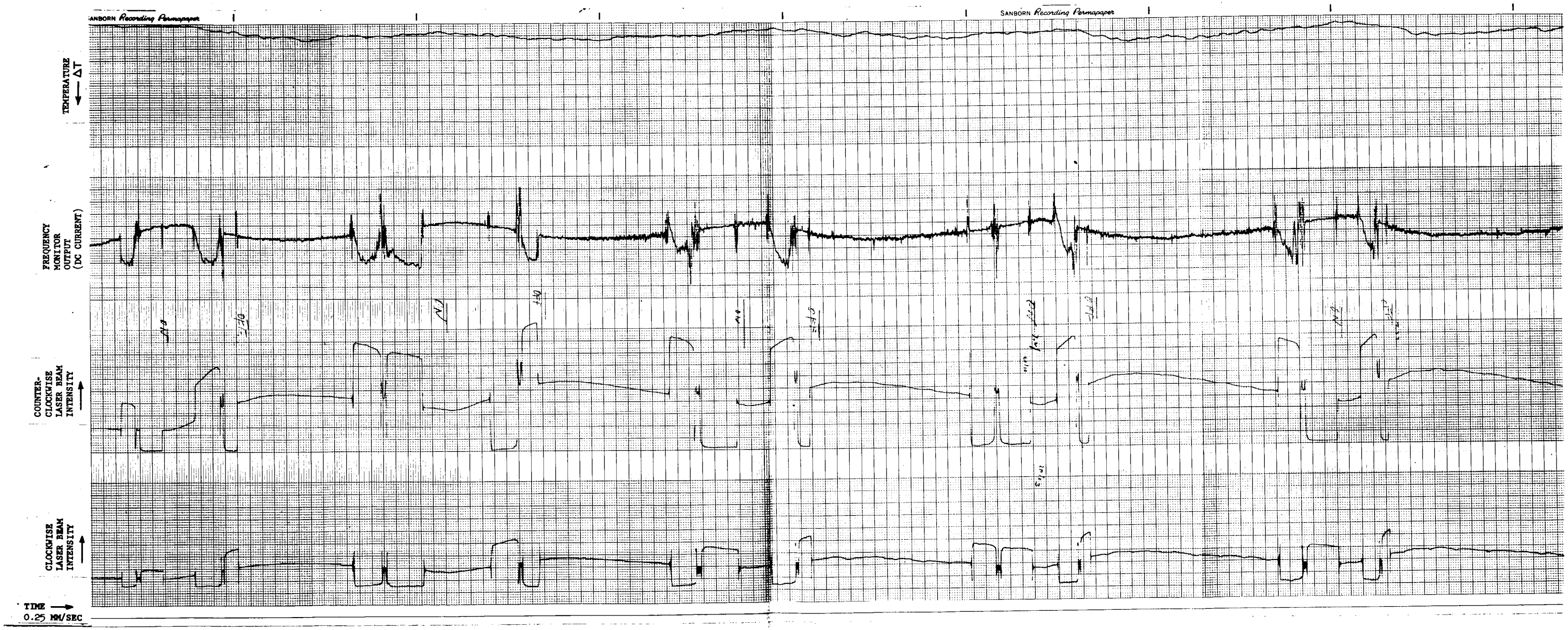

Figure 42 Mode Competition at 6.9 Torr Pressure, With Zeeman Frequency Monitor. (One cavity mode tuned about doppler center.)

Figure 43 Mode Competition at 6.9 Torr Pressure, With Zeeman Frequency Monitor. (One cavity mode tuned about doppler center. This is a continuation of Figure III-13.)

that into beam I_2.

The frequency monitor calibration is approximately 12MHz/mm, giving a competition width of approximately 50 MHz. The center spike is approximately 4 MHz wide.

22. RELATIONSHIP BETWEEN POSITION OF CENTER SPIKE AND GAIN MAXIMUM

As discussed in the section on the frequency monitor, zero d.c. feedback current output occurs at the frequency for which the laser beam experiences equal gain for both maximum excursions of the a.c. magnetic field. For a symetric gain curve, this frequency is the center of the atomic transition, or "true" doppler center. However, when the gain curve is assymetric due to pressure broadening or isotope broadening, the point of zero output will be shifted towards the point of maximum gain.

To consider this shift, first the magnitude of the a.c. magnetic field for optimum sensitivity will be calculated. Neglecting assymetric effects, the gaussian lineshape (normalized) is

$$g = \exp(-\xi^2) \tag{137}$$

If in an a.c. magnetic field the maximum zeeman splitting is ξ_z, the maximum differential gain is

$$\Delta g = \exp[-(\xi - \xi_z)^2] - \exp[-(\xi + \xi^2] \tag{138}$$

The sensitivity is the derivitive of Δg with respect to ξ, evaluated at $\xi = 0$, or

$$\Delta g' = 4\xi_z \exp - \xi_z^2 \tag{139}$$

Eq. (139) has a maximum at

$$\xi_z = \sqrt{2}/2 \tag{140}$$

Now consider the effect of the addition of another isotope whose transition center is shifted ξ_i from the center of the second isotope. If the relative number of atoms of the 2nd isotope is ϵ, the gain is

$$g = \exp(-\xi^2) + \epsilon \exp[-(\xi - \xi_i)^2] \tag{141}$$

The maximum differential gain in the presence of an a.c. magnetic field is

$$\Delta g = g(\xi \rightarrow \xi + \xi_z) - g(\xi \rightarrow \xi - \xi_z) \tag{142}$$

To find the frequency where the output of the frequency monitor is zero, one solves Eq. (142) for ξ when $\Delta g = 0$. When $\epsilon \ll 1$, then $\xi \ll 1$, and one finds

$$\xi_{zero} = \epsilon \exp(-\xi_i^2) \quad \frac{\sinh 2\xi_i\xi_z}{2\xi_z} \tag{143}$$

When the magnetic spliting is optimized, Eq (140, 143) gives

$$\xi_{zero} = \frac{\epsilon}{2} \exp(-\xi_i^2) \sinh 2\xi_i \tag{144}$$

For the Ne^{20} 1.15μ transition and when the second isotope is Ne^{22}, then $\xi_i = 0.56$ and Eq. (144) becomes

$$\xi_{zero} = 1.8\,\epsilon \text{ MHz} \qquad (\epsilon \text{ in percent}) \tag{145}$$

Using Eq. (141), the frequency at which the gain is a maximum was calculated and found to give the same shift as in Eq. 145.

The frequency monitor was filled with a single isotope such that $\epsilon = 10^{-2}$ percent. Thus the zero shift is much less than the sensitivity of the instrument.

The collision broadened lineshape is obtained from Eqs. (122,C18) and for $\eta \ll 1$ can be written as

$$g = \exp(-\xi^2) - \frac{2\eta'}{\pi}[1 - 2\xi F(\xi)] + cF(\xi) \tag{146}$$

The frequency at which the gain is a maximum is

$$\xi_{max} = c/2\,(1-2\eta') \tag{147}$$

The shift has been determined as 4.2 MHz/torr[18] for low pressures. This determines "c" as

$$c = 0.015p \qquad (p \text{ in torr}) \tag{148}$$

In obtaining Eq. (148), the relation[15]

$$\eta' = \frac{22p + 11}{500} \qquad (p \text{ in torr}) \tag{149}$$

has been used.

In the presence of an a.c. magnetic field, Eq. (142) holds for the differential gain, where the gain is given by Eq. (146). Isotope effects are neglected. To find the frequency where the output of the frequency monitor is zero, one again sets the differential gain equal to zero. Since $\xi_z = 2/2$ the Taylor expansion

$$F(\xi \pm \xi_z) = \pm F(\xi_z) + \xi F'(\xi_z) + \ldots \tag{150}$$

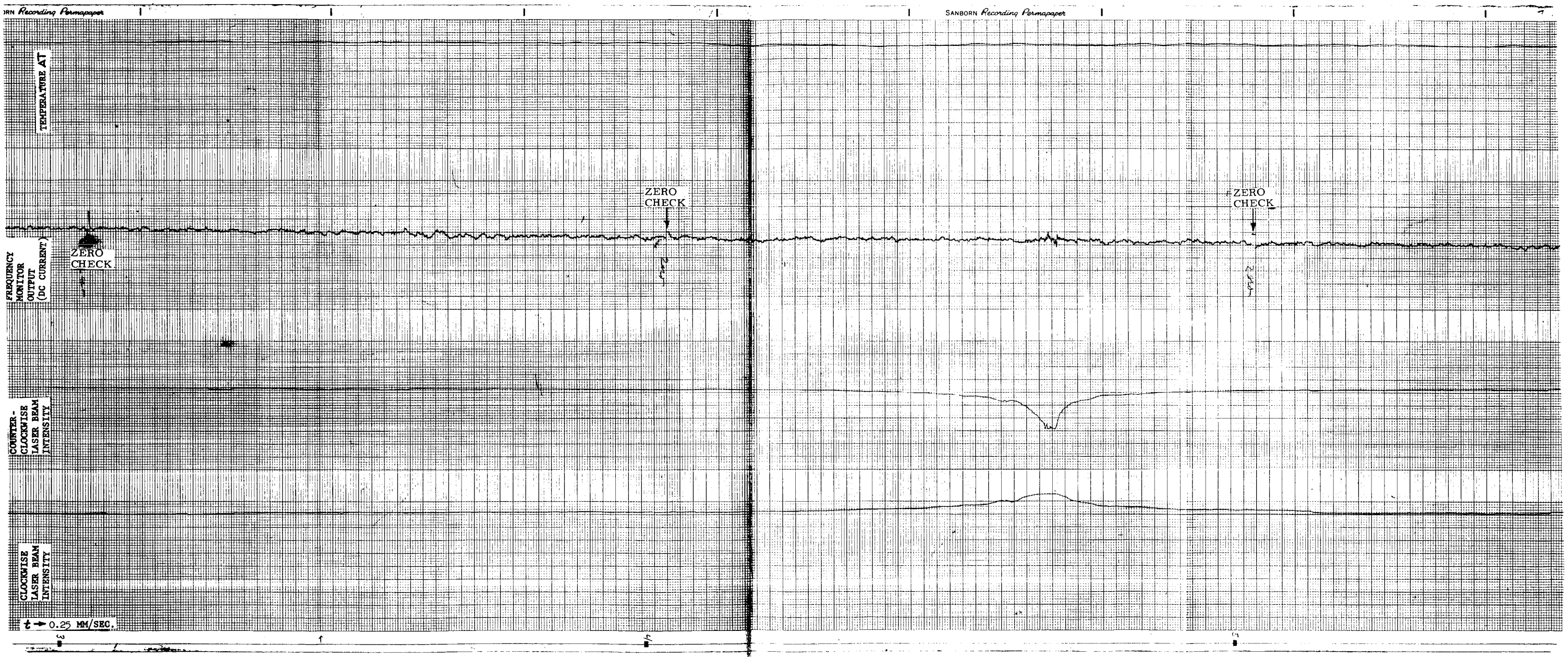

Figure 44 **Laser Gyro** Beam Intensities During Thermal Scanning. (Pressure of 3.2 Torr.)

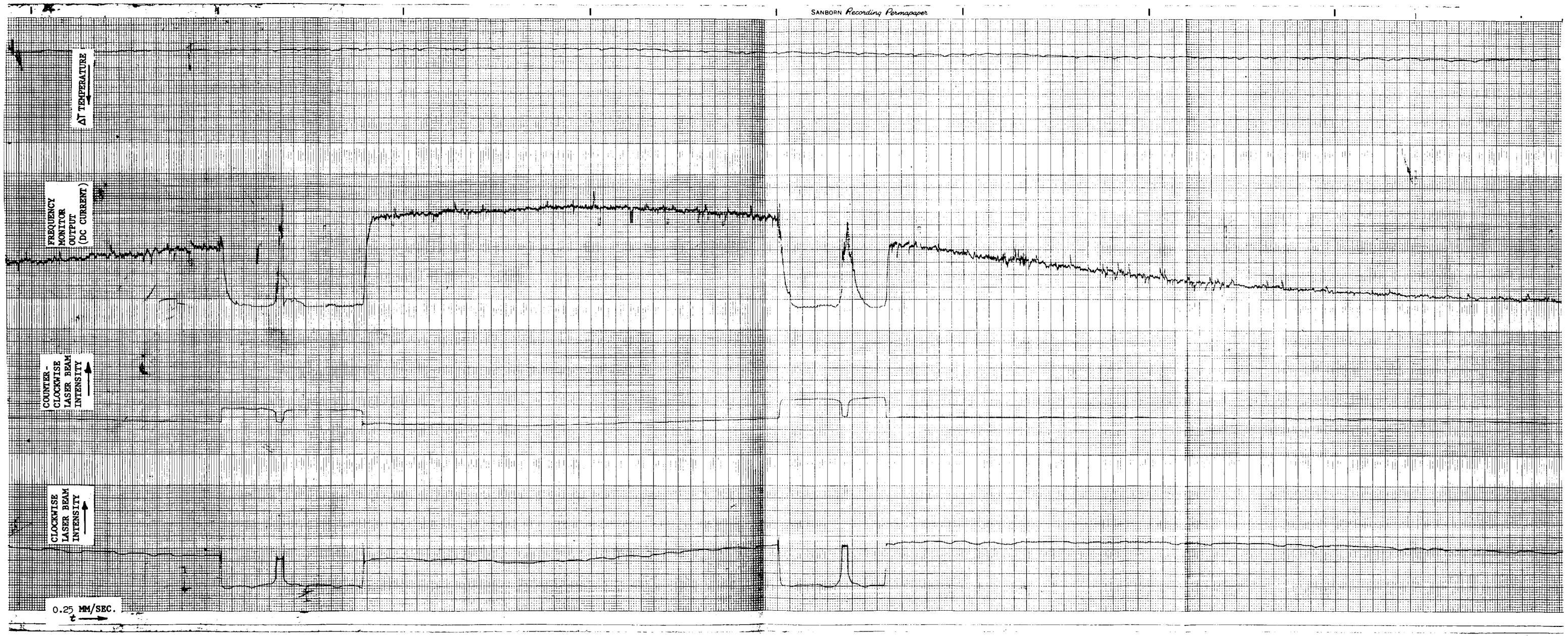

Figure 45 | Laser Gyro Beam Intensities During Thermal Scanning. (Pressure of 7.0 Torr.)

is used to give

$$\xi_{zero} \simeq \frac{c\,F(\xi_z)\,\exp(\xi_z^2)\,/\,2\xi_z}{1 - \frac{2\eta'}{\xi_z \pi^{\frac{1}{2}}} \exp \xi_z^2 [F(\xi_z) + \xi_z F'(\xi_z)]} \tag{151}$$

Using the optimum magnetic field splitting, Eq (151) becomes

$$\xi_{zero} = \frac{.38c}{(1-1.45\eta')} \tag{152}$$

Comparing Eq. (152, 147), it is seen the frequency at which the output of the frequency monitor is zero is below that at which the gain is a maximum. If the magnetic field were reduced such that the assymetry could be expressed by a linear function, the two expressions would be equal.

The frequency monitor gain cell was filled to a pressure of 6.4 torr. From Eqs. (147, 149) the shift of the gain maximum is 60 MHz to the high side. Note that at these pressures the frequency shift is no longer linear in pressure and Eq. (147) is only a rough approximation. From Eq. (152) the zero frequency monitor output point is 32 MHz.

In section 20 it has been shown that the center competition spike occurs within 2-3 MHz of the "true" doppler center. This is opposed to a "gain maximum" shift of 17 MHz for a laser pressure of 3.2 torr. Thus the seperation of 32 MHz between the zero frequency monitor output and the center competition spike should be readily observed. Figs. (44,45) show this effect. Figure (44) shows a slow thermal tune (decreasing frequency to the right) through the competition spike at the doppler center. The time scale is 0.25mm/sec. Points of "zero check" were placed on the output of the frequency monitor. It is seen that the center competition spike occurs well to the right (lower frequency) of the point where the frequency monitor output crosses the zero output. The frequency monitor calibration is 10-12 MHz/mm giving a seqaration of ~30-35 MHz.

Figure (45) shows one mode being tuned across the doppler center in an increasing and decreasing (frequency) direction. Note the slope of the frequency monitor. The gas pressure in the laser was 7.0 torr. The frequency monitor was tracking the clockwise beam, hence as the beam is extinguished, the output of the frequency monitor drifts. The "zero checks" on the frequency monitor have not been explicity marked but it can be observed that they lie ~29.5 mm up from the bottom

of the scale. In both cases the center spike is observed to lie 30-40 MHz on the low side of the zero frequency output of the frequency monitor.

It should be mentioned that the above was done while the laser was connected to a vacuum fill station and the gain tube was filled with the same gas and with the same fill station.

24. OPTICAL FEEDBACK

Backscattering of energy from one traveling wave into the direction of the other has bean shown to be a cause of mode competition. A method of controlling the mode competition is to reflect one of the transmitted beams back into the cavity and into the direction of the other beam.

The reflection mechanism was a 90° prism rather than a mirror. The alignment of the prism is much simpler since precise alignment is required in only one axis. A schematic of the optical feedback technique is shown in Fig (46). It is seen that energy from the counter clockwise beam is retroreflected into the beam traveling in the clockwise direction.

Figure (47) shows a strip chart recording of the intensities of the oppositely directed beams as a function of tuning three cavity modes across the doppler gain profile. The gas pressure was 3.2 torr. It is noticed that the half maximum width of the center competition spike has increased from the no external feedback value of 2-3MHz to the feedback value of 30 MHz. The offcenter competition spikes have also increased in width. Also the competition is such that the beam whose intensity increases, is always the clockwise beam. This is consistant with the mode competition model as shown in Figs (7,8).

The convention for labeling the beams I_1 or I_2 is that the back scattering coefficients satisfy $R_2 = KR_1$, $K<1$. The dominating source of backscattered energy is reflection by the prism of energy from the c.c.w. beam into the c.w. beam. Then the c.c.w. beam must be labeled I_1. Note that this labeling is different from the previous data. This was intentionally done so that external back scattering could reverse the direction of mode competition.

Referring to Fig (7) for I_2, it is seen that solution "c" dips down and agrees with the direction of competition in the c.c.w beam.

Since the beams are linearly polarized, a polarizer was inserted between the feedback prism and the laser. The amount of feedback was controlled as one mode was continuously scanned back and forth about the doppler center. It was observed that for decreasing amounts of feedback, the width of the competition region and depth both decreased. This is shown in Figs (48-50)

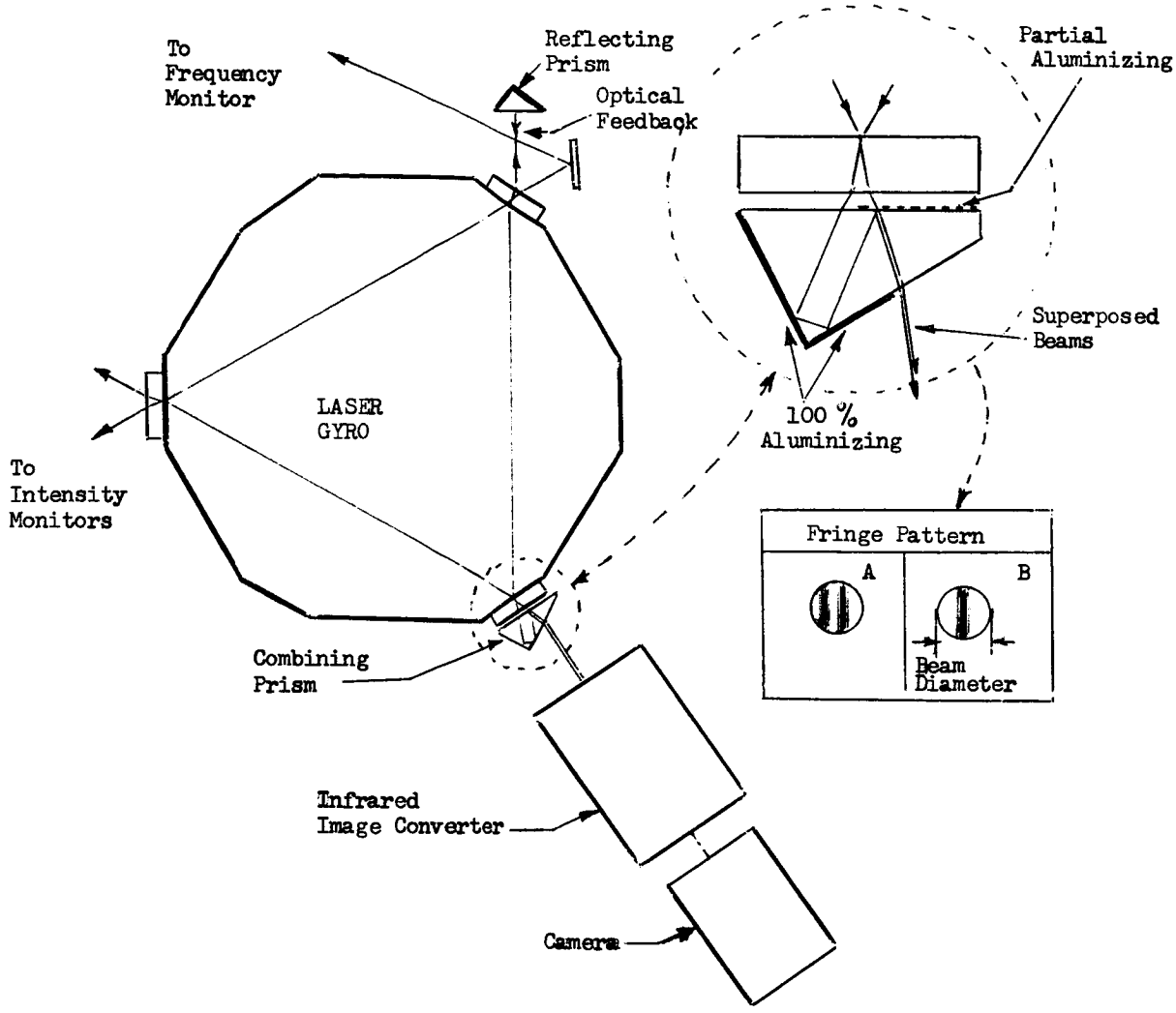

Figure 46 Fringe Measurement Method.

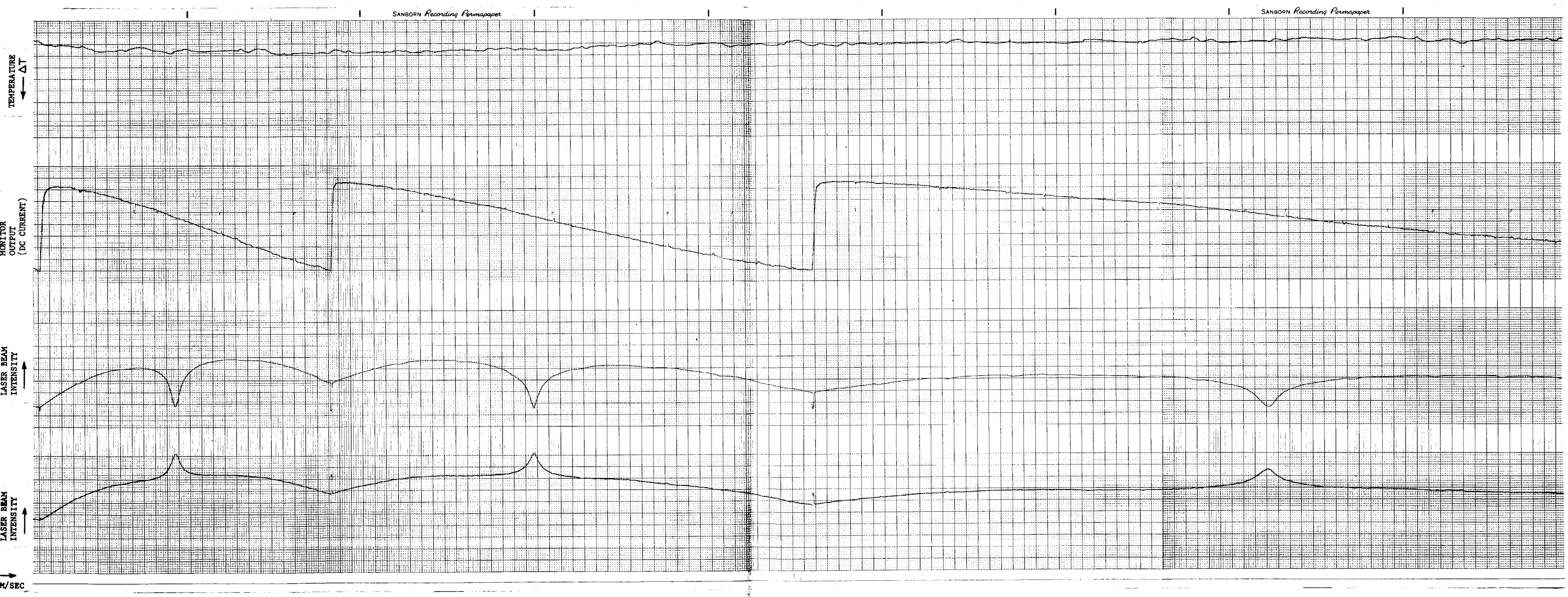

Figure 47 Mode Competition at 3.2 Torr Pressure, With Zeeman Frequency Monitor. Condition of maximum feedback.

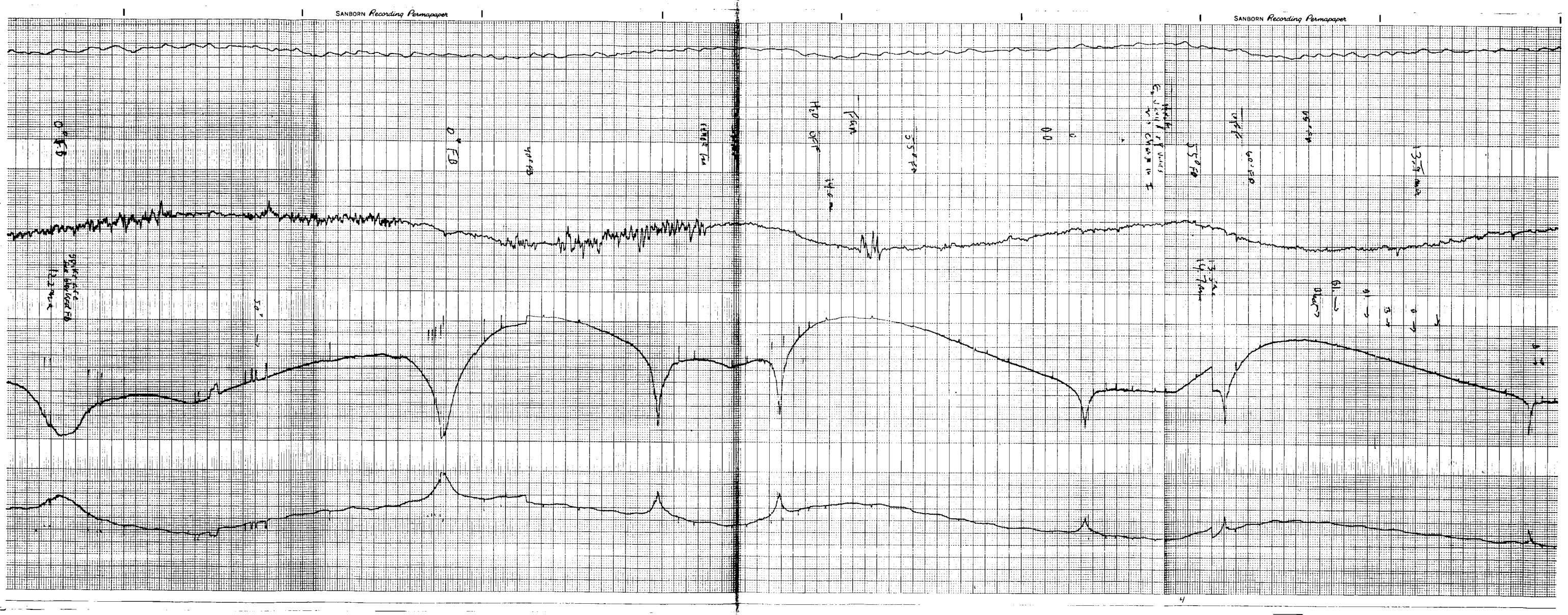

Figure 48 Mode Competition at 2.0 Torr Pressure, With Zeeman Frequency Monitor. (One cavity mode tuned about doppler center. Scans with varying amounts of optical feedback.)

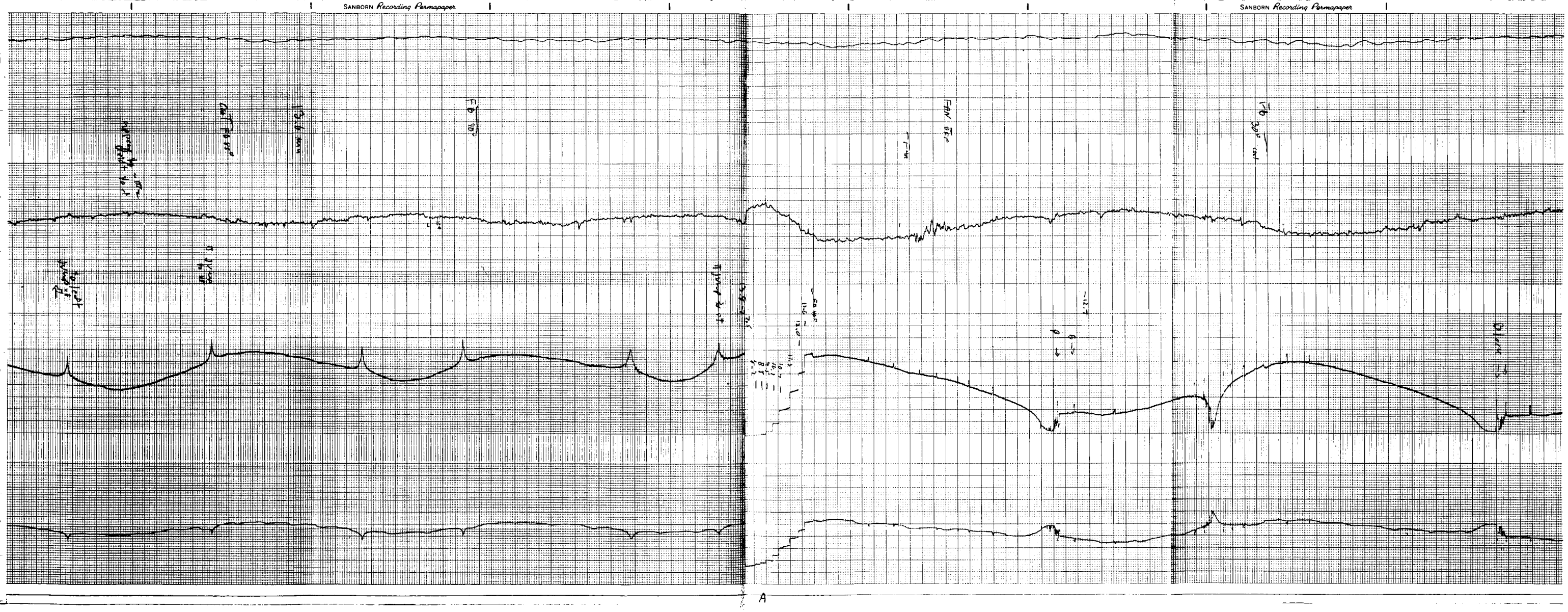

Figure 49 Mode Competition at 2.0 Torr Pressure, With Zeeman Frequency Monitor. (One cavity mode tuned about doppler center. Scans with varying amounts of optical feedback. This is a continuation of Figure III-21.)

Figure 50 Mode Competition at 2.0 Torr Pressure, With Zeeman Frequency Monitor. (One cavity mode tuned about doppler center. Scans with varying amounts of optical feedback. This is a continuation of Figure III-22.)

for a gas pressure of 2.0 torr. In Fig (48), the angle at which the polarizer was set, for the first three groups of back and forth cycles was 0^{o}, 40^{o}, 55^{o}, respectively. Maximum feedback is signified by 0^{o}. The last competition spike was for 65^{o}. The narrow spikes seen supperimposed on the intensity curves are the intensities when the feedback prism was momentarily blocked. In Fig (49) the second, third and fourth cycles are for 85^{o}, 90^{o}, 0^{o}, respectively. Note that the backscattering from the external prism causes a change in the direction of competition. Figure (50) shows competition spikes with maximum feedback. The last spike is for zero feedback. Note that the backscattering extinguishes the c.c.w. beam and that there is a long assymetric tail on the spike, on the high frequency side.

25. PHASE DIFFERENCE BETWEEN OPPOSITELY DIRECTED BEAMS

The phase difference between the oppositely directed beams was measured as a function of frequency tuning the laser oscillation across the doppler gain curve. The laser was connected to the fill station and the beams were frequency synchronized. The fringe pattern was formed by combining the beams with a single prism. Photographs of the fringe pattern were taken through an image converter using XXX film. Figure (46) shows the fringe measurement method.

Figure (51) shows the results of a typical frequency scan: The fringe pattern spacing was adjusted such that only two maximum, at most, occur. The phase difference is seen to be a constant over the doppler curve, with jumps of π at the mode competition points.

Figure (52) shows a slow seen across the doppler center for a pressure of 3.2 torr. A sequence of 4 sec exposures were taken at the indicated points. The fringe pattern results are shown in Figure (53). The vertical line signifies a reference which was obtained by superimposing a heated wire on the image converter. It is seen that a constant phase difference exists with a jump of π between frames 19 and 20. Referring to Figure (52) it is seen that this is the peak of the mode competition spike. The frequency monitor calibration is 10 - 12 MHz/mm, giving a mode competition spike width of 1.4-1.7 MHz. Figure (54) shows the results of a slower scan over a period of 5 hours. A portion of the recorder chart is shown in Fig (44). The times at which the fringe measurements were taken are noted at the bottom border. The frequency monitor output and the intensity outputs over the entire measurement period are sketched in Fig (54). Again, the results show a constant phase difference with a jump of π at the doppler center.

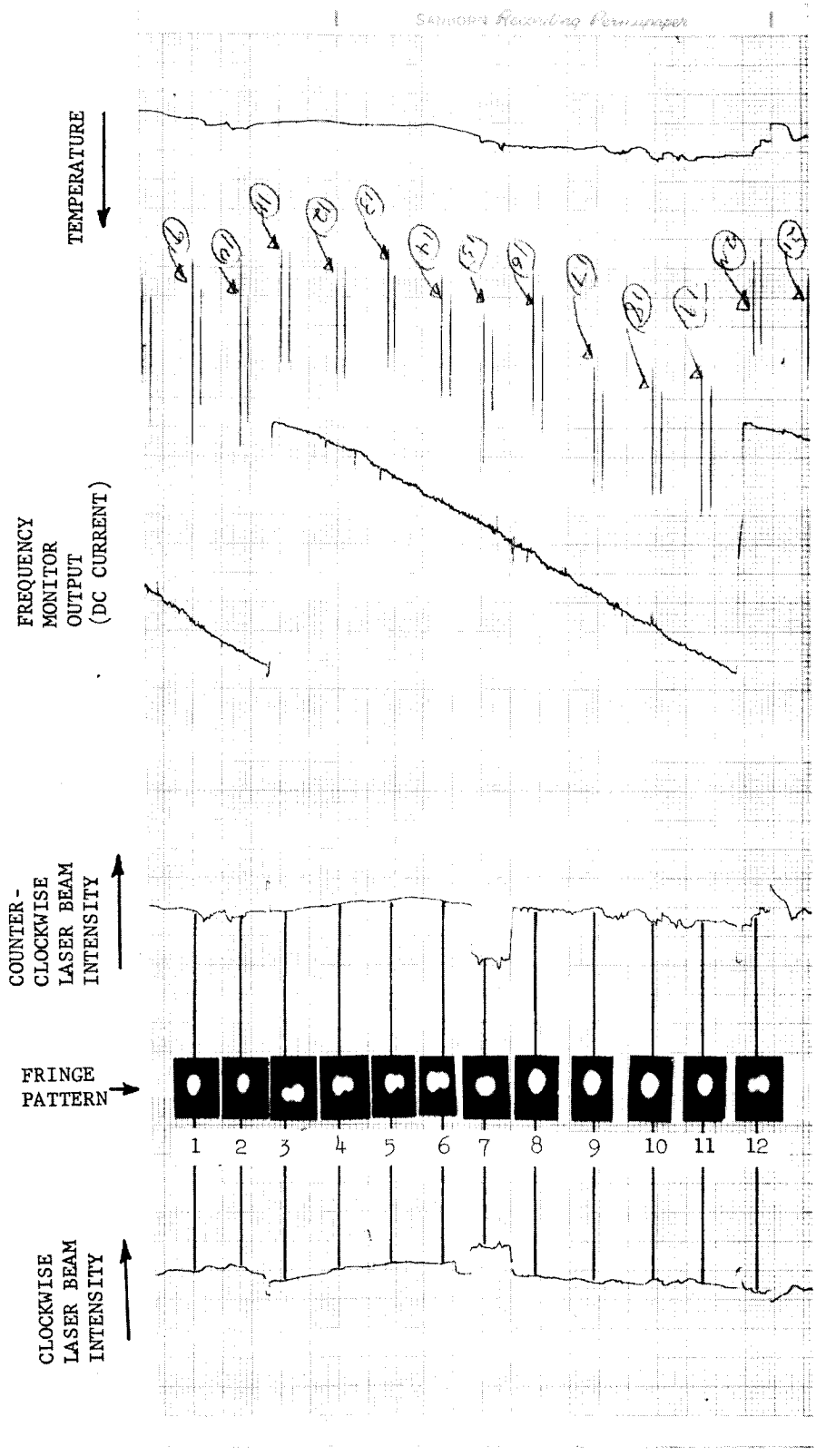

Figure 51 Laser Gyro Output and Corresponding Fringe Patterns During a Thermal Frequency Scan (Heating.).

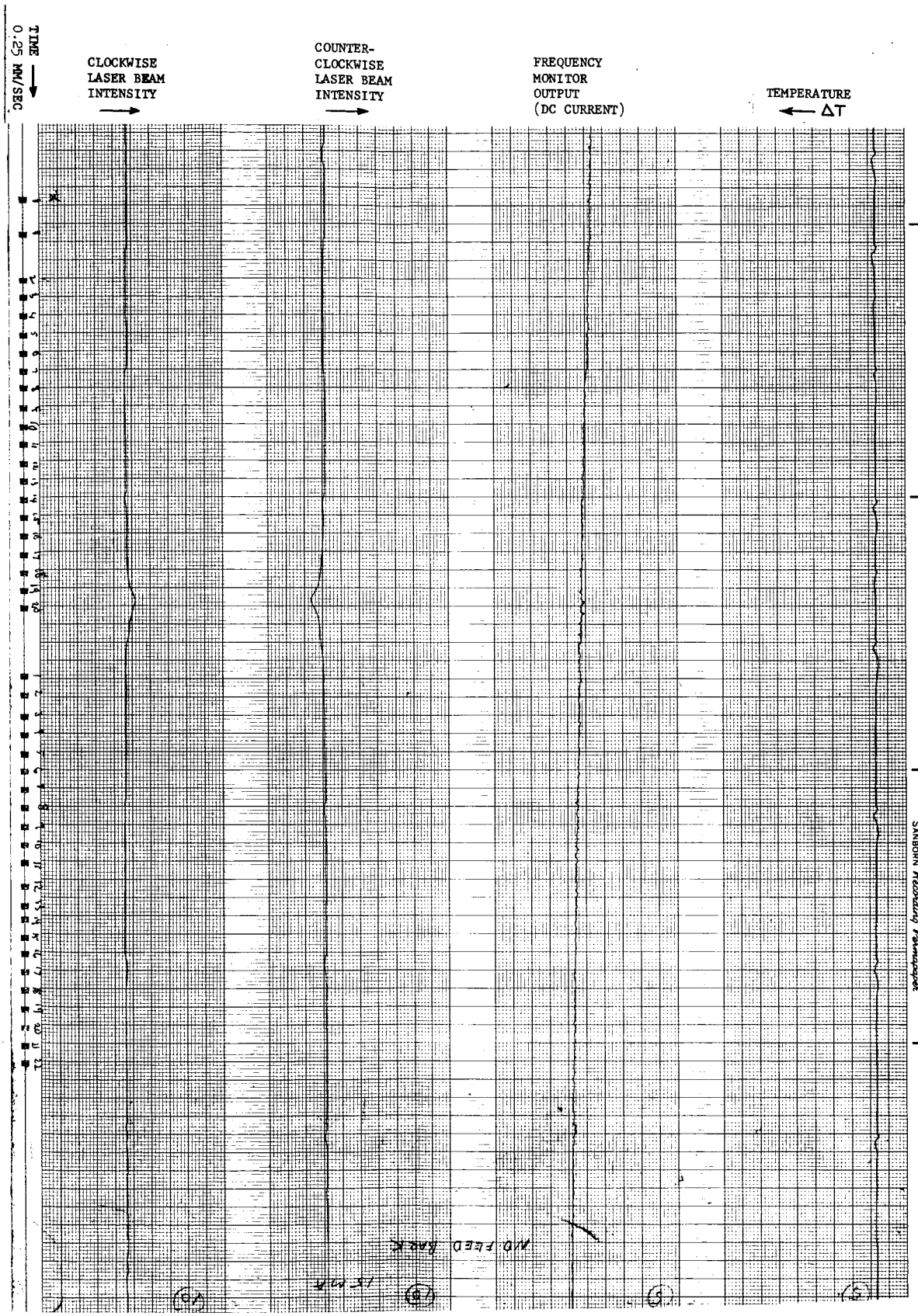

Figure 52 Laser Gyro Output Showing Times When Photographs of Fringe Pattern Were Made.

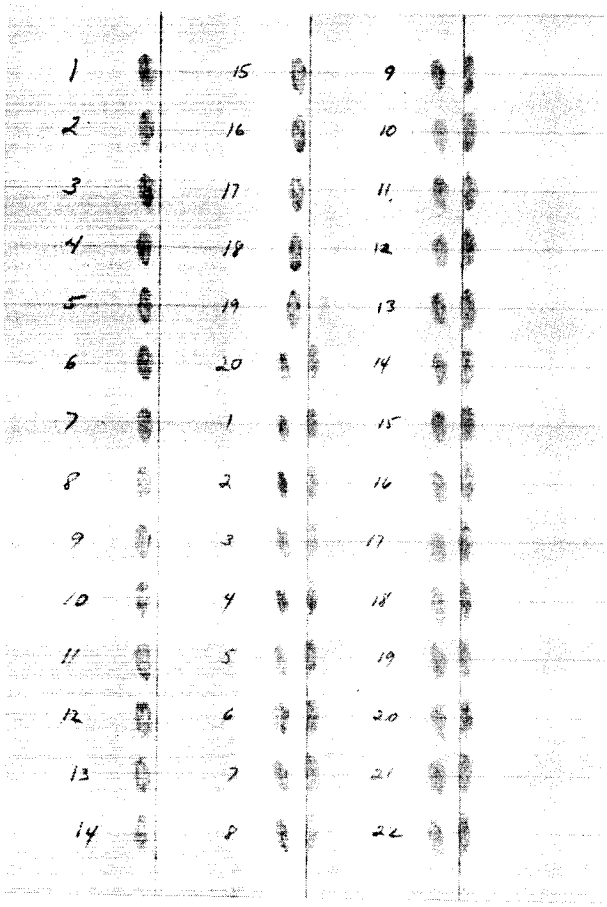

Figure 53 Sequential Map Made From Photographs of Fringe Pattern Position Taken During Thermal Frequency Scan. (Pressure of 3.2 Torr.)

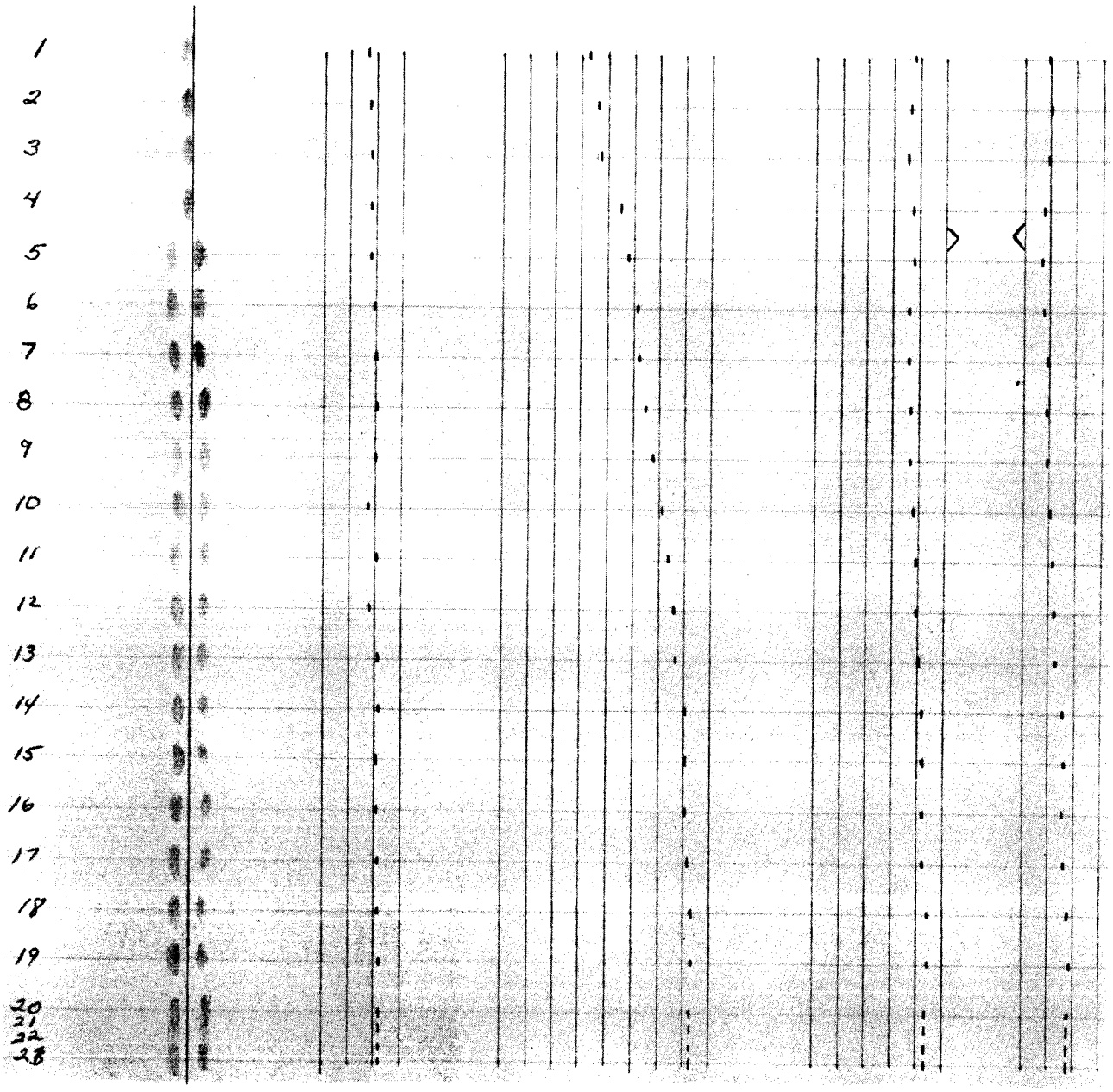

Figure 54 Sequential Map Made From Photographs of Fringe Pattern Position Taken During Thermal Frequency Scan. (Total Elapsed Time of 5 hours.)

26. ROTATION DRIFT DATA

As a means of investigating the stability of the laser when operated as an integrating gyro, a fringe pattern was formed from the outputs of the oppositely directed beams, as shown in Fig (46). When the laser is rapidly rotated, the two beams are unlocked in frequency and there is a motion of the fringe pattern at the frequency difference rate.

A direct measurement of the fringe pattern rate of motion determines the angular velocity at which the laser is rotated. A count of the number of fringe pattern cycles passing a fixed detector determines the angular displacement of the laser.

The laser was rapidly turned, first in one direction and then in the other. The magnitude of the rotation rate was the same for both directions and was much larger than the lock-in threshold. As the laser was turned in, say, the positive direction, positive counts accumulated. When the laser turned in the negative direction, negative counts were subtracted from the total. At the end of a fixed interval of 100 seconds (measured to a precision of better than 1 part in 10^6), the net number of counts were recorded. The net number of error counts attributed to a net displacement was estimated to be less than 10 counts.

If the laser were on a frame such that the optical paths for the oppositely directed rotating beams were equal (no null shift bias and no rotational motion such as earths rate) the net number of accumulated counts during the 100 second interval would be equal to the error counts. After five hours the average net accumulated counts per one hour interval was 16,288 counts, corresponding to a net rotation of 14.2 deg/hr. The accumulated counts per 100 second interval is shown in Fig. (55). A formal analysis is given in Appendix G.

The rotation was in the direction of the rotation of the earth and at this lattitude the net average bias null shift was 3.6 deg/hr. As a measure of the accuracy of the bias rotation a 1σ value was calculated as 0.34 deg/hr.

The method used in calculating the 1σ value is as follows. The time interval

Figure 55 Accumulated Counts vs Time

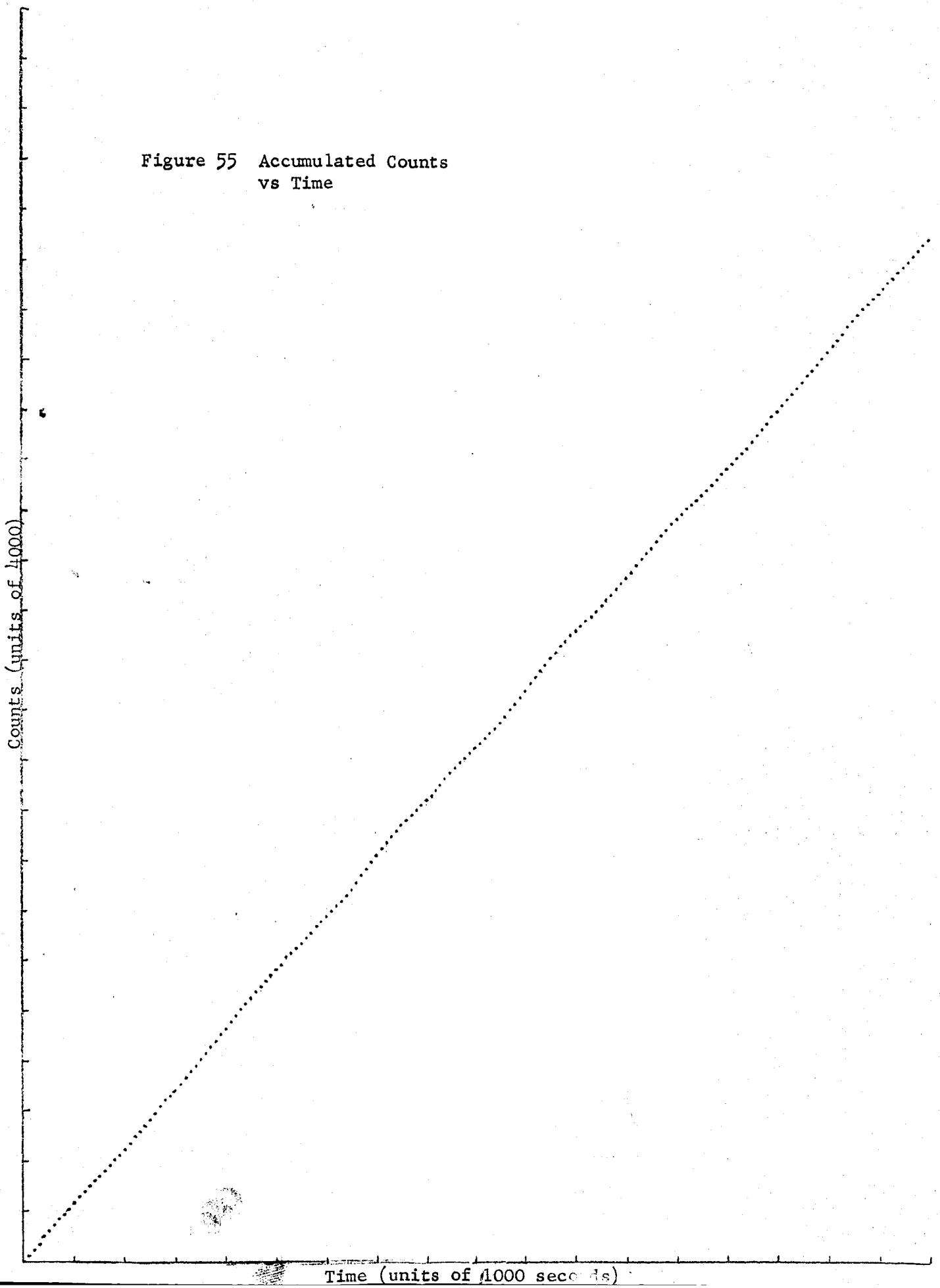

was chosen as one hour. The difference between accumulated counts over time intervals of 36 x 100 sec. = 1 hour was obtained for successive 100 second points. The RMS of the accumulated one hour counts was 388 counts which gave the above 1σ value.

The percentage of points which differed from the average one hour accumulated counts by: less than the 1σ value was 58.3 percent; less than the 2σ values was 96.9 percent; less than the 3σ value was 100.0 percent. Thus the distribution, compared to a normal distribution, is more flattened at the center and falls off slightly faster at the wings. The largest deviation from the mean was 2.17σ.

27. EQUIPMENT LIST

- Quartz Block Ring Laser and Dielectric Coated Mirrors (1.15μ):
- D.C. Power Supply for Laser:
- Detectors (two) for 1.15μ radiation, Hoffman EA7E1 Photovoltaic Silicon Cells:
- Infra-red Pass Optical Filters (two) for Detectors:
- D.C. Amplifiers for Detectors, (one) Kintel Model 207B and (one) Keithley Instruments Mode 610A Electrometer:
- Four Channel Sanborn Strip Chart Recorders:
- Thermistors (two) for Temperature Monitoring of Quartz Block:
- Zeeman Cell Frequency Monitor:
- Vacuum Fill Station and He^3 and Ne^{20} gas:
- Right Angle Prism (two) for Fringe Pattern and for Back Reflection:
- Optical Wedge
- Infra-red Image Convertor:
- Heat Transfer Plate for Thermal Tuning of Laser:
- Glan Thomson Prism Polarizer:
- 35 mm Camera (xxx Film) for Fringe Pattern Recording:
- Heated Wire for Fringe Pattern Reference
- Honeywell 1800 Computor:
- Honeywell 400 Computor:
- Rate Table-Lietz
- Optical Gate:
- Digital Counter, Computor Measurements Co. Model 2887A:

REFERENCES

1. F. Aronowitz, Phys. Rev., 139 A635 (1965)
2. W. M. Macek and D. T. M. Davis, Jr., Appl. Phys. Letters, 2, 67 (1963).
3. W. E. Lamb, Jr., Phys. Rev., 134 A1429 (1964).
4. W. M. Macek, et.al. Optical Masers Polytechnic Press, Bklyn, N.Y. 1963
5. R. A. McFarlane, W. R. Bennett, Jr. and W. E. Lamb, Jr. Appl. Phys. Letters, 2 189 (1963)
6. R. A. McFarlane, Phys. Rev 135 A543 (1964)
7. J. Haisma and G. Bouwhuis, Phys. Rev. Letters 12 287 (1964)
8. G. J. Sagna, Phys. Radium 4 177 (1964)
9. A. A. Michelson and H. G. Gale, Nature 115 566 (1925) Astrophys. J. 61 137 (1925)
10. A. H. Rosenthal, Jr. Opt. Soc. Am. 52 1143 (1962)
11. C. V. Heer, Phys. Rev., 134, 799 (1964)
12. W. E. Lamb, Jr., and T. M. Sanders, Jr., Phys. Rev. 119, 1901 (1960)
13. B. D. Fried and S. D. Conte, The Plasma Dispersion Function (Academic Press, Inc., New York, 1961)
14. W. R. Bennett, Jr., Phys. Rev. 126, 580 (1962); Quantum Electronic Paris 1963 (Columbia Univ. Press, New York, 1964), p. 441.
15. A Szoke and A. Javan, Phys. Rev. Letters 10, 521 (1963); Phys. Rev 145 137 (1965)
16. R. A. Fork and M. A. Pollock, Bull. Phys. Rev 139 A1408 (1965)
17. P. H. Lee and J. G. Atwood have reported, at the Quantum Electronics Conference (Phoenix 1966), mode competition and extinction of one of the beams due to differential losses of the order of 10^{-4}.
18. A. D. White, J. Quantum Electr., QE1 349 (1965) p. 352
19. A. Yildiz and C. H. Tang, Phys. Rev. 146 947 (1966)

APPENDIX A

Determination of Self-consistant Equations

Consider the field to be a linearly polarized plane wave with the Poynting vector in the z-direction. It is assumed that the field can be closed upon itself by some means without losing its plane wave properties. Thus Maxwell's equations can be solved in Cartesian coordinates for one dimension only. It is also assumed that the frame is rotating with a projection of the angular velocity of $(-\Omega_{rot})$ along the normal to the plane of the cavity.

The one-dimensional form of Maxwell's equations expressed in the rotating frame[11] are (MKS units)

$$\frac{\partial E}{\partial z} + \frac{\partial B}{\partial t} = 0 \quad , \tag{A1}$$

$$\frac{\partial H}{\partial z} + \frac{\partial D}{\partial t} + J = 0 \quad , \tag{A2}$$

$$B = \mu_o H - E \quad , \tag{A3}$$

$$D = \epsilon_o E + P - aH \quad , \tag{A4}$$

$$J = \sigma E + \sigma_s E_s \quad , \tag{A5}$$

Where

$$a = 2A\,\Omega_{rot}/(Lc^2) \tag{A6}$$

and L is the optical path of the cavity and A is the geometric area enclosed by L. Maxwell's equations are written only to first order in Ω_{rot}. The effects of a medium in the cavity have been taken into account, to first order, by considering L to be the optical path traversed by the light beam[19].

In Equation (A5) the current density has been written as the sum of two terms. The first represents the losses of the cavity and the fictional conductivity can be expressed in terms of the passive Q of the cavity as

$$\sigma/\epsilon_o = \omega/Q \tag{A7}$$

The second term in Equation (A5) represents losses due to forward scattering and back scattering. Whether or not this term is actually a loss will depend upon the phase of the scattered radiation with respect to the phase of the oscillations. This term and the term in P in Equation (A4) will be treated as a source term in the inhomogeneous wave equation for the electric field intensity.

Combining Equations (A1 - A5, A7) the one dimensional inhomogeneous wave equation for the electric field intensity becomes

$$-\frac{1}{\epsilon_o\mu_o}\frac{\partial^2 E}{\partial z^2} + \frac{\omega}{Q}\frac{\partial E}{\partial t} + \frac{\partial^2 E}{\partial t^2} + \frac{2a}{\epsilon_o\mu_o}\frac{\partial^2 E}{\partial z \partial t} = \frac{\omega^2 P}{\epsilon_o} - \frac{\sigma_s}{\epsilon_o}\frac{\partial E_s}{\partial t} \qquad (A8)$$

In Equation (A8) only terms linear in "a" have been retained and since the macroscopic polerization is nearly monochromatic, the second time derivative of P has been replaced by $-\omega^2 P$.

For the case of an empty lossless cavity (no scattering) containing two oppositely directed traveling waves, the solution of Equation (A8) gives

$$E(z,t) = E_1 \sin(Kz + \Omega t) + E_2 \sin(Kz - \Omega t). \qquad (A9)$$

This leads one to expand the solution of Equation (A8) into the set of empty cavity normal mode eigenfunctions (ECNME)

$$E(z,t) = \Sigma_n \left[A_n(t)\, U_n(z) + \tilde{A}_n(t)\, V_n(z)\right] \qquad (A10)$$

with

$$U_n(z) = \sin K_n z\ , \qquad (A11)$$

$$V_n(z) = \cos K_n z\ . \qquad (A12)$$

For a ring cavity of length L, E(z,t) satisfies periodic boundary conditions giving the wave number

$$K_n = 2\pi n/L\ . \qquad (A13)$$

The ECNME satisfy the equation

$$\left[\frac{d^2}{dz^2} + \epsilon_o \mu_o \Omega_n^2\right] \begin{pmatrix} U_n(z) \\ V_n(z) \end{pmatrix} = 0 \quad . \tag{A14}$$

Making use of the orthogonality properties of the ECNME, equations (A8, A10, A14) give the set of coupled equations for the time dependent coefficients of ECNME as

$$\frac{d^2 A_n}{dt^2} + \frac{\omega}{Q_n} \frac{dA_n}{dt} + \Omega_n^2 A_n - 2aK_n \frac{c^2 d\tilde{A}_n}{dt} = \frac{\omega}{\epsilon_o}^2 P_n - \frac{\sigma_s}{\epsilon_o} \frac{d}{dt} E_{sn} , \tag{A15}$$

$$\frac{d^2 \tilde{A}_n}{dt^2} + \frac{\omega}{Q_n} \frac{dA_n}{dt} + \Omega_n^2 \tilde{A}_n + 2 a K_n \frac{c^2 dA}{dt} = \frac{\omega}{\epsilon_o} \tilde{P}_n - \frac{\sigma_s}{\epsilon_o} \frac{d}{dt} \tilde{E}_{sn} , \tag{A16}$$

with

$$P_n(t) = (2/L) \int_o^L P(z,t)\, U_n(z)\, dz, \tag{A17}$$

$$\tilde{P}_n(t) = (2/L) \int_o^L P(z,t)\, V_n(z)\, dz, \tag{A18}$$

$$E_{sn}(t) = (2/L) \int_o^L E_s(z,t)\, U_n(z)\, dz, \tag{A19}$$

$$\tilde{E}_{sn}(t) = (2/L) \int_o^L E_s(z,t)\, V_n(z)\, dz. \tag{A20}$$

In Equations (A15, A16) the Q of each mode has been subscripted for greater generality.

As discussed by Lamb, for the case of the principal mode separation being much greater than the passive cavity width such that time dependent Fourier components of A_n which are far removed from the cavity resonance can be neglected, one can write

$$A_n(t) = E_{1n}(t) \cos \theta_{1n} + E_{2n}(t) \cos \theta_{2n} \tag{A21}$$

$$\tilde{A}_n(t) = E_{1n}(t) \sin \theta_{1n} - E_{2n}(t) \sin \theta_{2n} \tag{A22}$$

where

$$\theta_{in} = \omega_{in}t + \varphi_{in}(t) \qquad i = 1,2. \tag{A23}$$

The Fourier components of the polarization are written as "in phase" and "in quadrature" term with respect to frequency "one", or

$$P_n(t) = S_{1n}(t) \sin \theta_{1n} + C_{1n}(t) \cos \theta_{1n} \tag{A24}$$

$$\tilde{P}_n(t) = \tilde{S}_{1n}(t) \sin\theta_{1n} + \tilde{C}_{1n}(t) \cos \theta_{1n} \tag{A25}$$

In Equations (A21-A25), the time dependent coefficients are slowly varying with respect to optical frequencies. The form of equations (A21, A22) are such as to reduce, in an empty cavity to two oppositely directed traveling waves with different frequencies and amplitudes.

Now to consider the scattering source terms in Equations (A15, A16). Refer to Figure A1. It will be assumed that there exists some mechanism for

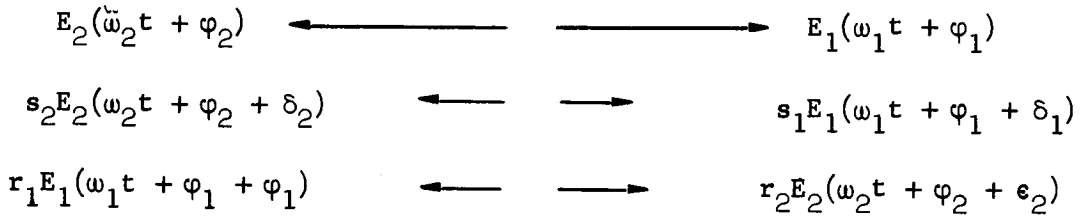

Figure A1. Scattering Source Terms

both forward and back scattering. For forward scattering, some of the energy from each beam is scattered in the same direction as the beam from which the scattered energy originated, but with some phase angle. For back scattering, some of the energy from each beam is scattered in the opposite direction of the beam from which the scattered energy originates, again with some aribitrary phase angle. Thus going in the same direction as beam "one", is scattered energy of the same frequency as beam "one" but with some phase difference, plus energy with the frequency of beam "two". The same type of statement applies to the energy traveling in the opposite direction. Using the traveling wave formalism as in Eqs. (A9, A10) and

substituting into Eqs. (A19, A20), the Fourier components of the scattering fields are found as

$$E_{sn} = r_{1n}E_{1n}\cos(\theta_{1n} + \epsilon_{1n}) + r_{2n}E_{2n}\cos(\theta_{2n} + \epsilon_{2n}) + s_{1n}E_{1n}\cos(\theta_{1n} + \delta_{1n}) + s_{2n}E_{2n}\cos(\theta_{2n} + \delta_{2n}) \tag{A26}$$

$$\tilde{E}_{sn} = -r_{1n}E_{1n}\sin(\theta_{1n} + \epsilon_{1n}) + r_{2n}E_{2n}\sin(\theta_{2n} + \epsilon_{2n}) + s_{1n}E_{1n}\sin(\theta_{1n} + \delta_{1n}) - s_{2n}E_{2n}\sin(\theta_{2n} + \delta_{2n}) \tag{A27}$$

The terms in r_{in} and s_{in} $(i = 1,2)$ signify energy being back and forward scattered, respectively, into the n^{th} mode traveling in the direction of the radiation oscillating at frequency ω_i. The $\underline{r}$ and $\underline{s}$ coefficients are the back and forward scattering coefficients, respectively, and are considered to be much less than unity.

Substituting Equations (A21-A27) into Equations (A15, A16) and equating coefficients of $\sin\theta_{1n}$ and $\cos\theta_{1n}$ to zero, four equations are obtained, which when manipulated give

$$\dot{E}_{1n} + \frac{\omega}{2Q_n}E_{1n} = \frac{\omega}{4\epsilon_o}(\tilde{C}_{1n} - S_{1n}) - \frac{\sigma_s}{2}r_{2n}E_{2n}\cos(\psi_n + \epsilon_{2n}) - \frac{\sigma_s}{2\epsilon_o}s_{1n}E_{1n}\cos\delta_{1n} \tag{A28}$$

$$\dot{E}_{2n} + \frac{\omega}{2Q_n}E_{2n} = \frac{\omega}{4\epsilon_o}\left[(\tilde{S}_{1n} - C_{1n})\sin\psi_n - (S_{1n} + \tilde{C}_{1n})\cos\psi_n\right] - \frac{\sigma_s}{2\epsilon_o}r_{1n}E_{1n}\cos(\psi_n - \epsilon_{1n}) - \frac{\sigma_s}{2\epsilon_o}s_2E_{2n}\cos\delta_{2n} \tag{A29}$$

$$(\Omega_{1n} - \dot{\theta}_{1n})E_{1n} = \frac{\omega}{4\epsilon_o}(C_{1n} + \tilde{S}_{1n}) + \frac{\sigma_s}{2\epsilon_o}r_{2n}E_{2n}\sin(\psi_n + \epsilon_{2n}) + \frac{\sigma_s}{2\epsilon_o}s_{1n}E_{1n}\sin\delta_{1n} \tag{A30}$$

$$(\Omega_{2n} - \dot{\theta}_{2n})\, E_{2n} = \frac{\omega}{4\epsilon_o}\left[(C_{1n} - \tilde{S}_{1n})\cos\psi_n - (S_{1n} + \tilde{C}_{1n})\sin\psi_n\right] - \frac{\sigma_s}{2\epsilon_o} r_{1n} E_{1n} \sin(\psi_n - \epsilon_{1n}) + \frac{\sigma_s}{2\epsilon_o} s_{2n} E_{2n} \sin\delta_{2n} \tag{A31}$$

where

$$\psi_n = \theta_{2n} - \theta_{1n} = (\omega_2 - \omega_1)t + (\varphi_2 - \varphi_1) \tag{A32}$$

is a slowly varying function of time. In the derivation of Equations (A27-A31), second time derivatives of slowly varying functions of time have been neglected.

It should be noticed that in Equations (A30, A31), the ECNME frequencies for the n^{th} mode, Ω_n, have been replaced by Ω_{1n}, where

$$\Omega_{2n} = \Omega_n + akn\, c^2 \tag{A33}$$

$$\Omega_{1n} = \Omega_n - aKn\, c^2 \tag{A34}$$

This occurred because of the coupling terms linear in "a" in Equations (A15, A16) and could be seen most easily by considering the solution of Equations (A15, A16) for an empty lossless cavity. For this case

$$E_s = Q^{-1} = P = 0$$

Expressing $A_n(t)$ and $\tilde{A}_n(t)$ by Eqs. (A21, A22) and substituting into Eqs. (A15, A16) for the empty cavity case, one finds, upon equating coefficients of $\sin\omega_{1n}t$ and $\cos\omega_{1n}t$ to zero, the equations

$$\omega_{2n}^2 - \Omega_n^2 - 2aK_n c^2 \omega_{2n} = 0 \tag{A35}$$

$$\omega_{1n}^2 - \Omega_n^2 + 2aK_n c^2 \omega_{1n} = 0 \tag{A36}$$

Since $\omega^2 - \Omega^2 \approx 2\omega(\omega - \Omega)$

Eqs. (A35, A36) become

$$\omega_{2n} = \Omega_n + aK_n c^2 \ , \tag{A37}$$

$$\omega_{1n} = \Omega_n - aK_n c^2 \ . \tag{A38}$$

In Eqs. (A37, A38), ω_{1n}, ω_{2n} are the ECNME Ω_{1n}, Ω_{2n} introduced in Eqs. (A30, A31). From the definition of "a" given in Eq. A6, the passive cavity frequency splitting is given by

$$\Omega_{2n} - \Omega_{1n} = (2\pi)\ 4A\ \Omega_{rot}/\lambda_n L \ . \tag{A39}$$

The physical significance of this cavity frequency splitting is that due to the cavity being located on a rotating frame, the resonant frequency is different for radiation traveling with and against the rotation.

APPENDIX B

Analysis of Lock-In Equation

The lock-in equation to be analyzed, is of the form

$$\dot{\psi} = \Delta\Omega + \frac{c}{L}\left[\rho_2 \cos(\psi+\epsilon_2) + \rho_1 \cos(\psi - \epsilon_1)\right] \tag{B1}$$

By simple manipulation, Eq. (B1) can be put into the form

$$\dot{\psi} = \Delta\Omega + \Delta\Omega_L \cos(\psi - \beta) \tag{B2}$$

where

$$\Delta\Omega_L = (c/L)\left[\rho_1^2 + \rho_2^2 + 2\rho_1\rho_2 \cos(\epsilon_1 + \epsilon_2)\right]^{1/2}, \tag{B3}$$

$$\text{Tan}\,\beta = \frac{\rho_1 \sin\epsilon_1 - \rho_2 \sin\epsilon_2}{\rho_1 \cos\epsilon_1 + \rho_2 \cos\epsilon_2} \tag{B4}$$

To simplify the integration of Eq (B2), initial conditions will be chosen so that at time $t = t_o$, $\psi = \beta$. Then Eq. (B4) becomes

$$\int_o^{\psi-\beta} \frac{dx}{\Delta\Omega + \Delta\Omega_L \text{Cos } x} = \int_{t_o}^{t} dt \tag{B5}$$

First consider the case when $\Delta\Omega > \Delta\Omega_L$. Then Eq. (B5) can be integrated[1] to give

$$\psi - \beta = 2\tan^{-1}\left[\left(\frac{K+1}{K-1}\right)^{1/2} \tan\left[\Delta\Omega_L (K^2-1)^{1/2} (t-t_o)/2\right]\right] \tag{B6}$$

where

$$K = \frac{\Delta\Omega}{\Delta\Omega_L} > 1 \tag{B7}$$

For the case when $K >> 1$, then

$$(K^2 \pm 1)^{1/2} \rightarrow K, \quad \Delta\Omega_L K \rightarrow \Delta\Omega$$

and Eq. (B6) reduces to

$$\psi = \beta + \Delta\Omega (t - t_o) \tag{B8}$$

---

1. Chemical Rubber Table of Integrals- 11th Edition 1957, P 293 No. 248

This is the expected result for the charge in the relative phase as a function of time in the absence of backscattering effects.

The period of time T, over which ψ change by 2π can be obtained from Eq. (B6) by writing Eq. (B6) for time t and time t=T. Then subtracting the two equations and taking the tangent of both sides, one finds

$$T = \frac{2\pi}{\Delta\Omega_L (K^2-1)^{1/2}} \tag{B9}$$

Using this period to define the observed frequency in the presence of back scattering, one finds

$$\Delta\omega = [\Delta\Omega^2 - \Delta\Omega_L{}^2]^{1/2} . \tag{B10}$$

This equation shows that the effective frequency difference between the oppositely directed traveling waves, defined in terms of the periodicity of the instantaneous phase difference is reduced from the no-backscattering value due to the mutual coupling between the beams. For small values of rotation or,

$$\Delta\Omega < \Delta\Omega_L ,$$

the beams are frequency locked, or a constant phase difference exists between the oppositely directed beams. This could be observed from direct integration of Eq. (B5) for the case of $K < 1$. From the table of integrals[1],

$$\Delta\Omega_L (1-K^2)^{1/2} (t - t_o) = \ln \left[\frac{(1-K^2)^{1/2} \tan \frac{1}{2} (\psi-\beta) + (1+K)}{(1-K^2)^{1/2} \tan \frac{1}{2} (\psi-\beta) - (1+K)} \right] \tag{B11}$$

As $t \to \infty$, Eq (B11) gives

$$\psi - \beta = 2 \tan^{-1} \frac{1+K}{1-K}^{1/2} \tag{B12}$$

Equation (B12) shows that the phase difference ψ, changes from $\psi = \beta + \pi$ at threshold (K = 1) to $\psi = \beta + \frac{1}{2}\pi$ at zero input rate. The phase conditions Eq. (B12) can also be obtained directly from Eq. (B12).

At values of K corresponding to rotations slightly above lock-in, Eq. (B6)

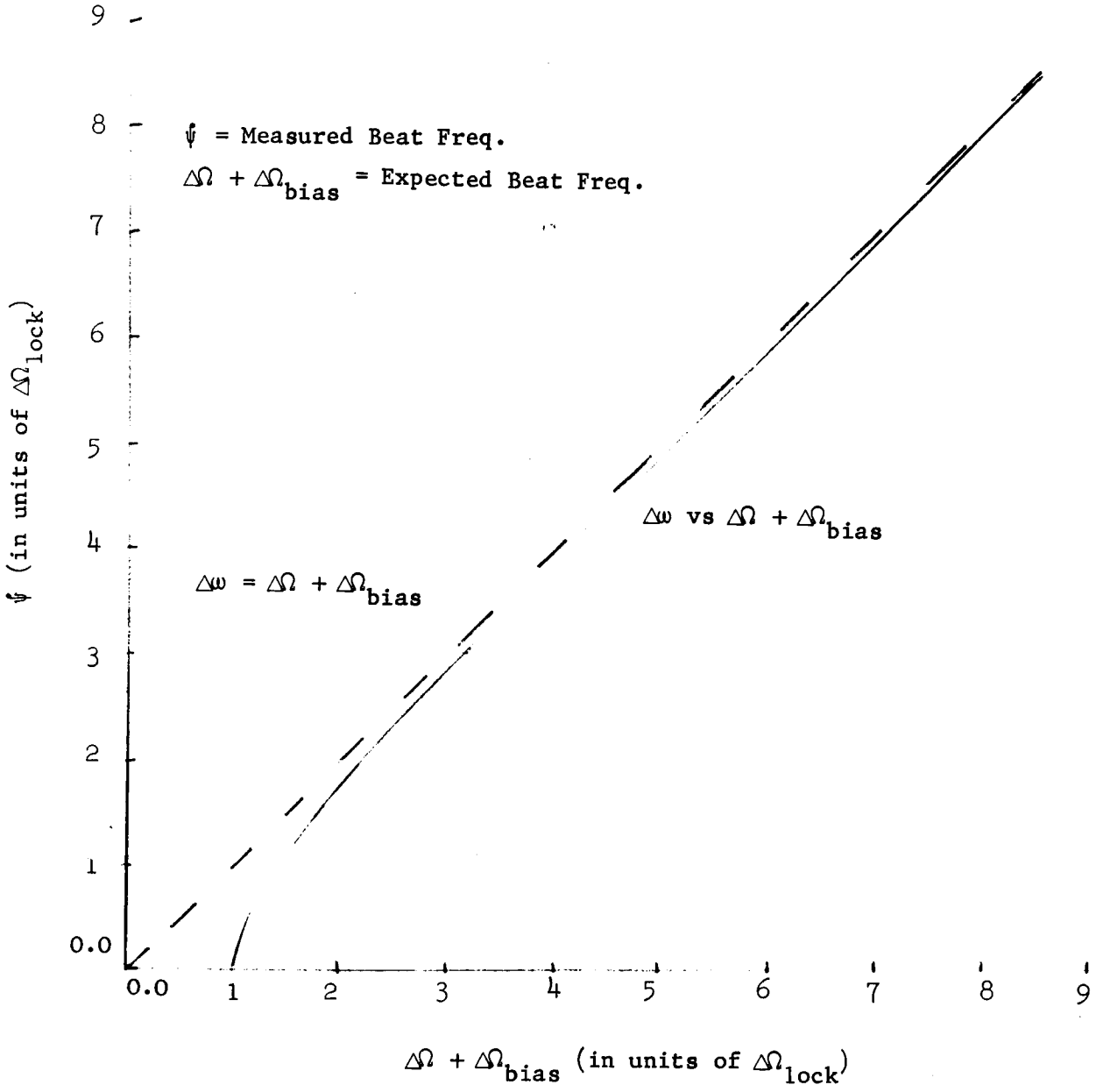

Figure 5. Measured Beat Frequency vs. Beat Frequency in the Absence of Backscatter

becomes (for $K = 1 + \delta$, $\delta << 1$)

$$\psi - \beta = 2 \tan^{-1}\left[(2/\delta)^{1/2} \tan[\Delta\Omega_L (\delta/2)^{1/2} (t - t_o)]\right] \qquad \text{(B13)}$$

Thus except for times when the tangent function is approximately zero, the phase difference is $\psi - \beta = \pi$, which is the threshold value. Thus slightly above lock in threshold the phase remains essentially constant over a period, and has a rapid jump of 2π. This gives rise to the so called distorted waveforms.

APPENDIX C

Determination of First Order Polarization

Using the single mode interaction as given by Equation (A60), the first order Fourier components of the polarization are given by:

$$\begin{Bmatrix} P_n^{(1)}(t) \\ \tilde{P}_n^{(1)}(t) \end{Bmatrix} = \frac{2i|\mu_{ab}|^2}{\hbar L} \int_{-\infty}^{\infty} W(v)dv\, T(v) \int_0^L N(z,t)dx \int_0^{\infty} d\tau' \exp -(\gamma_{ab} + i\omega)\tau' \tag{C1}$$

$$\begin{Bmatrix} U_n(z) \\ V_n(z) \end{Bmatrix} \left[\left[E_1 \cos\left[(\omega_1 + Kv)\, t' + \varphi_1\right] + E_2 \cos\left[(\omega_2 - Kv)t' + \varphi_2\right] \right] U_n(z) + \left[E_1 \sin\left[(\omega_1 + Kv)t' + \varphi_1\right] - E_2 \sin\left[(\omega_2 - Kv)t' + \varphi_2\right] \right] V_n(z) \right] + C.C.$$

where $\tau' = t - t'$ and $W(v)$ is the normalized velocity distribution. $T(v)$ is the proper Lorentz transformation necessary to transform the polarization back to the cavity frame.

The above expression is simplified by the rotating wave approximation. For example

$$\exp -(\gamma_{ab} + i\omega)\tau' \cos(\omega_1 + Ku)t' = \tag{C2}$$

$$\frac{i}{2} \exp - i\omega_1 t \exp -iKvt \exp -[\gamma_{ab} + i(\omega - \omega_1 - Ku)]\tau'$$

Only the negative frequency component of the cosine function is used to obtain Eq. (C2). The positive frequency component would give a term of the form

$$\exp -[\gamma_{ab} + i(\omega + \omega_1 + Kv)]\tau$$

and is neglected.

Thus in making the rotating wave approximation, Equation (C1) becomes

$$\begin{Bmatrix} P_n^{(1)} & (t) \\ \tilde{P}_n^{(1)} & (t) \end{Bmatrix} = \frac{i|\mu_{ab}|^2}{\hbar L} \int_{-\infty}^{\infty} W(v)dv\ T(v) \int_0^L N(z,t)dz \int_0^{\infty} d\tau' \begin{Bmatrix} U_n & (z) \\ V_n & (z) \end{Bmatrix}$$

$$\left[E_1 \exp -(i\omega_1 t + i\varphi_1 + iKvt + \gamma_{1-}\tau')(U_n(z) + iV_n(z)) + \right. \tag{C3}$$

$$\left. E_2 \exp -(i\omega_2 t + i\varphi_2 + iKvt + \gamma_{2+}\tau')(U_n(z) + iV_n(z)) \right] + \text{C.C.}$$

where

$$\gamma_{i\pm} + \gamma_{ab} + (\omega - \omega_i \pm Kv), \quad i = 1,2. \tag{C4}$$

Since $U \pm iV \sim \exp \mp iKz$, Equation (C3) is of the form

$$E_1 \exp - i(\omega_1 t + Kz) + E_2 \exp - i(\omega_2 t - Kz)$$

Now in transforming the traveling wave fields to the frame of the moving atom, fields of the form $(\omega t + Kz)$ were transformed such as to increase the frequency while fields of the form $(\omega t - Kz)$ were transformed such as to decrease the frequency. To transform the polarization back to the cavity frame, it is only necessary to make the reverse transformation.

Thus, $T(v)$ is exp iKvt and exp - iKvt for the term in E_1 and E_2, respectively. As a general rule, the Lorentz transformation can be carried out by placing the factor exp $\pm$ iKv next to each bracketed $U \pm iV$.

The ECNME are then written in exponential form and second harmonic spatical terms are neglected, or (neglecting the "n" subscript since only a single longitudinal mode is considered to be oscillating)

$$U \pm iV = \pm i \exp(\mp Kz),$$

and

$$U\,(U \pm iV) \simeq \frac{1}{2},$$

$$V\,(U \pm iV) \simeq \pm \frac{i}{2}.$$

The second harmonic spatial terms can be neglected as long as the population inversion density is slowly varying over spatial distances on the order of optical wavelengths. The effect of not making this approximation will be considered in a later section.

Thus Eq. (C3) becomes

$$P_n^{(1)}(t) = -\frac{i|\mu_{ab}|^2}{\hbar\, Ku\, \pi^{1/2}} \exp - i(\omega_1 t + \varphi_1) \int_{-\infty}^{\infty} dw \exp - w^2 \int_o^{\infty} dx$$

$$[E_1 \exp(-2\eta x + 2i(\xi_1 + w)x) + E_2 \exp(-i\psi\ 2\eta x + 2i(\xi_2 - w)x)] + \text{C.C.}, \tag{C5}$$

$$\tilde{P}_n^{(1)}(t) = \frac{|\mu_{ab}|^2}{\hbar Ku\, \pi^{1/2}} \exp - i(\omega_i t + \varphi_1) \int_{-\infty}^{\infty} dw \exp - w^2 \int_o^{\infty} dx$$

$$[E_1 \exp(-2\eta x + 2i(\xi_1 + w)x) - E_2 \exp(-i\psi - 2\eta x + 2i(\xi_2 - w)x)] + \text{C.C.} \tag{C6}$$

where the following substitutions have been made:

$x = \frac{1}{2}Ku\tau'$, $\eta = \gamma_{ab}/Ku$, $\xi_i = (\omega_i - \omega)/Ku$, $w = v/u$, and the velocity distribution has been chosen as Maxwellian, or

$$W(v)dv = (\pi)^{-\frac{1}{2}} \exp - w^2. \tag{C7}$$

Since

$$\pi^{-1/2} \int_{-\infty}^{\infty} dw \exp(-w^2 \pm 2iwx) = \exp -x^2 \tag{C8}$$

and defining the Hilbert transform of the Gaussian integral as

$$Z(\xi) = 2i \int_o^{\infty} \exp(-x^2 - 2\eta x + 2i\xi x)\, dx, \tag{C9}$$

Eqs. (C5, C6) can be written as

$$P_n^{(1)}(t) = -(A/2) \exp - (\omega_1 t + \varphi_1) [E_1 Z(\xi_1) + E_2 \exp(-i\psi) Z(\xi_2)] + \text{C.C.} \tag{C10}$$

$$\tilde{P}_n^{(1)}(t) = -(iA/2) \exp - (\omega_1 t + \varphi_1) [E_1 Z(\xi_1) - E_2 \exp(-i\psi) Z(\xi_2)] + \text{C.C.} \tag{C11}$$

The "in phase" and "in quadrature" Fourier components of the polarization, as defined in Eqs. (A24, A25), can be obtained as

$$S_n^{(1)}(t) = -A\left[E_1 Z_i(\xi_1) + E_2 \cos\psi\, Z_i(\xi_2) - E_2 \sin\psi Z_r(\xi_2)\right] \tag{C12}$$

$$C_n^{(1)}(t) = -A\left[E_1 Z_r(\xi_1) + E_2 \cos\psi\, Z_r(\xi_2) - E_2 \sin\xi Z_i(\xi_2)\right] \tag{C13}$$

$$\tilde{S}n^{(1)} = -A\left[E_1 Z_r(\xi_1) - E_2 \cos\psi\, Z_r((\xi_2) - E_2 \sin\psi Z_i(\xi_2)\right] \tag{C14}$$

$$\tilde{C}n^{(1)} = -A\left[E_1 Z_i(\xi_1) + E_2 \cos\psi\, Z_i(\xi_2) - E_2 \sin\psi Z_r(\xi_2)\right] \tag{C15}$$

Substituting Eqs. (C12- C15) into Eqs. (A28 - A31) and neglecting the scattering terms, the self-consistant equations, to first order, are found to be

$$E_j + \frac{1}{2}(\omega/Q_j)\, E_j = \frac{1}{2}(\omega/\epsilon_o)\, AE_j Z_i(\xi_j) \quad j = 1,2 \tag{C16}$$

$$(\Omega_j - \omega_j - \dot{\varphi}_j)\, E_j = -\frac{1}{2}(\omega/\epsilon_o)\, AE_j Z_r(\xi_j) \quad j = 1,2 \tag{C17}$$

For the doppler with much larger than the natural width ($\eta << 1$) the expansion of Equation (C9) gives

$$Z_i(\xi) = \sqrt{\pi}\, \exp -\xi^2 - 2\eta\,[1 - 2\xi\, F(\xi)] + O(\eta^2) \tag{C18}$$

$$Z_r(\xi) = -2F(\xi) + \sqrt{\pi}\, \xi\eta\, \exp -\xi^2 + O(\eta^2) \tag{C19}$$

with $F(\xi)$ given by

$$F(\xi) = \exp(-\xi^2) \int_o^{\xi} \exp x^2\, dx\,, \tag{C20}$$

$$\simeq \xi\,(1 - 2\xi^2/3) \qquad \xi << 1 \tag{C21}$$

APPENDIX D

Determination of Second Order Polarization

The second order population inversion density is given as[2]

$$\Delta \rho^{(2)}(z,v,t) = T(v)\Delta \rho^{(o)}(z,v,t) \int_o^\infty d\tau' \int_o^\infty d\tau'' \, [\exp(-\gamma_a \tau') + \exp(-\gamma_b \tau')] \exp -(\gamma_{ab} + i\omega)\tau'' \; V_{ba}(t') \; V_{ab}(t'') + C.C. \tag{D1}$$

where the substitutions $\tau' = t - t'$, $\tau'' = t' - t''$, have been made and the interaction is given by Equation (38). The zero'th order population inversion density (inversion in the absence of stimulated emission) is given by

$$\Delta \rho^{(o)}(z,v,t) = W(v) \; N(z,t) \tag{D2}$$

Making use of the rotating wave approximation, only the positive and negative frequency components of $V_{ba}(t')$ and $V_{ab}(t'')$, respectively, give contributions. The interaction terms then have the form

$$V_{ba}(t') \sim E_1 \exp[i(\omega_1 + Kv)t' + \varphi_1] \; (U - iV) + E_2 \exp[i(\omega_2 - Kv)t' + \varphi_2] \; (U + iV) \tag{D3}$$

$$V_{ab}(t'') \sim E_1 \exp[-i(\omega_1 + Kv)t'' - \varphi_1] \; (U + iv) + E_2 \exp[-i(\omega_2 - Kv)t'' - \varphi_2] \; (U - iV) \tag{D4}$$

The cross terms in $E_1 E_1$ have the factor $(U \pm iV)^2 \sim \exp \mp 2iKz$ and can be neglected. The interaction terms are then of the form

$$V_{ba}(t'') \; V_{ab}(t'') \sim [E_1^2 \exp i(\omega_1 + Kv) \; \tau'' + E_2^2 \exp i(\omega_2 - Kv)\tau''] \; (U+iV) e^{iKvt} \; (U - iV) e^{-iKvt} \tag{D5}$$

In Equation (D5) the Lorentz transformation has been carried out by the rule stated in Appendix C.

The double integral on Equation (D1) can now by evaluated to give:

$$\Delta \rho^{(2)}(z,v,t) = -\eta \Delta \rho^{(o)}(z,v,t) \left[[I_1 [\eta - I(\xi_1 + w)]^{-1} + I_2[\eta - i(\xi_2 - w)]^{-1} \right] + C.C. \tag{D6}$$

where

$$W(v)\, dv = (\pi)^{-1/2} \exp(-w^2)\, dw, \tag{D7}$$

$$w = v/u \tag{D8}$$

Combining the complex congugate term in Eq. D6 and writing

$$\Delta \rho = \Delta \rho^{(o)} + \Delta \rho^{(2)} \tag{D9}$$

and averaging over the cavity length, one gets

$$\Delta \rho\ (v,t) = \bar{N}(t)\ W(v)\ [1 - 2I_1 \mathcal{L}(\xi_1 + v/u) - 2I_2 \mathcal{L}(\xi_2 - v/u)] \tag{D10}$$

where

$$\bar{N}\ (t) = \frac{1}{L} \int_o^L N\ (z,t)\ dz \tag{D11}$$

APPENDIX E

Determination of Third Order Polarization

The third order Fourier components of the polarization are given by

$$\begin{matrix} P_n^{(3)}(t) \\ \tilde{P}_n^{(3)}(t) \end{matrix} = -\frac{2i|\mu|^4}{L} \int_o^\infty W(v)\, T(v)dv \int_o^L N(z,t)dz \int_o^\infty d\tau' \int_o^\infty d\tau'' \int_o^\infty d\tau'''$$

$$\exp -(\gamma_{ab} + i\omega)\,\tau' \,[\exp -\gamma_a \tau'' + \exp -\gamma_b \tau''] \qquad \text{(E1)}$$

$$[\exp -(\gamma_{ab} + i\omega)\,\tau''' + C.C.] \begin{matrix} U_n(z) \\ V_n(z) \end{matrix}$$

$$V_{ab}(t')\, V_{ba}(t'')\, V_{ab}(t''') + C.C.$$

where the substitutions

$$\tau' = t - t',\ \tau'' = t' - t'',\ \tau''' = t'' - t''' \qquad \text{(E2)}$$

have been made and the interaction is given by Equation (38).

The first step to be made towards the evaluation of Eq. (E1) is the rotating wave approximation. However in making the rotating wave approximation, great care must be taken in including all the terms that might possibly give a contribution to the third order polarization.

From Eq. (38), the interaction $V_{ab}(t')$, $V_{ba}(t'')$, $V_{ab}(t''')$, respectively, can be written as

$$V_{ab}(t') = [1] = \frac{1}{2} E_1 \quad (U - iV) \exp i\,[(\omega_1 + Ku)\,(t - \tau') + \varphi_1] +$$

$$(U + iV) \exp -i[(\omega_1 + K_u)\,(t - \tau') + \varphi_1] +$$

$$\frac{1}{2} E_2 \quad (U + iV) \exp i\,[(\omega_2 - Ku)\,(t - \tau') + \varphi_2] + \qquad \text{(E3)}$$

$$(U - iV) \exp -i[(\omega_2 - Kv)\,(t - \tau') + \varphi_2]$$

$$V_{ab}(t'') = [2],\ V_{ab}(t''') = [3]$$

Equation (13) is used to obtain [2] and [3] by letting

$t - \tau'$ $t - \tau''$ in [2] -E2-

$t - \tau'$ $t - \tau' - \tau'' - \tau'''$ in [3]

The Lorentz transformation T(v), to transform the polarization back to the cavity frame can now be caried out. Following the rule introduced in Appendix C, all factors $(U \pm iV)$ are replaced by $(U \pm iV) \exp(\pm iKvt)$.

The interaction is then divided into positive and negative frequency components. For example $[1] = [1] + [1]$, where $[1]$, $[1]$, represents the part of [1] containing $\exp(i\omega t)$, $\exp(-i\omega t)$, respectively.

Then the interaction [1 2 3] can be written as eight terms. The terms [+ + +] and [- - -] can be neglected since they introduce polarization components at three times the optical frequency. The terms

$$[+ + -],\ [+ - +],\ [- + +] \tag{E4}$$

introduce frequency components of the form $\exp i(\omega_1 t + \varphi_1)$. Recall that the formalism discriminates in favor of frequency ω_1 by writing

$$\omega_2 t + \varphi_2 = \psi + \omega_1 t + \varphi_1 ,$$

where ψ is slowly varying with respect to optical frequencies.

The three terms in Eq. (E4) give zero contribution under the rotating wave approximation. This can be seen by noting that each individual interaction that has a positive frequency has a factor in τ' of the form $\exp(-i\omega_1\tau')$. In Eq (E1) the interaction term is multiplied by a factor of the form $\exp(-i\omega\tau')$. Thus there are three factors of the form $\exp(-i\omega\tau')$ and one of the form $\exp(i\omega\tau)$, which under the rotating wave approximation, gives zero contribution. The three remaining terms are

$$[- + -],\ [- - +],\ [+ - -] \tag{E5}$$

These terms can be simplified by the rotating wave approximation and by

neglecting rapidly varying special terms (as in the calculation of the first order polarization in Appendix C). The resulting terms in Eq. (E5) can be written as

$$[E_1 (U + iv) \exp (- \gamma_{1-}\tau') + E_2 (U - iV) \exp (-i\psi - \gamma_{2+}\tau')] \qquad \text{(E6)}$$

$$[E_1^2 \exp -\gamma_{1-}\tau''' + E_2^2 \exp (- \gamma_{2+}\tau''') + C.C.] +$$

$$E_1^2 E_2 (U - iV) \exp(-i\psi - \gamma_{2+}\tau' + i (\omega_2 - \omega_1 - 2Kv) \tau'') [\exp (-\gamma_{2+}\tau''') +$$

$$\exp (-\gamma^*_{1-}\tau''')] +$$

$$E_1 E_2^2 (U + iV) \exp (-\gamma_{1-}\tau') -i (\omega_2 - \omega_1 - 2Kv) \tau'')[\exp -\gamma_{1-}\tau''' +$$

$$\exp - \gamma^*_{2+}\tau'''] ,$$

where

$$\gamma_{i\pm} = \gamma_{ab} + i (\omega - \omega_i \pm Kv) \qquad i = 1,2. \qquad \text{(E7)}$$

Using just the first term in Eq (E6), the third order Fourier components of the polarization given by Eq. (E1) become

$$\begin{Bmatrix} P_n^{(3)}(I) \\ \tilde{P}_n^{(3)}(I) \end{Bmatrix} = \frac{i |\mu|^4}{4\hbar^3 L} \exp -i(\omega_1 t + \varphi_1) \int_o^L N(z,t)\, dz \int_{-\infty}^{\infty} W(v)\, dv \int_0^{\infty}\!\!\int\!\!\int d\tau' d\tau'' d\tau'''$$

$$[\exp (-\gamma_a \tau'') + \exp (-\gamma_b \tau'')] \begin{Bmatrix} U \\ V \end{Bmatrix} [E_1 (U + iV) \exp (-\gamma_{1-}\tau') + \qquad \text{(E8)}$$

$$E_2 (U - iV) \exp (-i\psi - \gamma_{2+}\tau')] [E_1^2 \exp (-\gamma_1 - \tau''') + E_2^2 \exp(-\gamma_{2+}\tau''') +$$

$$= c.c.] + C.C.$$

Rapidly varying spatial terms are neglected so that

$$U^2 = V^2 \simeq \frac{1}{2} \quad , \; UV \simeq 0 \qquad \text{(E9)}$$

and the following substitutions are made

$$x = \frac{1}{2} Ku\tau' \quad , \quad y = \frac{1}{2} Ku\tau'' \quad , \quad w = \frac{v}{u} \tag{E10}$$

$$\eta = \frac{\gamma_{ab}}{Ku} \qquad \xi_i = \frac{\omega_i - \omega}{Ku} \qquad i = 1,2 \tag{E11}$$

$$I_i = \frac{|\mu|^2 E_i^2}{2\gamma_a \gamma_b \hbar^2} \quad i = 1,2 \qquad A = \frac{|\mu|^2 \bar{N}}{\hbar \, Kn} \tag{E12}$$

The integral over $d\tau''$ is easily evaluated and defining

$$\bar{N} = \frac{1}{L} \int_o^L N(z,t)dz , \tag{E13}$$

Eq. (E8) becomes

$$P_n^{(3)}(I) = 2i\eta \, A \exp - i(\omega_1 t + \varphi_1) \iint_o^\infty dxdy \exp[-2\eta(x+y)] \tag{E14}$$

$$\pi^{-1/2} \int_{-\infty}^{\infty} dw \exp(-w^2) \left[E_1 \exp 2i(\xi_1 + w)x + E_2 \exp(-i\psi + 2i(\xi_2 - w)x)\right]$$

$$\left[I_1 \exp 2i(\xi_1 + w)y + I_2 \exp 2i(\xi_2 - w)y + c.c.\right] + c.c.$$

Since

$$\int_{-\infty}^{\infty} \exp(-w \pm 2aw) \, dw = \sqrt{\pi} \exp(-a^2) \tag{E15}$$

and writing

$$P_n^{(3)}(I) = F \exp -i(\omega_1 t + \varphi_1) + c.c , \tag{E16}$$

$$F = F_+ + F_- , \tag{E17}$$

it is found that

$$F_- = 2iA\eta \iint_o^\infty dxdy \exp[-2\eta(x+y) - (x-y)^2] \left[E_1 I_1 \exp 2i\xi_1 (x-y) + \right.$$

$$E_1 I_2 \exp 2i(\xi_1 x + \xi_2 y) + E_2 I_1 \exp\left[-i\psi + 2i(\xi_2 x + \xi_1 y)\right] + \tag{E18}$$

$$\left. E_2 I_2 \exp\left[\mp i\psi + 2i\,\xi_2 (x-y)\right]\right] ,$$

$$F_+ = 2iA\eta \iint_0^\infty dxdy \exp\left[-2\eta(x+y) - (x+y)^2\right] \Big[E_1I_1 \exp 2i\xi_1 (x+y) +$$

$$E_1I_1 \exp 2i(\xi_1 x - \xi_2 y) + E_2I_2 \exp\left[-i\psi + 2i\xi_2 (x+y)\right] + \qquad \text{(E19)}$$

$$E_2I_1 \exp\left[-i\psi + 2i(\xi_2 x - \xi_1 y)\right]\Big].$$

The integrand in Eq. (E18) can be evaluated by the substitution

$$\alpha = x + y \quad , \quad \beta = x - y$$

$$\iint_0^\infty dxdy = \frac{1}{2} \int_{-\infty}^{0} d\beta \int_{-\beta}^{\infty} d\alpha + \frac{1}{2} \int_0^\infty d\beta \int_\beta^\infty d\alpha \qquad \text{(E20)}$$

Then using the definition of the Hilbert transform of the Gaussian as found in Eq. (C9), Eq (E18) becomes

$$F_- = \frac{iA}{2} \left[E_1I_1 Z_i(\xi_1) + E_2I_2 \exp(-i\psi) Z_i(\xi_2)\right.$$

$$\left. -i(E_1I_2 + E_2I_1)\left(\frac{\eta + i\xi}{\eta}\right) \mathcal{L}(\xi) \ \bar{Z}(\xi)\right] , \qquad \text{(E21)}$$

where

$$\bar{Z}(\xi) = \frac{1}{2}\left[Z(\xi_1) + Z(\xi_2)\right] . \qquad \text{(E22)}$$

The integral in Eq. (E19) can be evaluated with the same substitution as in Eq. (E20) but with the order of integration so that

$$\iint_0^\infty dxdy = \frac{1}{2} \int_0^\infty d\alpha \int_{-\alpha}^{\alpha} d\beta \qquad \text{(E23)}$$

Equation (E19) is then evaluated to give

$$F_+ = iA\eta \Big[E_1I_1[1 + (\xi_1 + i\eta) Z(\xi_1)] + E_2I_2 \exp(-i\psi)[1 + (\xi_2 + i\eta) Z(\xi_2)]$$

$$-\frac{1}{4\xi} E_1I_2 [Z(\xi_1) + Z^*(\xi_2)] - \frac{1}{4\xi} E_2I_1 \exp(-i\psi)[Z^*(\xi_1) + Z(\xi_2)]\Big]$$

At this point the significance of the "Doppler approximation", made in Lamb's paper[2] can be seen. In the "Doppler Limit" (die) for $\eta \ll 1$, the term $\exp - (x \pm y)^2$ can be treated as a delta function in $x \pm y$.

Since the range of integration for x and y is only over positive values, the dominant contribution comes from the term in $(x - y)$, which is F_-. Referring to Eqs. (E21, E24), it is seen that the contribution from F_- is an order of η^{-1} bigger than the contribution from F_+.

To evaluate the self-consistant equations, it is seen from Eqs. (A28-A31) that the following combinations of terms are required.

$$\begin{array}{l} S - \tilde{C} \\ (S + \tilde{C}) \cos\psi + (C - \tilde{S}) \sin\psi \\ C + \tilde{S} \\ (C - \tilde{S}) \cos\psi + (S - \tilde{C}) \sin\psi \end{array} \qquad \text{(E21)}$$

The "in phase" and "in quardrature" parts of the Fourier components of the polarization are defined in Eqs. (A24, A25). Using Eq. (16) to define F one can write

$$F = \Omega [A + B \exp(-i\psi)]/2 \qquad \text{(E22)}$$

and similar relations for $\tilde{F}$, $\tilde{A}$, $\tilde{B}$.

Then as seen from Eq. (E8), P_m and $\tilde{P}_m$ are related such that A, B, $\tilde{A}$, $\tilde{B}$, are of the form

$$\begin{array}{l} A \sim U (U + iV) a \\ B \sim U (U - iV) b \\ \tilde{A} \sim V (U + iV) a \\ \tilde{B} \sim V (U - iV) b \end{array} \qquad \text{(E23)}$$

When rapidly varying spacial terms are neglected such that $U^2 = V^2 = \frac{1}{2}$, $UV = 0$, then

$$\tilde{A} = iA, \qquad \tilde{B} = iB \qquad \text{(E24)}$$

By substitution, it can now be shown that the combination of terms given in Eq (E21) take the simple form of

$$2A_i,\ 2A_r,\ 2B_i,\ 2B_r, \text{ respectively} \qquad \text{(E24a)}$$

It should be emphasized at this point that there is no ψ dependence in the coefficients A and B. Thus as long as the polarization can be put in the form of Eq (E23), no terms in ψ arise in the self-consistant equation, which could lead to lock-in. Referring back to Eq. (E6), which is the general form of the interaction after the rotating wave approximation and the neglecting of the rapidly varying spacial terms, it is seen that Eq. (E23) holds. Thus for a single oscillating longitudinal mode (one pair of oppositely directed traveling waves) no combination tone is generated in the non-linear medium which could lead to frequency locking.

Using F_- (the polarization contribution in the "doppler limit") as given by Eq. (E21) as given by Eq. (E21) the self-consistant equations, to third order, can be written as

$$\dot{E}_1 + \frac{1}{2}(\omega/Q)E_1 = \frac{1}{2}(\omega/\epsilon_o)AE_1 \; Z_i(\xi_1) - I_1 Z_i(\xi_1) - I_2 \mathcal{L}(\xi)\,[\bar{Z}_i + (\xi/\eta)\bar{Z}_r] \tag{E25}$$

$$\dot{E}_2 + \frac{1}{2}(\omega/Q)E_2 = \frac{1}{2}(\omega/\epsilon_o)AE_2 \; Z_i(\xi_2) - I_2 Z_i(\xi_2) - I_1 \mathcal{L}(\xi)\,[Z_i + (\xi/\eta)\bar{Z}_r] \tag{E26}$$

$$(\omega_1 + \dot{\varphi}_1 - \Omega_1) = \frac{1}{2}(\omega/\epsilon_o)A \; Z_r(\xi_1) + I_2 \mathcal{L}(\xi)\,[(\xi/\eta)\bar{Z}_i - \bar{Z}_r] \tag{E27}$$

$$(\omega_2 - \dot{\varphi}_2 - \Omega_2) = \frac{1}{2}(\omega/\epsilon_o)A \; Z_r(\xi_1) + I_1 \mathcal{L}(\xi)\,[(\xi/\eta)\bar{Z}_i - \bar{Z}_r] \tag{E28}$$

The contribution to the polarization arising from F_+, as given by Eq. (E24), can be evaluated using the same technique. Adding this contribution to the self-consistant equations changes the backeted terms on the right hand side of Eqs. (E25, E27). They take on the form

$$Z_i(\xi_1) - I_1\,[(1 + 4\eta^2)Z_i(\xi_1) - 2\eta(1 + \xi_1 Z_r(\xi_1))] - I_2 \mathcal{L}(\xi) \times [\bar{Z}_i(\xi) - \frac{\eta}{\xi}\bar{Z}_r(\xi)] \tag{E29}$$

$$Z_r(\xi_1) + (\xi/\eta) I_2 \mathcal{L}(\xi)\left[\bar{Z}_i - (\eta/\xi)^2 \bar{Z}_r - \frac{1}{2}\left[1 + (\eta/\xi)^2\right]\left[Z_i(\xi_1) - Z_i(\xi_2)\right]\right] + 2\eta I_1\,[\xi_1 Z_i(\xi_1) + \eta Z_r(\xi_2)] \tag{E30}$$

where use has been made of the identity

$$(\eta/\xi) - (\xi/\eta)\,\mathcal{L}(\xi) = (\eta/\xi)\,\mathcal{L}(\xi) \tag{E31}$$

Similar equations to Eqs (E29, E30) hold for beam "two".

If the delta function approximation[2] were made, the bracketed parts on the right hand side of Eqs (E25, E27) would read

$$Z_i(\xi_1) - \sqrt{\pi}\, I_1 - \sqrt{\pi}\, I_2\, \mathcal{L}(\xi) \tag{E32}$$

$$Z_r(\xi_1) + (\xi/\eta)\sqrt{\pi}\, I_2\, \mathcal{L}(\xi) \tag{E33}$$

Thus the delta function approximation not only neglects terms on the order of η, but also neglects gaussian factors in the third order polarization terms. The neglect of these factors is not too serious for the treatment of a "pure" single isotope type gas, but for a mixture of isotopes, leads to incorrect results.

Now to consider the part of the interaction given by the second and third terms in Eq. (E6). Substituting into the polarization expression given by Eq. (E1) and using the substitutions given by Eqs. (E10, E11) and writing $z = \frac{1}{2} Ku\tau''$, one finds

$$\begin{pmatrix} P_n^{(3)}(II) \\ \tilde{P}_n^{(3)}(II) \end{pmatrix} = \frac{2i|\mu|^4 \sqrt{N}\, \exp -i(\omega_1 t + \varphi_1)}{\hbar^3 \sqrt{\pi}\, (Ku)^3} \iiint_0^\infty dx\,dy\,dz \exp -2\eta(x+y) \begin{pmatrix} U \\ V \end{pmatrix}$$

$$[\exp(-2\eta_a z) + \exp(-2\eta_b z)] \Big[E_1^2 E_2\, (U - iV) \exp[-i\psi + 2i(\xi_2 - w)\, x$$

$$+2i(\xi_2 - \xi_1 - 2w)\, z] \exp 2i(\xi_2 - w)\, y + \exp -2i(\xi_1 + w)\, y \Big]$$

$$E_1 E_2^2 \exp[2i(\xi_1 + w)\, x - 2i(\xi_2 - \xi_1 - 2w) z] \Big[\exp 2i(\xi_1 + w)\, y + \tag{E34}$$

$$\exp -2i(\xi_2 - w)\, y \Big] \Big] + C.C.$$

If one carries out the dw integration first it can be seen that all the terms give a factor of exp - $(x + y + z)^2$. Thus in the "doppler limit" all the terms in Eq (E34) are of the order of $\eta << 1$, or smaller. Equation (E34) was not evaluated. Thus to be consistant, all the terms on the order of η in the third order polarization, should be neglected. It should also always be remembered that the resulting equations only hold for $\eta << 1$.

APPENDIX F

Calculation of Backscatter Correction to Polarization

In writing the interaction in the presence of backscatter, it is now assumed that the steady state radiation field is composed of two sets of oppositely directed traveling waves. The second set is generated from backscattering of the first set, as shown in Fig A1. The expression for the first order polarization is that given by Eq. (C1), except that the interaction field now reads

$$\Big[E_1 \cos[(\omega_1 + Kv)t' + \varphi_1] + E_2 \cos[(\omega_2 - Kv)t' + \varphi_2] + r_1 E_1 \cos[(\omega_1 - Kv)t' + \varphi_1] + r_2 E_2 \cos[(\omega_2 + Kv)t' + \varphi_2] \Big] U + \Big[E_1 \sin[(\omega_1 + Kv)t' + \varphi_1] - E_2 \sin[(\omega_2 - Kv)t' + \varphi_2] + -r_1 E_1 \sin[(\omega_1 - Kv)t' + \varphi_1] + r_2 E_2 \sin[(\omega_2 + Kv)t' + \varphi_1] \Big] V \tag{F1}$$

Making the rotating wave approximation, neglecting rapidly varying spacial terms and integrating over the cavity length, the first order Fourier component of the polarization becomes

$$P_n^{(1)} = \frac{-i|\mu|^2 \bar{N}}{2\hbar} \int_o^\infty dv W(v) \int_o^\infty d\tau' \Big[E_1 \exp - i(\omega_1 t + \varphi_1) \exp(-\gamma_{1-}\tau') + r_1 \exp(-\gamma_{1+}\tau' - i\varepsilon_1) + E_2 \exp -i(\omega_2 t + \varphi_2) \exp(-\gamma_{2+}\tau') + r_2 \exp(-\gamma_{2+}\tau' - i\varepsilon_2) \Big] + C.C. \tag{F2}$$

$$\tilde{P}_n^{(1)} = i P_n^{(1)} [r_1, r_2, E_2 \to -r_1, -r_2, -E_2] \tag{F3}$$

The notation is identical to that in Appendix C.

Using a Maxwellian velocity distribution and integrating over velocity, Eqs. (F2,F3) become

$$P_n^{(1)} = -iA \exp -(\omega_1 t + \varphi_1) \int_0^\infty dx \exp (-x^2 - 2\eta x)\Big[[\, 1 + r_1 \exp(-i\epsilon_1)]$$

$$E_1 \exp\left|2i\xi_1 x\right| + [1 + r_2 \exp(-i\epsilon_2)]\, E_2 \exp (-i\psi + 2i\, \xi_2 x)]\Big] + C.C. \tag{F4}$$

$$\tilde{P}_n^{(1)} = i\, P_n^{(1)} [r_1, r_2, E_2 \rightarrow -r_1, -r_2, -E_2] \tag{F5}$$

The integrals in Eqs (F4, F5) can be expressed in terms of the Hilbert transform of the Gaussian integral to give

$$P_n^{(1)} = F \exp -i(\omega_1 t + \varphi_1) + C.C. \tag{F6}$$

$$\tilde{P}_n^{(1)} = \tilde{F} \exp -i(\omega_1 t + \varphi_1) + C.C. \tag{F7}$$

$$F = -\frac{A}{2} [E_1 (1 + r_1 \exp - i\epsilon_1)\, Z(\xi_1) + E_2 (1 + r_2 \exp -i\epsilon_2) \exp (-i\psi)$$

$$Z(\xi_2)] \tag{F8}$$

$$\tilde{F} = iF [r_1, r_2, E_2 \rightarrow -r_1, -r_2, -E_2] \,. \tag{F9}$$

Writing

$$F = \tfrac{1}{2}[A + B \exp -i\psi] \,, \tag{F10}$$

$$\tilde{F} = \tfrac{1}{2}[\tilde{A} + \tilde{B} \exp(-i\psi)] \,, \tag{F11}$$

it can be seen from Eqs. (F8, F9) that

$$\tilde{A} = iA\,(-r_1) \,, \tag{F12}$$

$$\tilde{B} = -iB\,(-r_2) \,. \tag{F13}$$

Hence Eq. (E24) is not satisfied and the factors in the self-consistant equations will not take the simple form as given in Eq (E24a). By substitution, it is found that

$$S\text{-}\tilde{C} = [A_i(r_1) + A_i\,(-r_1)] + [B_i(r_2) - B_i(-r_2)] \cos\psi +$$

$$[B_r(r_2) - B_r(-r_2)] \sin\psi \tag{F14}$$

$$C + \tilde{S} = [A_r(r_1) + A_r(-r_1)] + [B_r(r_2) - B_r(-r_2)] \cos\psi + [B_i(r_2) - B_i(-r_2)] \sin\psi \quad . \tag{F15}$$

Using Eqs (F8, F10, F12, F13), it is found that

$$A_i = -A E_1 [(1 + r_1 \cos\epsilon_1) Z_i(\xi_1) - r_1 \sin\epsilon_1 Z_r(\xi_1)] \tag{F16}$$

$$A_r = -A E_1 [(1 + r_1 \cos\epsilon_1) Z_r(\xi_1) + r_1 \sin\epsilon_1 Z_i(\xi_1)] \tag{F17}$$

$$B_i = -A E_2 [(1 + r_2 \cos\epsilon_2) Z_i(\xi_2) - r_2 \sin\epsilon_2 Z_r(\xi_2)] \tag{F18}$$

$$B_r = -A E_2 [(1 + r_2 \cos\epsilon_2) Z_r(\xi_2) + r_2 \sin\epsilon_2 Z_i(\xi_2)] \tag{F19}$$

Using Eqs (F14-F19) and Eqs (A28-A31) the first order self-consistant equations become

$$\dot{E}_1 + \frac{\omega}{2Q_1} E_1 = \frac{\omega A}{2\epsilon_o} [E_1 Z_i(\xi_1) + r_2 E_2 Z_i(\xi_2) \cos(\psi + \epsilon_2) - Z_r(\xi_2) \sin(\psi + \epsilon_2)] \tag{F20}$$

$$(\omega_1 + \dot{\varphi}_1 - \Omega_1) E_1 = \frac{\omega A}{2\epsilon_o} [E_1 Z_r(\xi_1) + r_2 E_2 Z_r(\xi_2) \cos(\psi + \epsilon_2) + Z_i(\xi_2) \sin(\psi + \epsilon_2)] \tag{F21}$$

Equations for beam "two" are obtained by letting $1 \rightarrow 2, 2 \rightarrow 1$ and $\psi \rightarrow -\psi$.

APPENDIX G

Analysis of Rotation Drift Data

From Eq. (54), the instantaneous frequency difference between the oppositely directed beams is of the form

$$\Delta\omega = \Delta\Omega_R + \Delta\Omega_B + \Delta\Omega_L \cos(\psi-\beta) \tag{G1}$$

The average observed frequency difference is, from Eq. (56)

$$\Delta\omega = [(\Delta\Omega_R + \Delta\Omega_B)^2 - \Delta\Omega_L{}^2]^{1/2} \tag{G2}$$

Assuming the quantities on the right hand side of Eq. (G2) to be time independent, a time integration of Eq. (56) gives

$$N = T\,[(\Delta\Omega_R + \Delta\Omega_B)^2 - \Delta\Omega_L{}^2]^{1/2} \tag{G3}$$

where N is the number of cycles in a time T for a frequency $\Delta\omega$.

If the laser is rotated first in one direction and then in the other direction with the same $|\Delta\Omega_R|$, then Eq. (G3) can be written for both cases as

$$N_+ = T\,[(\Delta\Omega_R + \Delta\Omega_B)^2 - \Delta\Omega_L{}^2]^{1/2} \tag{G4}$$

$$N_- = T\,[(\Delta\Omega_R - \Delta\Omega_B)^2 - \Delta\Omega_L{}^2]^{1/2} \tag{G5}$$

For the case of the rotation rate being much greater than the bias rate and the lock-in threshold, a binomial expansion of Eqs. (G4, G5) gives,

$$N_+ - N_- = 2\,T\,\Delta\Omega_B \tag{G6}$$

Thus the difference in counts when the laser is rotated in opposite directions is just equal to the bias counts. For the case of the experiment discussed in section 26, earth's rate is included in the bias term.